STRUCTURAL AND MECHANISTIC STUDIES OF
MAMMALIAN MITOCHONDRIAL RNAS

Christie Nicole Jones

A dissertation submitted to the faculty of the University of North Carolina at Chapel Hill in
partial fulfillment of the requirements for the degree of Doctor of Philosophy in the Department
of Chemistry.

Chapel Hill
2008

Approved by:

Linda Spremulli

Kevin Weeks

Nancy Thompson

Gary Pielak

Dorothy Erie

ABSTRACT

Christie N. Jones: Structural and mechanistic studies of mammalian mitochondrial RNAs
(Under the direction of Linda L. Spremulli)

The mammalian mitochondrial genome encodes 13 proteins, which are synthesized at

the direction of 9 monocistronic and two dicistronic mRNAs. These mRNAs lack both 5' and

3' untranslated regions. The mechanism by which the specialized mitochondrial translational

apparatus locates start codons and initiates translation of these leaderless mRNAs is currently

unknown. To better understand this mechanism, the secondary structures near the start

codons of all 13 open reading frames have been analyzed using RNA SHAPE chemistry. The

extent of structure in these mRNAs as assessed experimentally is distinctly lower than would

be predicted by current algorithms based on free energy minimization alone. We find that the

5' ends of all mitochondrial mRNAs are highly unstructured. The first 35 nucleotides for all

mitochondrial mRNAs form structures with free energies less favorable than -3 kcal/mol,

equal to or less than a single typical base pair. The start codons, which lie at the very 5' ends

of these mRNAs, are accessible within single stranded motifs in all cases, making them

potentially poised for ribosome binding. These data are consistent with a model in which the

specialized mitochondrial ribosome preferentially allows passage of unstructured 5'

sequences into the mRNA entrance site to participate in translation initiation.

The mitochondrial tRNA genes are hot spots for mutations that lead to human

disease. A single point mutation (T4409C) in the gene for human mitochondrial tRNA^{Met}

(hmtRNA^{Met}) has been found to cause mitochondrial myopathy. This mutation results in the

replacement of U8 in hmtRNA^{Met} with a C8. Here we show that the single U8C mutation leads to a failure of the tRNA to respond conformationally to Mg^{2+}. This mutation results in a drastic disruption in the structure of the hmtRNA^{Met}, which significantly reduces its aminoacylation. We have used structural probing and molecular reconstitution experiments to examine the structures formed by the normal and mutated tRNAs. In the presence of Mg^{2+} the normal tRNA displays the structural features expected of a tRNA. However, even in the presence of Mg^{2+}, the mutated tRNA does not form the cloverleaf structure typical of tRNAs. Thus, we believe that this mutation has disrupted a critical Mg^{2+} binding site on the tRNA required for formation of the biologically active structure. This work establishes a foundation for understanding the physiological consequences of the numerous mitochondrial tRNA mutations that result in disease in humans.

ACKNOWLEDGMENTS

I would like to begin by thanking my mentor and friend Dr. Linda Spremulli for all of her help and support throughout my time in her lab. She has been a constant source of encouragement and enthusiasm. I am forever gratefully for the love of biochemistry that she has instilled in me.

I would also like to thank past members of the Spremulli lab for their contribution to this work. In particular, special thanks go to Domenick Grasso who was a constant source of encouragement and amusement during his time in the lab and Angie Spencer who laid the foundation for the tRNA^{Met} project. Thanks also to Kim Hung, a very talented undergraduate student that I had the pleasure of working with on the mRNA project.

I am very appreciative of the scientific help and support that I have received from Dr. Kevin Weeks and his lab, in particular Kevin Wilkinson and my good friend Caia Duncan. I am also grateful to Dr. Paul Agris and his laboratory for insightful discussions about tRNA^{Met}.

Finally, I would like to thank all of my family and friends for their constant love and support. In particular, I thank my wonderful lifelong friends Stacy and Rebecca for providing a distraction from science. Lastly, special thanks go to my parents and grandparents who have always believed that I could accomplish whatever I tackled. Thanks for believing in me!

TABLE OF CONTENTS

LIST OF TABLES

LIST OF FIGURES

ABBREVIATIONS

A_{260} or A_{280} or A_{600}	absorbance at the indicated wavelength (nm)
ADP	adenosine diphosphate
ATP	adenosine triphosphate
aa-tRNA	aminoacyl-tRNA
ATP8 or ATP6	ATP synthase subunit 8 or 6
βME	β-mercaptoethanol
COI, II or III	cytochrome oxidase subunit I, II or III
CytB	cytochrome B
D-arm or –loop or -stem	dihydrouridine arm or loop or stem
DMSO	dimethyl sulfoxide
DTT	dithiothreitol
EDTA	ethylenediaminetetraacetic acid
$EF\text{-}Tu_{mt}$	mitochondrial elongation factor Tu
GDP	guanosine $5'$-diphosphate
GTP	guanosine $5'$-triphosphate
$hmtRNA^{Met}$	human mitochondrial $tRNA^{Met}$
$IF2_{mt}$	mitochondrial initiation factor 2
$IF3_{mt}$	mitochondrial initiation factor 3
IPTG	isopropyl-β-D-thiogalactopyranoside
Met-tRNA	methionyl-tRNA
MTF_{mt}	mitochondrial methionyl-tRNA transformylase
mtMetRS	mitochondrial methionyl-tRNA synthetase

ND1-6	NADH dehydrogenase subunit 1-6
NMIA	N-methylisatoic anhydride
OXPHOS	oxidative phosphorylation
PAGE	polyacrylamide gel electrophoresis
PCR	polymerase chain reaction
PMSF	phenylmethylsulfonyl fluoride
ROS	reactive oxygen species
SAFA	semi-automated footprinting analysis
SHAPE	selective 2′-hydroxyl acylation analyzed by primer extension
Tris	Tris-(hydroxymethyl)aminomethane
T-arm or – loop or –stem	thymidine arm or loop or stem
Ψ	pseudouridine
1M7	1-methyl-7-nitro-isotoic anhydride

CHAPTER 1

MECHANISM OF PROTEIN SYNTHESIS

INTRODUCTION

Mitochondria are membrane bound, subcellular organelles found in eukaryotic cells. They are believed to have derived from bacteria that were engulfed by early eukaryotic cell precursors. Mitochondria are known as the powerhouses of the cell and through oxidative phosphorylation (OXPHOS) generate 90% of the cell's energy in the form of ATP. Present in the inner membrane of the mitochondrion are a series of multi-protein complexes through which electrons are transported and ultimately delivered to molecular oxygen (Fig. 1-1). Electron transport generates an electrochemical proton gradient across the membrane; the flow of protons back across the membrane drives the formation of ATP by the ATP synthase complex *(1)*.

There are over 80 proteins that constitute the OXPHOS machinery. The majority of these proteins are encoded within the nuclear genome, translated in the cytoplasm and imported into the mitochondrion. However, a few of the protein subunits are encoded within the unique mitochondrial genome. The size and content of the mitochondrial genome varies greatly across species. For example, the mitochondrial genome of plants is commonly greater than 100 kilo base pairs (kbp) compared to the human mitochondrial genome of only about 13 kbp. The human mitochondrial genome is small and compact encoding only 13 proteins that all function in OXPHOS and also encodes 2 rRNAs and 22 tRNAs (Fig. 1-2). The double-stranded, circular genome is organized so that 12 of 13 protein encoding genes are encoded on a single strand of the genome. The protein encoding genes are delineated by the tRNA genes that are dispersed on both strands of the genome *(2)*.

FIGURE 1-1. The inner mitochondrial membrane showing the oxidative phosphorylation pathway. Electrons are transferred from NADH through the 4 complexes of the electron transfer chain: complex I (NADH dehydrogenase), complex II (succinate dehydrogenase, not shown), complex III (cytochrome reductase) and complex IV (cytochrome oxidase). From complex IV, the electrons reduce molecular oxygen to water. The flow of electrons through the complexes provides the energy used to pump protons across the inner membrane, from the matrix to the intermembrane space, forming a proton gradient. The flow of protons down the concentration gradient, through complex V (ATP synthase), results in the formation of ATP from ADP and inorganic phosphate (P_i).

Fig. 1-1

mitochondrion

Outer mitochondrial membrane

Intermembrane Space

Inner mitochondrial membrane

High [H^+]

low [H^+]

H^+

H^+

H^+

H^+

e^-

I

III

IV

V

$\frac{1}{2}O_2$

H_2O

ADP + Pi

ATP
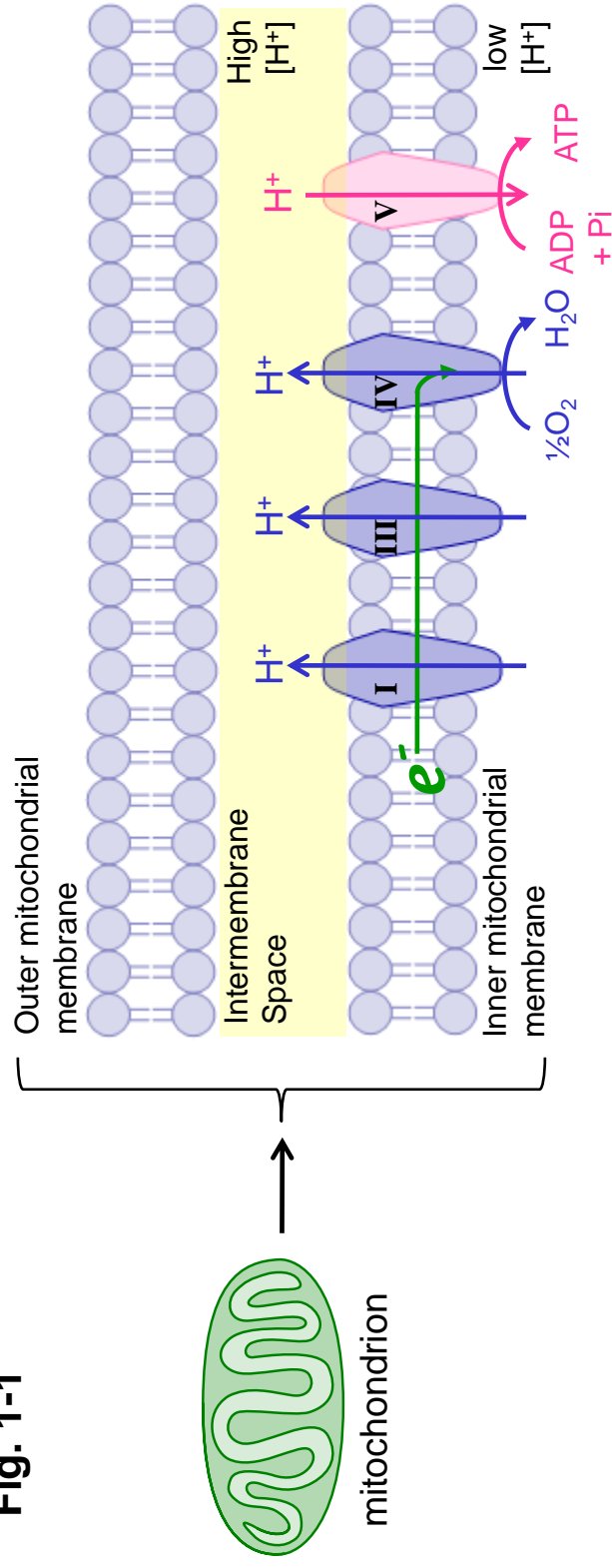
FIGURE 1-2. Organization of the human mitochondrial genome. The mitochondrial genome encodes 13 protein subunits of the oxidative phosphorylation pathway (pink, purple, orange and yellow). In addition, the genome encodes all 22 tRNAs (white) and the 2 rRNAs (green) required for protein synthesis in mammalian mitochondria. The tRNA genes are designated by their 1 letter amino acid abbreviation. The origins of replication (O_H and O_L) and transcription promoters (P_H and P_L) are shown. This figure was taken and modified from www.mitomap.org.

Fig. 1-2
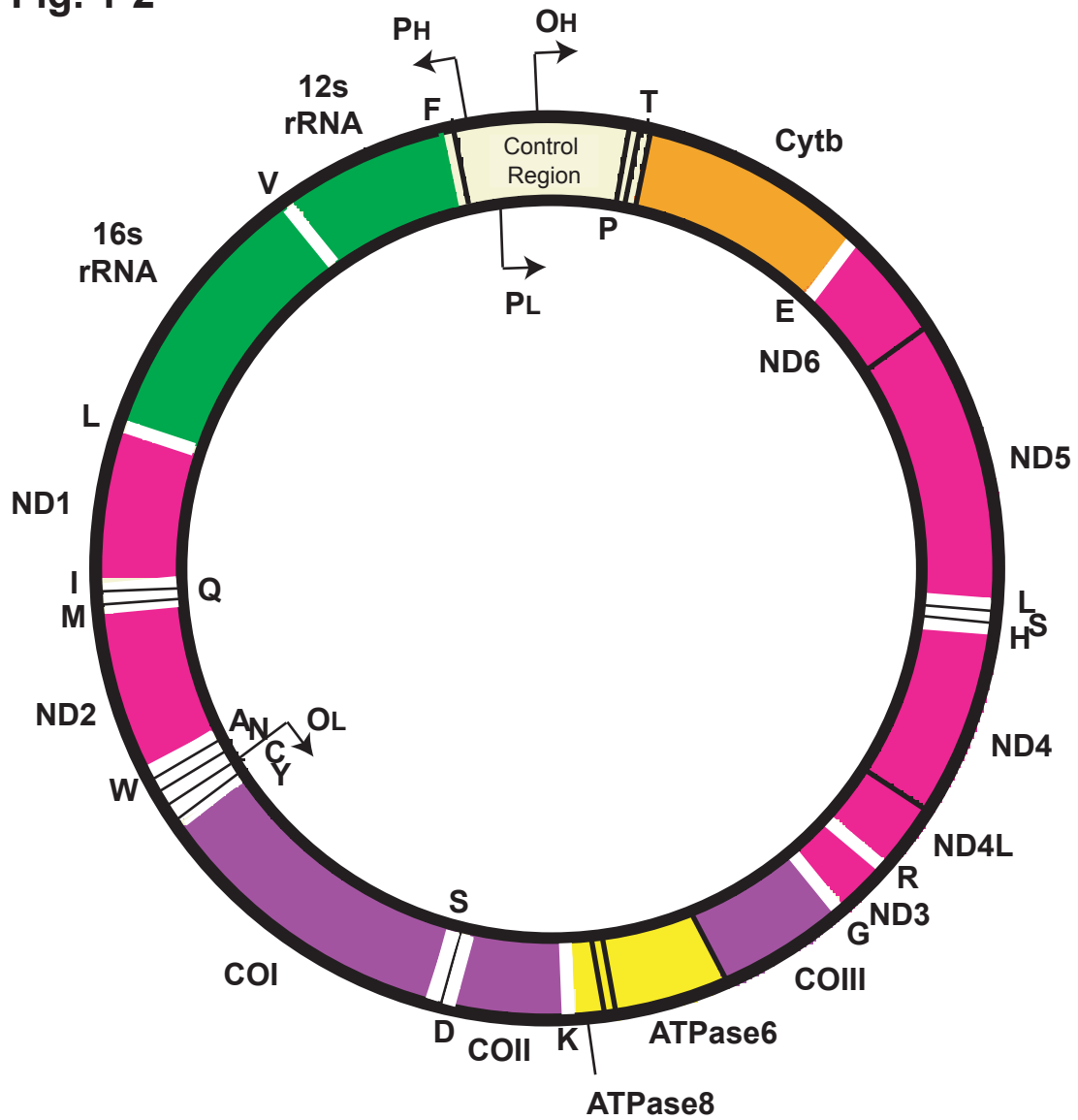
modified from mitomap.org

An unavoidable by-product of OXPHOS is the generation of reactive oxygen species (ROS), such as superoxide. Most of the ROS generated in mitochondria are scavenged by enzymes or non-enzymatic antioxidants *(3)*. However, damage to the mitochondrial DNA (mtDNA) by ROS does occur. The close proximity of the mtDNA, in the matrix of the mitochondrion, to the ROS generating OXPHOS pathway leads to a much higher mutation rate compared to nuclear DNA. Mitochondrial polymerases lack base-excision repair so are ill equipped to deal with ROS-induced DNA damage. Therefore, mutations are prevalent in mitochondrial DNA *(3,4)*.

There are multiple mitochondria in each cell and 100-10,000 copies of mtDNA in each mitochondrion. Mutations that are caused by ROS induced damage may only affect a subset of the mtDNA. When a mutation is only present in some copies of the mtDNA the mutation is considered heteroplasmic. A mutation present in all copies is homoplasmic. For heteroplasmic mutations, a critical number of mutated mtDNA copies must be present in a mitochondrion for disease to result. Therefore, the onset of disease and loss of energy production may be gradual and may depend on the cell type affected *(5,6)*.

Diseases caused by mutation of mtDNA can result from damage to one of the mitochondrial encoded OXPHOS proteins or may result from damage to one of the tRNAs. While the rate of mtDNA mutation is generally high, the mutation rate of the tRNAs is disproportionately high. The tRNA genes only constitute ~10% of the genome, but account for over half of the disease causing mutations *(4,7)*. The mitochondrial tRNAs are, therefore, considered hotspots for mutations that cause disease in humans.

PROTEIN SYNTHESIS IN PROKARYOTES

The mechanism of protein synthesis in prokaryotes occurs on the 70S ribosome (Fig. 1-3). The 70S ribosome is composed of two subunits; both the large subunit (50S) and the small subunit (30S) are required for protein synthesis along with additional protein factors, tRNAs and mRNA. The ribosome is composed of multiple protein and RNA components that are assembled to form the protein synthesizing ribozyme. The ribosome contains 3 sites: the aminoacyl-tRNA site (A-site) where aminoacyl-tRNAs are delivered, the peptidyl site (P-site) where the peptide carrying tRNA is positioned and the exit site (E-site) where deacylated tRNAs are positioned for release. The 30S subunit contains the mRNA binding cleft and the catalytic peptidyl transferase center is on the 50S subunit (Fig. 1-3) *(8)*.

The mechanism of protein synthesis is divided into 3 phases: initiation, elongation and termination (Fig. 1-4). During initiation the ribosome loads onto the mRNA, the start codon of the mRNA is located and positioned at the P-site of the ribosome and finally the initiator tRNA (fMet-tRNA$_f^{Met}$) binds to the P-site of the ribosome forming the correct codon/anticodon interaction. Subsequently, during the elongation phase, amino acids are added to a growing peptide chain in response to the mRNA codon sequence. Finally, during termination a stop codon is positioned at the A-site of the ribosome signaling the end of protein synthesis, release of the newly formed peptide and dissociation of the ribosome *(9)*.

Initiation phase of protein synthesis

The current model for initiation of protein synthesis in prokaryotes (Fig. 1-5) begins by dissociation of the 70S ribosome into its 30S and 50S subunits. Initiation factor 3 (IF3)

FIGURE 1-3. X-ray crystal structure of the *T. thermophilus* 70S ribosome and subunits at 5.5Å resolution. *(A)* The crystal structure of the 30S ribosomal subunit viewed from the subunit interface side. The subunit is shown with mRNA (pink) and tRNAs positioned at the A-site (red), P-site (green) and E-site (yellow). The decoding center near the A-site is indicated by an arrow. *(B)* The crystal structure of the 50S subunit viewed from the subunit interface side. The subunit is shown with tRNAs at the 3 sites (colored as in A). The peptidyl transferease center where peptide bonds are formed is circled. *(C)* The crystal structure of the 70S ribosome with the 30S (blue) and 50S (yellow) subunits shown. The 3 tRNA binding sites are visible at the subunit interface. Based on *(31)*.

Fig. 1-3

A) 30S subunit

E
P
A
mRNA
decoding site
30S

B) 50S subunit

L7/L12
L1
peptidyl transferase center

C) 70S ribosome

50S
30S
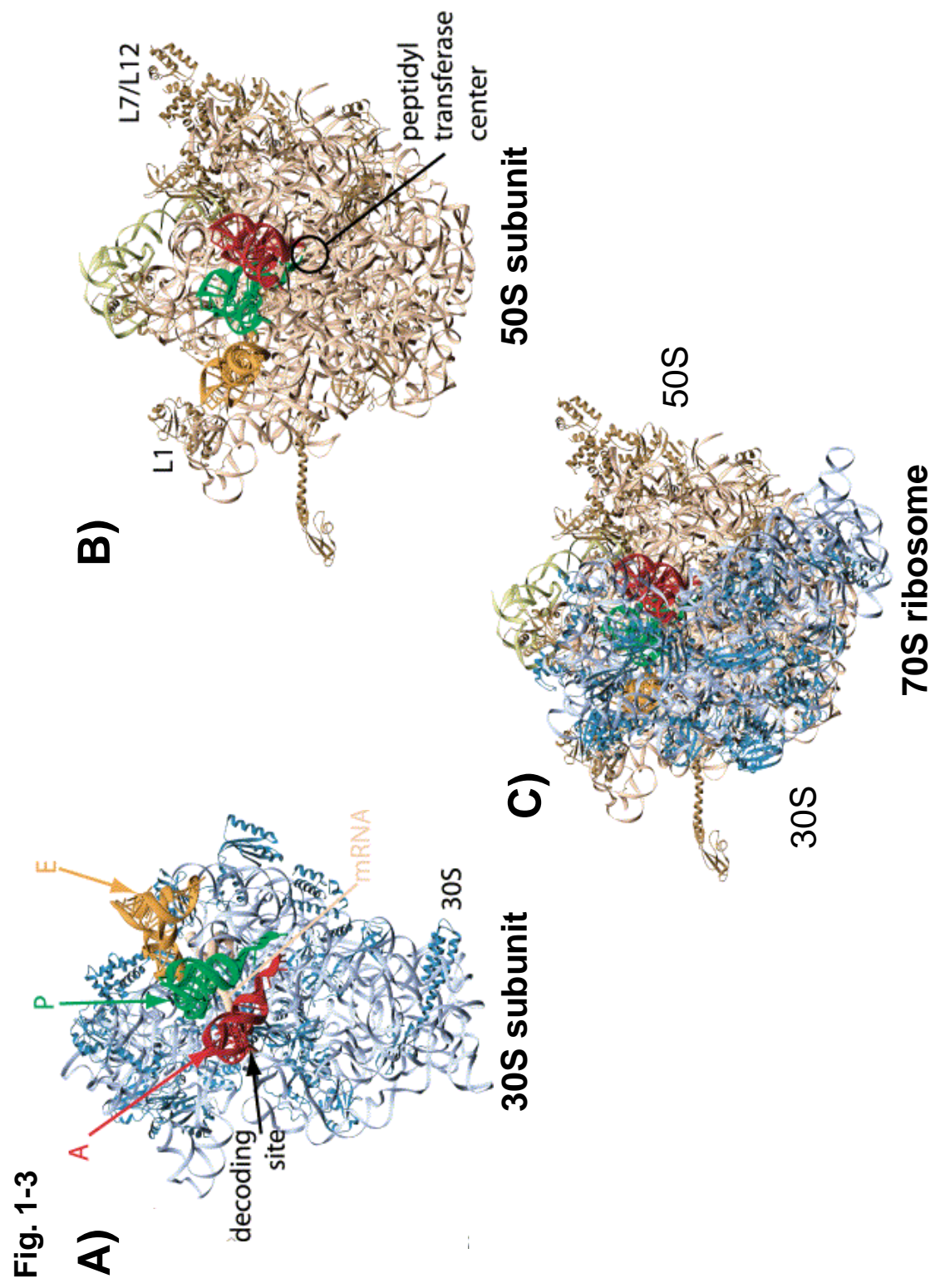
FIGURE 1-4. Cartoon representation of the three phases of protein synthesis: initiation, elongation and termination. During initiation the ribosome (green) must locate the start codon of the mRNA (blue) and form the proper codon:anticodon interaction with the initiator tRNA at the P-site of the ribosome. After initiation the cyclic elongation phase begins. During elongation the ribosome and mRNA move exactly 3 nucleotides relative to one another signaling delivery of a new amino acid, the newly delivered amino acids are incorporated into the nascent peptide chain (pink). When a stop codon is positioned at the A-site then termination occurs and the ribosomal subunits, peptide and mRNA are released.

Fig. 1-4

Initiation

5' —— AUG ———— UGA —— 3'

Met

Ribosome

Elongation

Nascent polypeptide

5' —— AUG ———— UGA —— 3'

Termination

5' —— AUG ———— UGA —— 3'

Protein

50S

30S

12
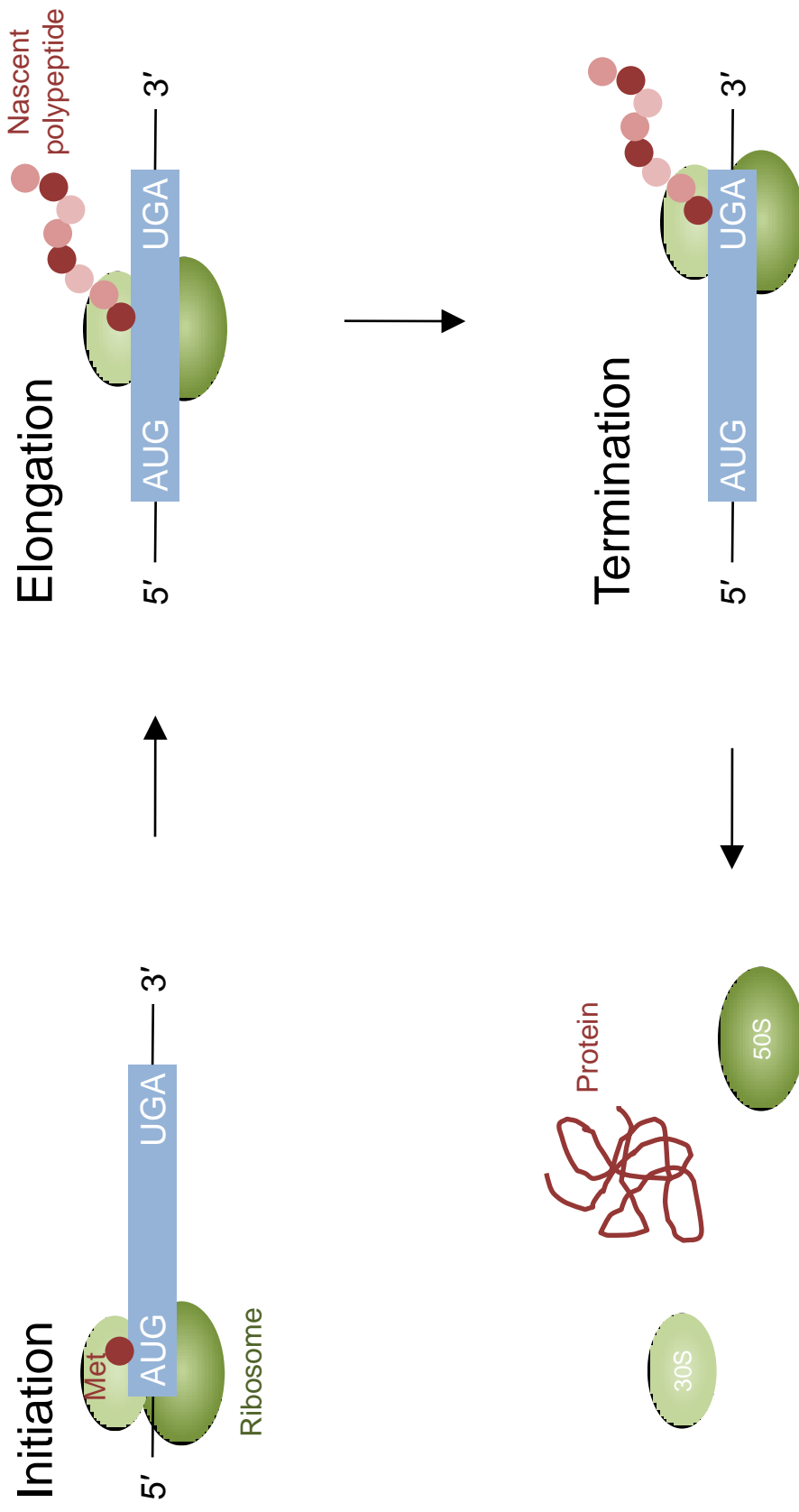
FIGURE 1-5. A model for the initiation phase of protein synthesis in prokaryotes. Initiation

begins with the 70S ribosome in equilibrium with its 50S and 30S subunits. Binding of IF3 to

the 30S subunit shifts the equilibrium toward dissociation of the ribosome. IF1 and IF2 then

bind to the 30S subunit, followed by the initiator fMet-tRNA and the mRNA to form the pre-

initiation complex. The 30S initiation complex is formed when the mRNA is properly

positioned with its start codon at the P-site of the ribosome. The binding of the 50S subunit to

the 30S initiation complex results in release of the initiation factors and formation of the 70S

initiation complex. The 70S initiation complex is prepared for the elongation phase of

protein synthesis.

Fig. 1-5

70S

50S   30S

IF3

30S

IF2:GTP

IF1

AUG

fMet

UAC

30S

fMet

UAC
AUG

30S Initiation
Complex

Proofread

fMet

UAC
AUG

Pre-Initiation
Complex

GDP + Pi

fMet

UAC
AUG

70S Initiation
Complex

14
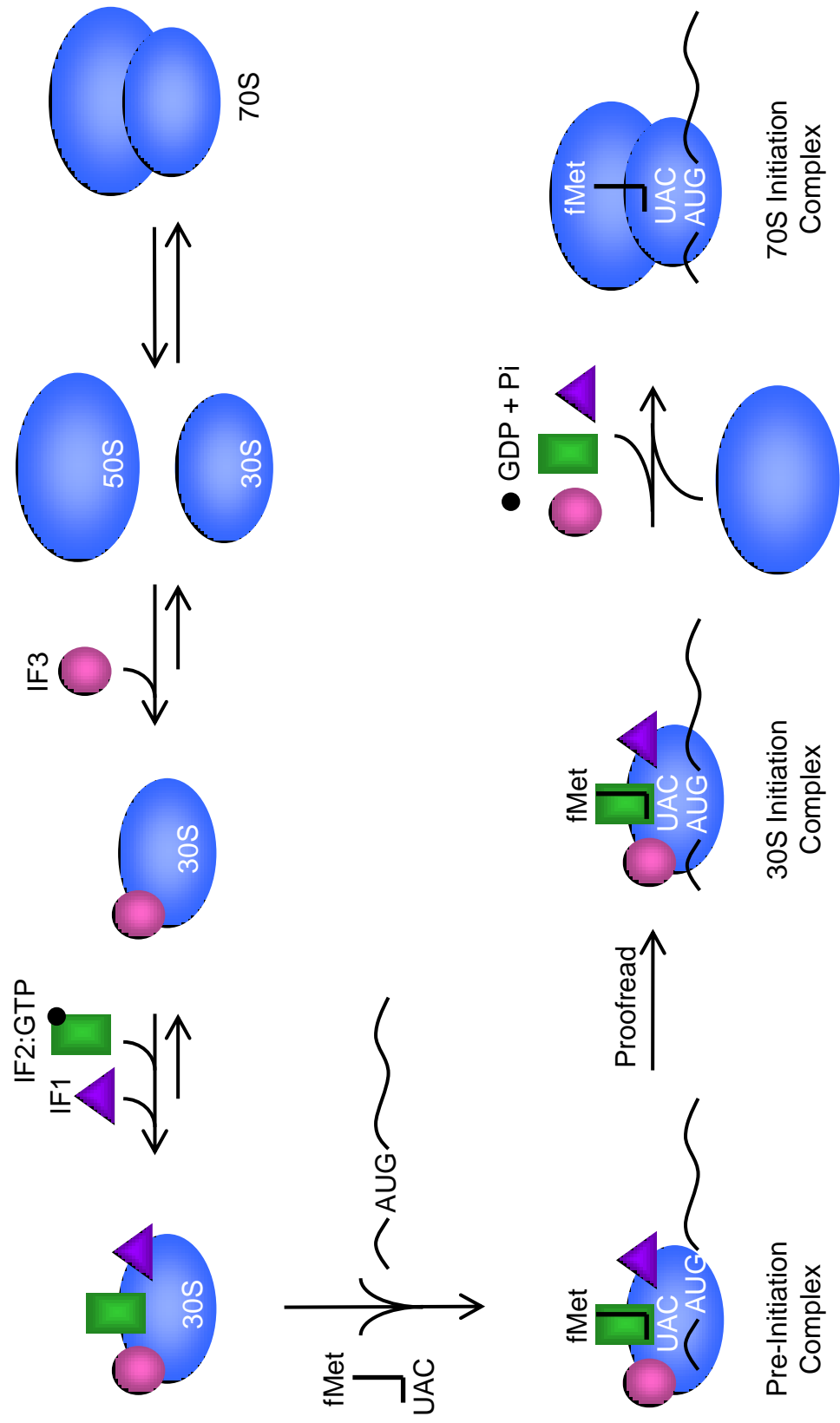
binds to the 30S subunit preventing its re-association with the 50S subunit and initiation

factor 1 (IF1) binds to the 30S:IF3 complex to prevent premature binding of aminoacyl-

tRNAs (aa-tRNAs) *(10)*. Subsequently, initiation factor 2 (IF2) binds to the complex to

stimulate binding of the initiator fMet-tRNA$_f^{Met}$ to the P-site of the ribosome. To facilitate

proper positioning of the complex on the mRNA the initiation factor:30S complex recognizes

and binds to the Shine-Dalgarno sequence to form a pre-initiation complex. A stable

initiation complex is formed when the correct codon:anticodon interaction occurs at the P-

site of the 30S subunit. Once the 30S initiation complex is formed the 50S subunit binds to

the complex triggering release of the initiation factors. The 70S initiation complex is then

poised to enter the elongation phase of protein synthesis.

Elongation phase of protein synthesis

The elongation phase begins with the 70S initiation complex containing the fMet-

tRNA$_f^{Met}$ at the P-site of the ribosome and empty A- and E-sites. The mRNA is positioned

with the AUG start codon forming a codon:anticodon interaction at the P-site of the ribosome

with the second codon positioned at the A-site. An aa-tRNA is delivered to the A-site as a

ternary complex with EF-Tu and GTP. The tRNA delivered depends on the identity of the

codon at the A-site. A cognate codon:anticodon interaction achieved at the A-site of the

ribosome triggers hydrolysis of GTP from the ternary complex and release of EF-Tu:GDP

from the ribosome. The EF-Tu:GDP complex interacts with its guanine nucleotide exchange

factor EF-Ts off the ribosome to re-generate the active EF-Tu:GTP complex that can then

bind an additional aa-tRNA. On the ribosome, the P-site amino acid (formylmethionine) is

transferred to the amino acid of the newly delivered A-site aa-tRNA and a peptide bond is

formed through the action of the peptidyl transferase center on the 50S subunit. This reaction leaves a deacylated tRNA at the P-site and a peptidyl-tRNA at the A-site. The G-protein, elongation factor G (EF-G), then catalyzes the translocation event that places the deacylated tRNA at the E-site, the peptidyl-tRNA at the P-site and moves the ribosome exactly 3 nucleotides relative to the mRNA placing a new codon at the A-site. The cyclic process then proceeds as a new ternary complex is delivered to the A-site (Fig. 1-6) *(9)*.

Termination phase of protein synthesis

Termination occurs when the codon present at the A-site of the ribosome is a stop codon. This triggers binding of either release factor 1 (RF-1) or release factor 2 (RF-2), both tRNA mimics, to the A-site. RF-1 recognizes the stop codons UAG or UAA and RF-2 recognizes UAA or UGA. Release factor 3 (RF-3) then binds to either RF-1 or RF-2 causing the release of either RF-1 or -2 from the A-site and release of the nascent peptide from the P-site. Subsequently, the GTP of RF-3 is hydrolyzed releasing the factor from the ribosome. The binding of the ribosome recycling factor (RRF) and EF-G to the ribosome signals release of the deacylated P-site tRNA and the mRNA from the ribosome *(9)*.

PROTEIN SYNTHESIS IN MITOCHONDRIA

The mechanism of protein synthesis in prokaryotes is used as a foundation for understanding this mechanism in mammalian mitochondria. The similarity between the two mechanisms is largely attributed to the homology between the translation factors involved in protein synthesis and similarities in antibiotic sensitivity *(1)*. Though the basic mechanisms

FIGURE 1-6. A model for the elongation phase of protein synthesis in prokaryotes. Elongation is a cycle which begins with a deacylated tRNA at the E-site of the ribosome ready for release and a peptidyl-tRNA at the P-site. The next aa-tRNA is delivered to the A-site of the ribosome in complex with EF-Tu and GTP and the deacylated-tRNA is released. Once the new aa-tRNA is delivered to the A-site, GTP is hydrolyzed and the EF-Tu:GDP complex is released. A peptide bond is formed between the A-site amino acid and the P-site peptide to form a peptide that is one amino acid longer and is positioned at the A-site. EF-G catalyzes the movement of the ribosome along the mRNA in a GTP dependent manner, once again placing a deacylated-tRNA at the E-site for release and the peptidyl-tRNA at the P-site.

Fig. 1-6

EF-Tu:GTP:aa-tRNA

EF-Tu:GDP

Peptide Bond Formation

EF-G

GDP

GTP
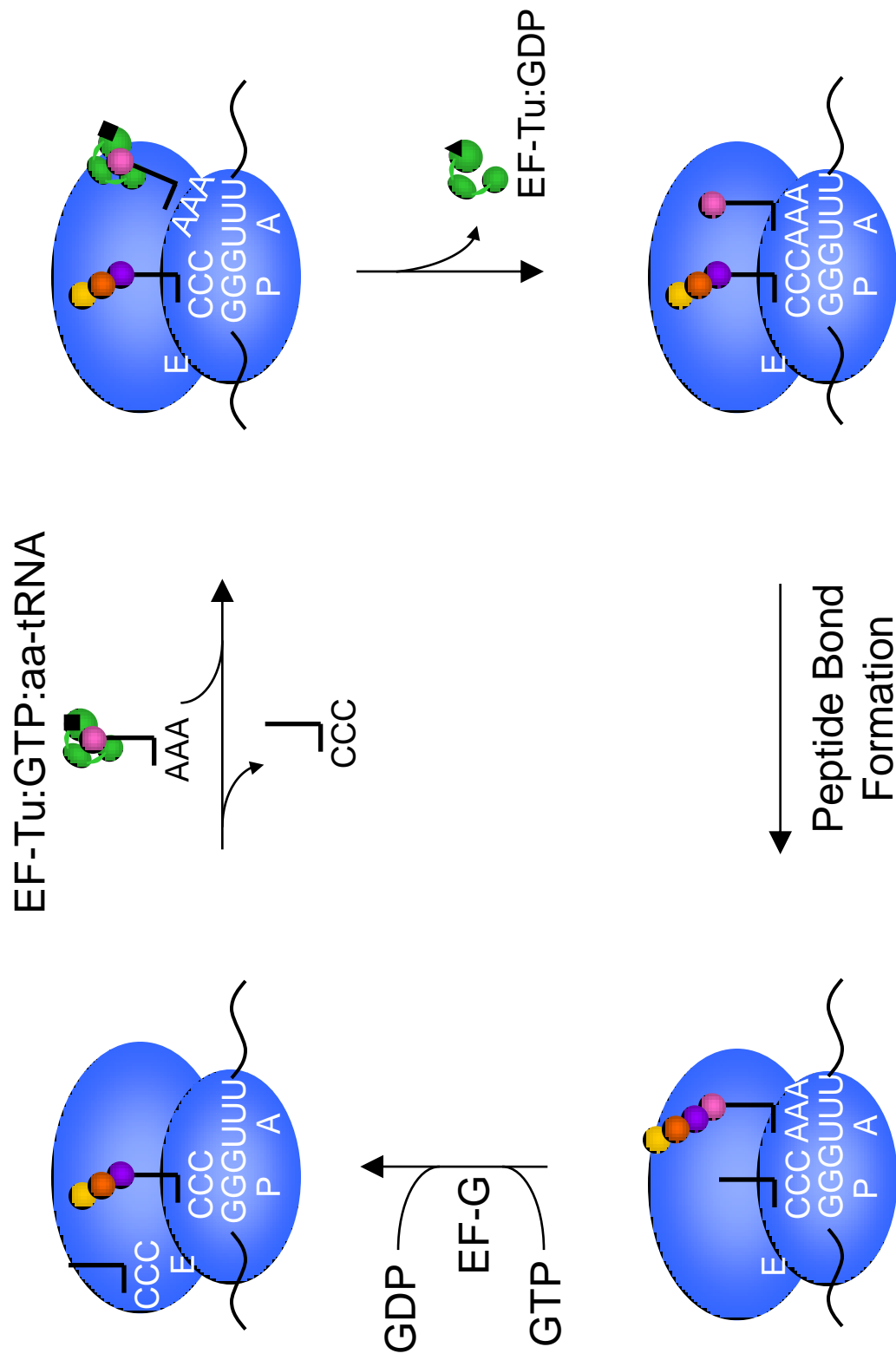
are similar, important differences exist (Table 1-1). In the following paragraphs the two systems will be compared.

Mitochondrial ribosomes

The mitochondrial ribosome is quite different from the ribosomes found in prokaryotes though they share a similar function. The mitochondrial ribosome is composed of 2/3 protein and only 1/3 RNA, while the prokaryotic ribosome is 2/3 RNA and 1/3 protein. The mitochondrial ribosome (2.7 MDa, 55S) has a larger molecular weight than the prokaryotic ribosome (2.3 MDa, 70S), but its smaller sedimentation coefficient suggests the particle is less dense. The mitochondrial ribosome, like the bacterial ribosome, is composed of two subunits. However, the mitochondrial subunits are 28S and 39S, compared to the 30S and 50S subunits of prokaryotes *(11)*.

Mitochondrial mRNAs

In mammalian mitochondria the mRNAs differ in both structure and genetic code from prokaryotic mRNAs. In prokaryotes, the canonical mRNA contains the Shine-Dalgarno (SD) sequence upstream of the start codon, this sequence base pairs with the anti-SD sequence at the 3′ end of the 16S rRNA of the small subunit and is important for placement of the start codon at the P-site of the ribosome for initiation. Mitochondrial mRNAs lack the SD sequence and the anti-SD sequence is missing from the small subunits RNA. Mitochondrial mRNAs are also not capped on the 5′ end like cytoplasmic eukaryotic mRNAs. They are, however, polyadenylated on their 3′ ends like the mRNAs in the cytoplasm of eukaryotes. Interestingly, the genetic code used in mitochondria also differs

Table 1-1. Comparison of the translation systems from prokaryotes and mammalian mitochondria

	Prokaryotes	Mitochondria
mRNAs	Shine-Dalgarno sequence in 5' UTR	No Shine-Dalgarno sequence or 5' cap
Ribosomes	30S & 50S subunits 2/3 RNA	28S & 39S subunits 2/3 protein
Initiator tRNA	formylated	formylated
tRNA^{Met}	Separate initiator, and elongator	One serves as both initiator and elongator
Initiation factors	IF1, IF2, IF3	IF2$_{mt}$ and IF3$_{mt}$

from that found in both prokaryotes and the cytoplasm of eukaryotes. Mammalian

mitochondria use both AUG and AUA as methionine codons, but canonically AUA codes for

isoleucine. Also, UGA has been reassigned as a tryptophan codon instead of a stop codon. In

addition to the canonical UAA and UAG stop codons, mammalian mitochondria also use

AGA and AGG as stop codons instead of as arginine codons.

Mitochondrial initiation factors

Mitochondrial translation factors are homologous to prokaryotic factors and generally

share their function, but significant differences also exist. Mitochondria contain IF2 and IF3

homologs (IF2$_{mt}$ and IF3$_{mt}$), but a homolog of IF1 has not been identified. IF2$_{mt}$ is an ~85

kDa G-protein. Like its prokaryotic homolog the primary function of IF2$_{mt}$ is to promote the

binding of fMet-tRNA$_f^{Met}$ to the small ribosomal subunit during initiation. *E. coli* IF2 is a 6

domain protein *(12)*. IF2$_{mt}$ has domains corresponding to III-VI of the *E. coli* factor *(13)* and

contains a 37 amino acid insertion between domains V and VI (Fig. 1-7). Recent work has

shown that in the presence of IF2$_{mt}$, an *E. coli* IF2 knockout no longer requires IF1,

suggesting that the IF2$_{mt}$ insertion may play the role of IF1 in mitochondria *(14)*.

IF3$_{mt}$ shares only 20-26% identity with prokaryotic IF3. Though only partially

homologous, IF3$_{mt}$ performs many of the same functions as its prokaryotic homologs

including an ability to dissociate ribosomes and to stimulate initiation complex formation

(15). The mitochondrial factor contains extension on both its N- and C-terminal ends (Fig. 1-

8) and the role of these extensions has recently been reported. Derivatives of the protein

lacking the extensions have been shown to have an increased affinity for binding to the 39S

FIGURE 1-7. Domain organization of *E. coli* and mitochondrial IF2. *E. coli* IF2 is a 6

domain G-protein that stabilizes the initiator tRNA at the P-site of the ribosome during

initiation. The homologous mitochondrial IF2 (IF2$_{mt}$) lacks domains I and II and contains an

insertion between domains V and VI that is postulated to functional replace IF1 in

mitochondrial protein synthesis.

Fig. 1-7

E. coli IF2

| I | II | III | G Domain | V | VI |

IF2$_{mt}$

| III | G Domain | V | | VI |

← 37 amino acid insertion
Functional IF1?

23

FIGURE 1-8. Domain organization of *E. coli* and mitochondrial IF3. *E. coli* IF3 contains 2 domains separated by a flexible linker and during initiation dissociates the ribosome into subunits and promotes initiation complex formation. The homologous mitochondrial IF3 (IF3$_{mt}$) contains N- and C-terminal extensions. These extensions prevent IF3$_{mt}$ from detrimental binding to the 39S subunit and allow for IF3$_{mt}$ dissociation upon 39S joining. IF3$_{mt}$ also contains an N-terminal mitochondrial important leader sequence.

Fig. 1-8

E. coli IF3

N-terminal domain — Linker — C-terminal domain

IF3mt

Leader — N-terminal extension — N-terminal domain — Linker — C-terminal domain — C-terminal extension
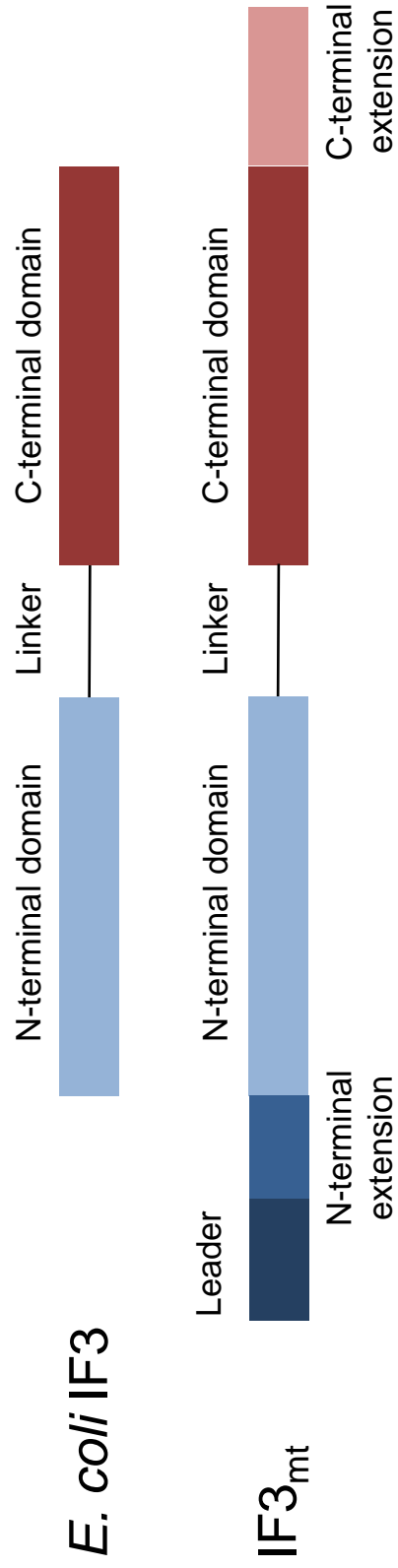
subunit, suggesting that the role of the extensions is to allow proper dissociation of the factor from the ribosome upon 39S joining *(16)*.

Mitochondrial tRNA^{Met}

The initiator tRNA in mammalian mitochondria differs substantially from that found in prokaryotes (Fig. 1-9). In prokaryotes and the cytoplasm of eukaryotes there are separate tRNA^{Met} species that function as either the initiator tRNA or as an elongator tRNA. However, in mammalian mitochondria there is a single tRNA^{Met}. This single tRNA functions in both elongation and is formylated for use in initiation. This single tRNA also decodes both the AUG and AUA codons *(17,18)*. The multiple roles of this tRNA, necessitates that the tRNA be structurally unique from canonical initiator tRNAs. Canonical initiator tRNAs are characterized by a set of structural features which are important for their function. The mammalian mitochondrial tRNA^{Met} contains some of the features characteristic of an initiator tRNA, but some of these features are conspicuously absent, while other interesting features are present.

Most initiator tRNAs, including the mammalian mitochondrial tRNA^{Met}, contain an anticodon stem with a GGG●CCC sequence forming 3 consecutive G:C base pairs. The GC pairs are important for targeting the tRNA to the P-site of the ribosome for use in initiation. This structural element likely affects the structure of the adjacent anticodon loop and may affect the ability of the loop to be accommodated at the P-site of the ribosome. The G:C structural element may also form important interactions with the ribosome itself.

Following the anticodon stem is a 7 nucleotide loop that is conserved from prokaryotes to mitochondria. Interestingly, animal mitochondrial tRNA^{Met} contains an

FIGURE 1-9. Comparison of *E. coli* initiator tRNA and human mitochondrial tRNA$^{\text{Met}}$. *(A)* The *E. coli* initiator tRNA contains the structural elements that characterize prokaryotic initiator tRNAs. These features include the 3 consecutive G●C base pairs (pink) at the base of the anticodon stem, the conserved Pu11●Py24 base pair (orange) in the D-stem and the non-Watson-Crick base pair at the top of the acceptor stem (green). *(B)* The human mitochondrial tRNA$^{\text{Met}}$ (hmtRNA$^{\text{Met}}$) contains some of the elements that characterize prokaryotic initiator tRNAs, but lacks others. HmtRNA$^{\text{Met}}$ contains the 3 consecutive G●C base pairs and the Pu11●Py24 base pair. However, hmtRNA$^{\text{Met}}$ contains a weak A●U base pair at the top of the acceptor stem, more similar to an elongator tRNA. HmtRNA$^{\text{Met}}$ contains features of both an initiator and an elongator tRNA, which is necessary because the tRNA must function in both initiation and elongation.

Fig. 1-9

A

E. coli initiator

B

human mitochondrial

28
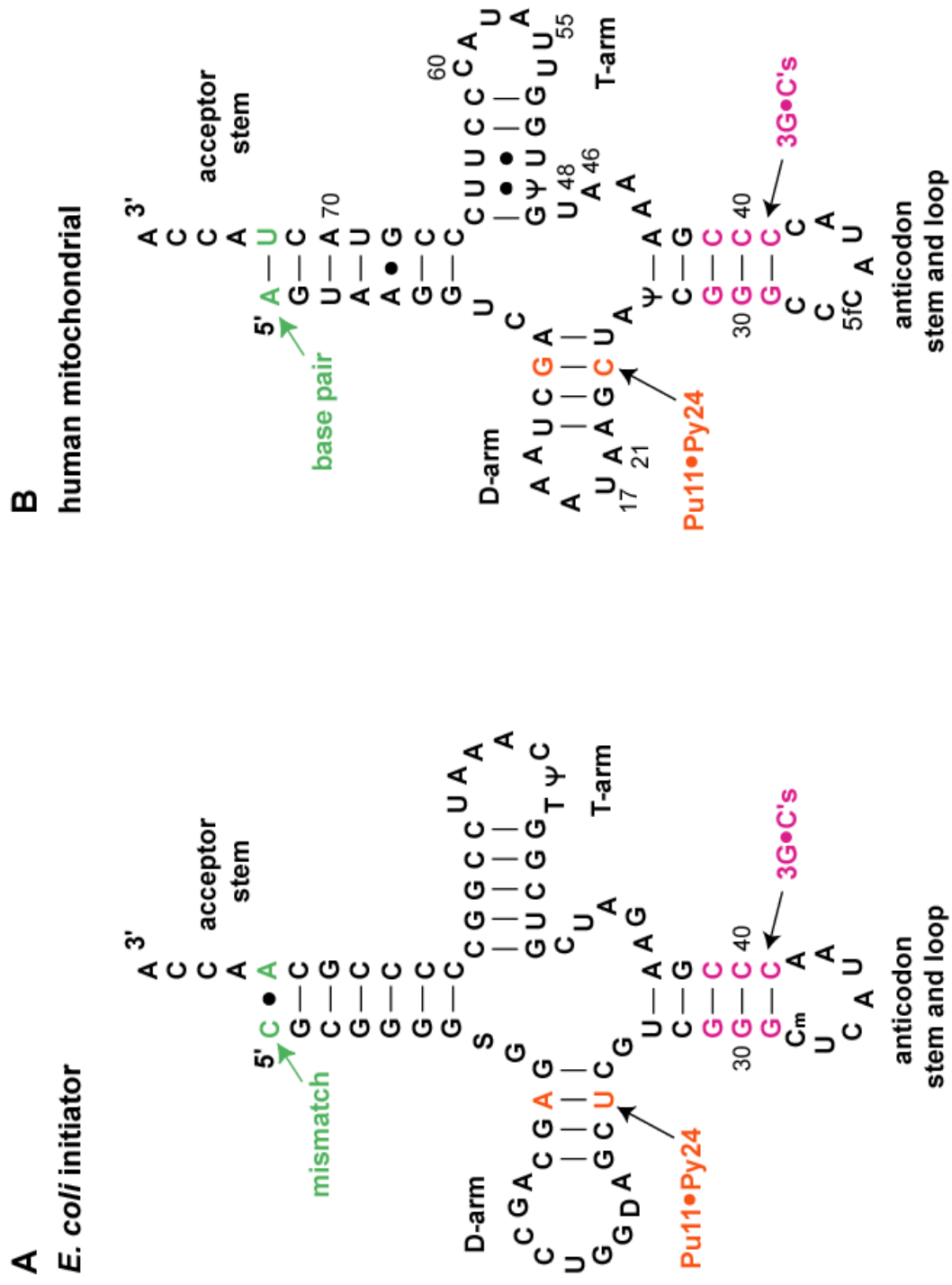
unusual 5-formylcytosine modification at position 34 of the anticodon loop *(17-19)*. We are currently investigating whether this unique modification may be important for allowing the hmtRNA to decode both the AUG and AUA codons.

One of the most important elements distinguishing initiator and elongator tRNAs is the base pair at the top of the acceptor stem. Prokaryotic initiator tRNAs never contain a Watson-Crick base pair at the top of the acceptor stem. This mismatch serves as an anti-determinant, preventing the initiator tRNA from binding to EF-Tu and being used in elongation. The prokaryotic elongator tRNA, however, has a strong G:C base pair at this position. Mutagenesis has shown that a tRNA with a weaker A:U base pair at this position interacts with EF-Tu more weakly than a tRNA with a strong G:C *(20)*. The hmtRNA^{Met}, interestingly, contains the weaker A:U base pair at this position. In this way, the hmtRNA^{Met} resembles a weak elongator tRNA.

In the D-stem of prokaryotic initiator tRNAs a conserved base pair exists between a purine at 11 and a pyrimidine at 24 (Pu11●Py24) and in elongator tRNAs the opposite base pair (Py11●Pu24) exists *(20)*. The importance of this conserved Pu11●Py24 interaction is unknown. It is, however, conserved in the hmtRNA^{Met}. It is possible that this interaction is important for formylation of the tRNA for use in initiation *(20)*.

The dual role of hmtRNA^{Met} in both initiation and elongation requires that the tRNA interact with protein factors involved in both phases of translation (Fig. 1-10). To be used during protein synthesis the tRNA must be aminoacylated by the human mitochondrial methionyl-tRNA synthetase (hmMetRS) to form Met-tRNA^{Met}. The Met-tRNA must then bind to EF-Tu$_{mt}$:GTP to form the ternary complex for delivery to the A-site of the ribosome during elongation. Conversely, Met-tRNA must also be formylated by the human

FIGURE 1-10. The life cycle of human mitochondrial tRNA$^{\text{Met}}$ (hmtRNA$^{\text{Met}}$). HmtRNA$^{\text{Met}}$ is used in both the initiation and elongation phases of protein synthesis in mitochondria. The tRNA must first be aminoacylated by hmMetRS to form Met-tRNA. Once aminoacylated, the Met-tRNA can be formylated by MTF$_{\text{mt}}$ to form fMet-tRNA, which is then delivered to the P-site of the ribosome for use in initiation. Conversely, the Met-tRNA can bind to EF-Tu for delivery to the A-site of the ribosome during elongation.

Fig 1-10

Methionyl-tRNA synthetase (MetRS)

Met

Methionyl-tRNA transformylase (MTF)

fMet

EF-Tu

EF-Tu:GTP:Met-tRNA
to the A site of the ribosome
Elongation

IF2

IF2:fMet-tRNA^Met
to the P site of the ribosome
Initiation

5'

3'

31
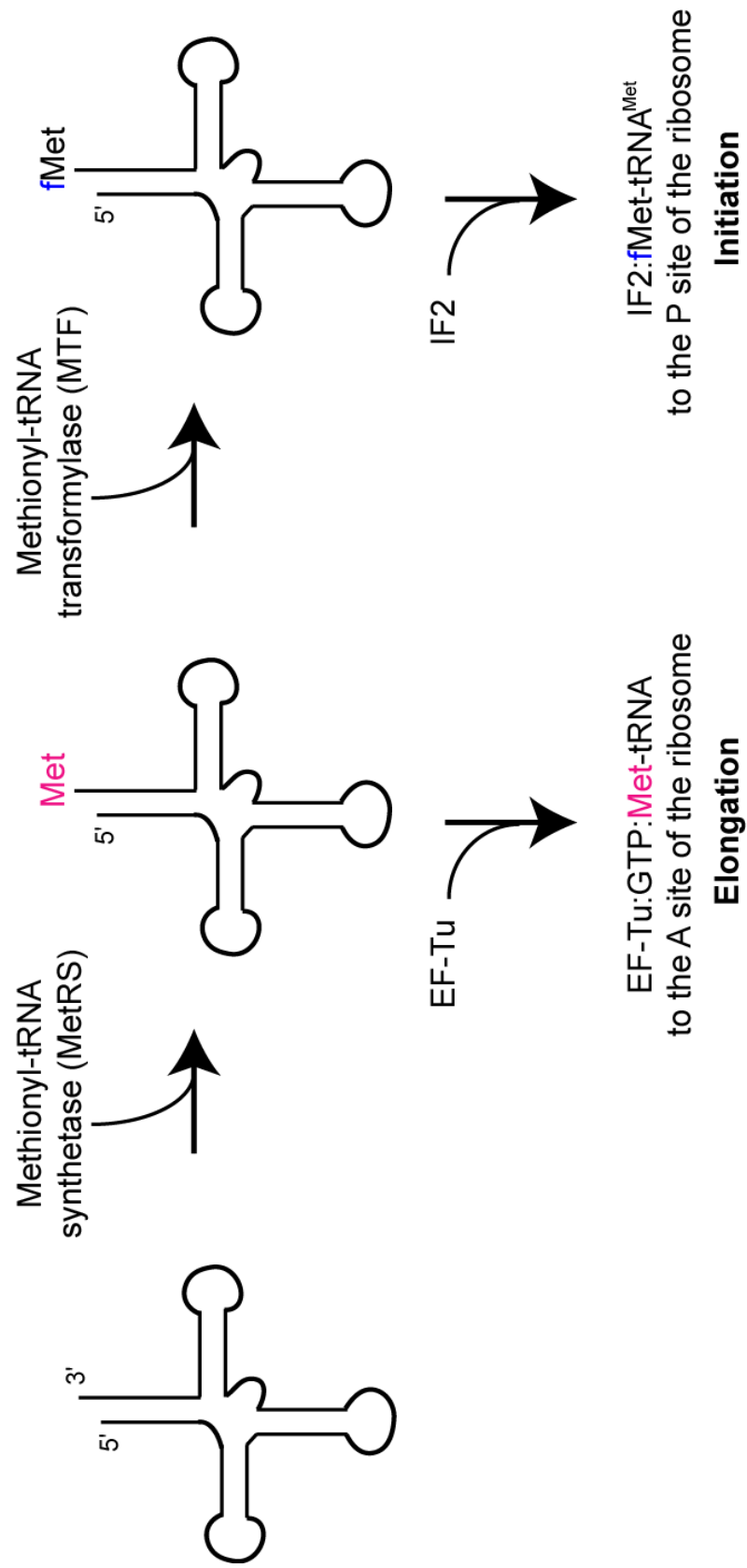
mitochondrial methionyl-tRNA transformylase (hmMTF) to form fMet-tRNA^{Met} for delivery to the P-site of the ribosome during initiation. This complex life cycle of hmtRNA^{Met} is unique to mammalian mitochondria. A more thorough understanding of how the tRNA is partitioned between the initiation and elongation phases of protein synthesis is being pursued.

For hmtRNA^{Met} to be used in either phase of translation it must first be aminoacylated by hmMetRS to form Met-tRNA. HmMetRS is homologous to its prokaryotic counterpart, *E. coli* MetRS, and both enzymes are categorized as Class I synthetases (21). The enzyme functions in a multi step process, in the first step the carboxyl group of methionine is activated by attachment of the amino acid to the α-phosphate of ATP to form the 5′-aminoacyl adenylate. In the second step, the amino acid is transferred to the 2′-OH of the terminal A residue in tRNA^{Met} and AMP is released. During the spontaneous transesterification step the amino acid is transferred from the 2′-OH to the 3′-OH of the terminal residue to form Met-tRNA. Class II synthetases add the amino acid directly to the 3′-OH of the terminal residue, thereby avoiding the transesterification step *(22)*.

MetRS, like other class I synthetases, is characterized by conserved structural elements *(22)*. The catalytic center contains a Rossman fold (pink in Fig. 1-11) with the HIGH signature sequence. The two halves of the Rossman fold are separated by a connectivity peptide (CP, green in Fig. 1-11). In *E. coli* the CP domain contains a Zn^{2+} binding knuckle structure. The Zn^{2+} binding region is absent in hmMetRS *(23)*. Following the Rossman fold is a small domain containing the signature sequence KMSKS (orange in Fig. 1-11). The C-terminal domain (blue in Fig. 1-11) follows and packs against the KMSKS domain *(24)*. An insertion helix in the Rossman domain, along with the CP domain, is thought to be important for positioning the acceptor helix of the tRNA at the catalytic site of

FIGURE 1-11. Crystal structure of *E. coli* MetRS and domain alignment of *E. coli* and

hmMetRS. *(A)* Domain alignment of hmMetRS with *E. coli* MetRS. The enzyme is

composed of 4 domains. The Rossman fold domain (pink) is separated by a connectivity

peptide (green), which in *E. coli* MetRS binds Zn^{2+}. The Rossman domain is followed by the

KMSKS domain (orange) and the C-terminal domain (blue). *E. coli* MetRS contains an

extension on its C-terminus and hmMetRS has an N-terminal signal sequence for import into

mitochondria. *(B)* X-ray crystal structure of *E. coli* MetRS at 2Å resolution (1qqt). The

domains are colored as in (A). The location of the single Zn^{2+} that binds to *E. coli* MetRS is

shown as a black sphere in the connective peptide.

Fig. 1-11
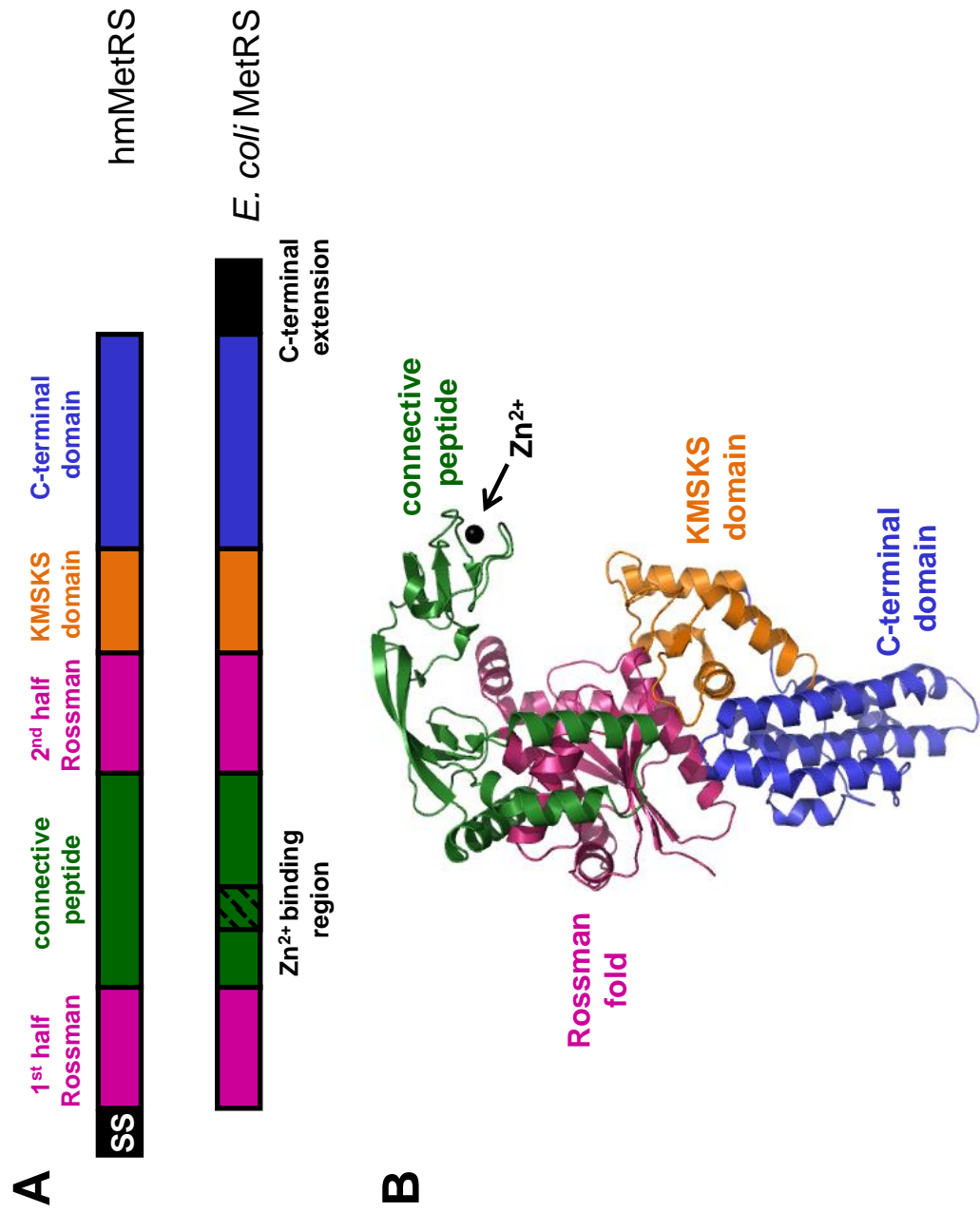
the Rossman domain *(24)*. Methionine binds in a cleft formed between two helices of the Rossman fold *(24)*. Residues in the C-terminal domain serve as either positive or negative determinants for tRNA binding, allowing only tRNAs with the CAU anticodon to bind *(24)*. In this way, MetRS specifically aminoacylates only tRNA^{Met}.

Once aminoacylated, human mitochondrial Met-tRNA^{Met} can either be formylated by MTF$_{mt}$ for use in initiation or bind to EF-Tu for use in elongation. MTF$_{mt}$ catalyzes the transfer of a formyl group from N^{10}-formyltetrahydrofolate to the amino group of methionine to form *N*-formylmethionine *(25,26)*. MTF$_{mt}$ is homologous to *E. coli* MTF which is a two domain protein separated by a linker (Fig. 1-12) *(27)*. The *E. coli* enzyme requires several structural elements in its substrate tRNA: a mismatch at the top of the acceptor stem, a Pu11●Py24 base pair in the D-stem, a G2●C71 base pair in the acceptor stem, A at position 73 and aminoacylation of the tRNA with methionine *(28)*. The *E. coli* initiator tRNA is positioned with its D-stem contacting the C-terminal domain of *E. coli* MetRS and a loop of the enzyme near the active site contacting the acceptor stem. In contrast, MTF$_{mt}$, lacks the active site loop so is not expected to make extensive contact with the acceptor stem of Met-tRNA *(26)*. This is supported by evidence that MTF$_{mt}$ does not require a G2●C71 base pair or a mismatch at the top of the acceptor stem. Interestingly, MTF$_{mt}$ is sensitive to the presence of a Pu11●Py24 base pair in the D-stem, so the interactions of this stem with the enzyme may be similar to those occurring with the *E. coli* enzyme. The major determinate for formylation by MTF$_{mt}$ appears to be the identity of the amino acid (methionine) and secondarily the presence of the Pu11●Py24 base pair *(26)*.

For human mitochondrial Met-tRNA^{Met} to be used during elongation it must be sequestered by EF-Tu$_{mt}$ to prevent formylation. EF-Tu binds GTP and aa-tRNA to form a

FIGURE 1-12. Crystal structure and domain organization of *E. coli* MTF. *(A) E. coli* MTF is composed of an N-terminal domain (blue) and a C-terminal domain (pink) separated by an elongated linker (green). *(B)* X-ray crystal structure of *E. coli* MTF at 2Å resolution (1fmt). The domains are colored as in (A).

Fig. 1-12

A

E. coli MTF

| N-terminal domain | linker | C-terminal domain |

B

N-terminal domain

linker

C-terminal domain
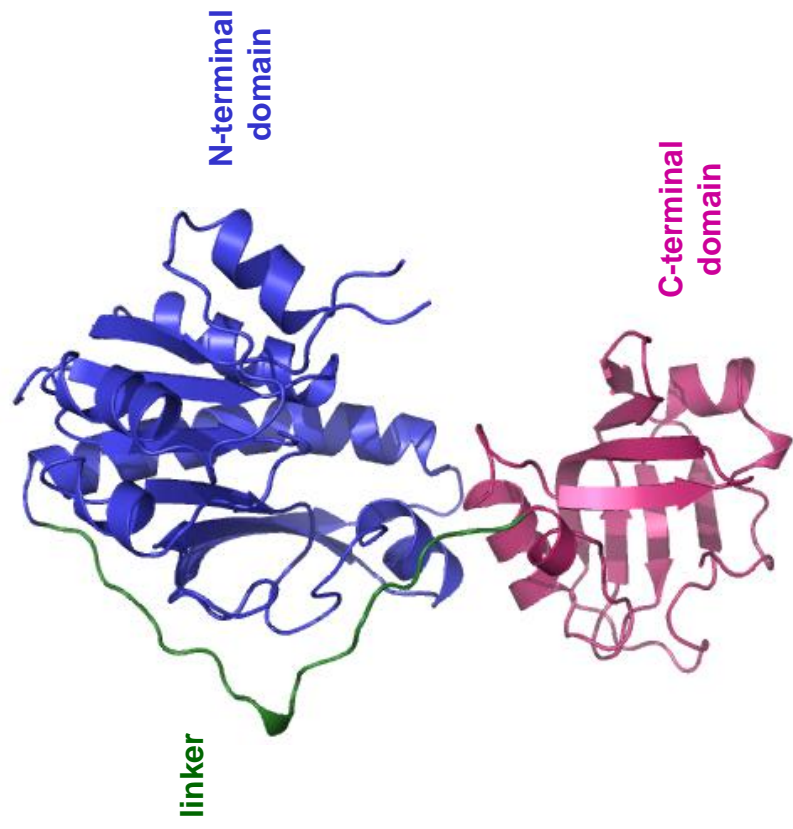
ternary complex (EF-Tu$_{mt}$:GTP:aa-tRNA). The ternary complex delivers the aa-tRNA to the A-site of the ribosome. GTP hydrolysis triggers release of EF-Tu:GDP from the ribosome. Subsequently, EF-Ts$_{mt}$ exchanges GDP for GTP on EF-Tu to form the aa-tRNA binding competent EF-Tu:GTP complex.

EF-Tu$_{mt}$ is a ~46 kDa G-protein composed of 3 domains *(29)* (EF-Tu$_{mt}$:GDP, Fig. 1-13) and is highly homologous to prokaryotic EF-Tu. The N-terminal domain, domain 1, of EF-Tu$_{mt}$ binds GTP/GDP and an associated Mg^{2+}. A crystal structure of the ternary complex formed between *T. aquaticus* EF-Tu, GDPNP and yeast Phe-tRNA shows that the 3′ end of the aa-tRNA binds between domains 2 and 3 of EF-Tu and that the 5′ end of the aa-tRNA contacts all three domains *(30)*. When compared to *T. aquaticus* and *E. coli* EF-Tu, EF-Tu$_{mt}$ contains an extra helical region at its C-terminus. This extra helix is modeled to contact the tRNA. This additional contact may be important for stabilizing the weakly structured mitochondrial tRNAs in the ternary complex *(29)*.

FIGURE 1-13. Crystal structure of bovine EF-Tu$_{mt}$ bound to GDP at 1.94Å resolution (PDB 1d2e). EF-Tu$_{mt}$ is composed of 3 structural domains. The N-terminal domain (domain 1, blue) binds GTP/GDP (orange) with an associated magnesium ion (Mg^{2+}, black). Domain 1 is connected to domain 2 (pink) by a linker (grey). The 3′ end of aa-tRNAs is predicted to bind between domains 2 and 3 (green) and the 5′ end is believed to interact with all 3 domains (aa-tRNA not shown).

GDP

Mg²⁺

Domain 1

linker

Domain 2

Domain 3

Fig. 1-13

40
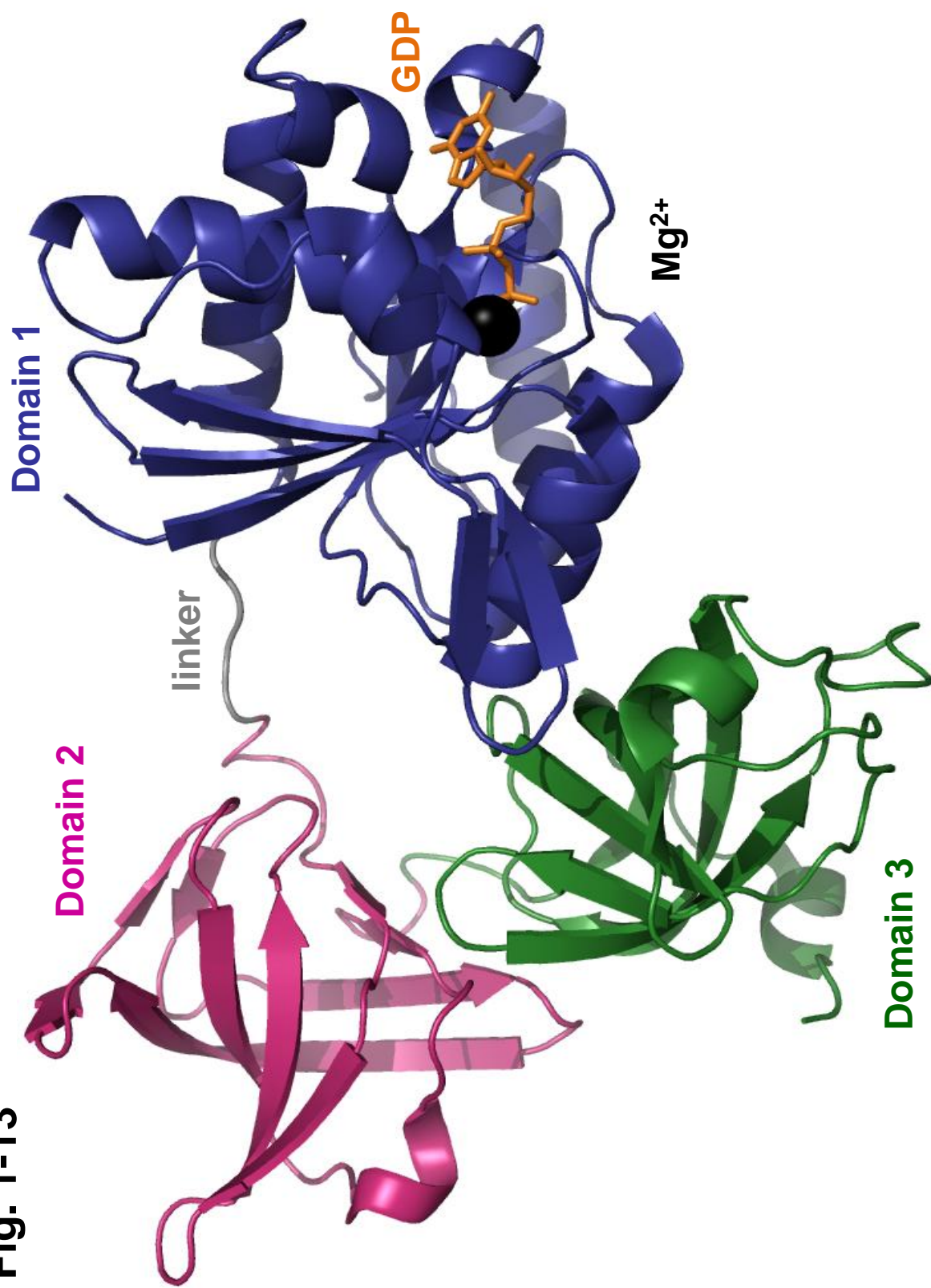
REFERENCES

1. Scheffler, I. (1999) *Mitochondria*. Wiley-Liss, Inc., New York.

2. Ojala, D., Montoya, J. and Attardi, G. (1981) tRNA punctuation model of RNA processing in human mitochondria. *Nature* **290:** 470-474.

3. Gao, L., Laude, K. and Cai, H. (2008) Mitochondrial pathophysiology, reactive oxygen species, and cardiovascular disease. *Vet. Clin. N. Am-Small.* **38**: 137-155.

4. Scaglia, F. and Wong, L.-J. (2008) Human mitochondrial transfer RNAs: Role of pathogenic mutation in disease. *Muscle Nerve.* **37**: 150-170.

5. Taylor, R.W. and Turnbull, D.M. (2005) Mitochondrial DNA mutations in human disease. *Nat. Rev. Genet*. **6**: 389-402.

6. Scheper, G.C., van der Knaap, M.S. and Proud, C.G. (2007) Translation matters: protein synthesis defects in inherited disease. *Nat. Rev. Genet*. **8**: 711-723.

7. Florentz, C., Sohm, B., Tryoen-Toth, P., Putz, J. and Sissler, M. (2003) Human mitochondrial tRNAs in health and disease. *Cell Mol. Life Sci*. **60**: 1356-1375.

8. Green, R. and Noller, H. (1997) Ribosomes and translation. *Ann. Rev. Biochem.* **66**: 679-716.

9. Steitz, T.A. (2008) A structural understanding of the dynamic ribosome machine. *Nat. Rev. Mol. Cell Bio.* **9**: 242-253.

10. Moazed, D., Samaha, R.R., Gualerzi, C. and Noller, H.F. (1995) Specific protection of 16 S rRNA by translational initiation factors. *J. Mol. Biol.* **248**: 207-210.

11. O'Brien, T.W., Denslow, N.D., Anders, J. and Courtney, B. (1990) The translation system of mammalian mitochondria. *Biochim. Biophys. Acta* **1050**: 174-178.

12. Mortensen, K., Kildsgaard, J., Moreno, J.M.P., Steffensen, S., Egebjerg, J. and Sperling-Petersen, H. (1998) A six-domain structural model for *Escherichia coli* translation initiation factor 2. Characterization of twelve surface epitopes. *Biochem. Biophys. Res. Comm.* **46**: 1027-1041.

13. Spencer, A.C. and Spremulli, L.L. (2004) Interaction of mitochondrial initiation factor 2 with mitochondrial (f)Met-tRNA. *Nucleic Acids Res.* **32**: 5464-5470.

14. Gaur, R., Grasso, D., Datta, P.P., Krishna, P.D.V., Das, G., Spencer, A., Agrawal, R.K., Spremulli, L. and Varshney, U. (2008) A single mammalian mitochondrial translation initiation factor functionally replaces two bacterial factors. *Mol. Cell* **29**: 180-190.

15. Koc, E.C. and Spremulli, L.L. (2002) Identification of mammalian mitochondrial translational initiation factor 3 and examination of its role in initiation complex formation with natural mRNAs. *J. Biol. Chem.* **277**: 35541-35549.

16. Haque, M.E., Grasso, D. and Spremulli, L.L. (2008) The interaction of mammalian mitochondrial translational initiation factor 3 with ribosomes: evolution of terminal extensions in IF3mt. *Nucleic Acids Res.* **36**: 589-597.

17. Takemoto, C., Koike, T., Yokogawa, T., Benkowski, L., Spremulli, L.L., Ueda, T., Nishikawa, K. and Watanabe, K. (1995) The ability of bovine mitochondrial transfer RNA[Met] to decode AUG and AUA codons. *Biochimie* **77**: 104-108.

18. Takemoto, C., Ueda, T., Miura, K. and Watanabe, K. (1999) Nucleotide sequences of animal mitochondrial tRNAs[Met] possibly recognizing both AUG and AUA codons. *Nuc. Acids Symp. Ser.* **42**: 77-78.

19. Tomita, K., Ueda, T. and Watanabe, K. (1997) 5-formylcytidine (f5C) found at the wobble position of the anticodon of squid mitochondrial tRNA(Met)CAU. *Nuc. Acids Symp. Ser.* **37**: 197-198.

20. RajBhandary, U. and Chow, C. (1995) Initiator tRNAs and initiation of protein synthesis. U. RajBhandary and D. Soll, eds. *tRNA: Structure, biosynthesis and function*. (Washington, D.C.: ASM Press), pp. 511-528.

21. Deniziak, M.A. and Barciszewski, J. (2001) Methionyl-tRNA synthetase. *Acta Biochim. Pol.* **48**: 337-350.

22. Meinnel, T., Mechulam, Y. and Blanquet, S. (1995) Aminoacyl-tRNA synthetases: Occurance, structure and function. U. RajBhandary and D. Soll, eds. *tRNA: Structure, biosynthesis and function*. (Washington, D.C.: ASM Press), pp. 251-292.

23. Spencer, A.C., Heck, A.H., Takeuchi, N., Watanabe, K. and Spremulli, L.L. (2004) Characterization of the human mitochondrial methionyl-tRNA synthetase. *Biochem.* **43**: 9743-9754.

24. Mechulam, Y., Schmitt, E., Maveyraud, L., Zelwer, C., Nureki, O., Yokoyama, S., Konno, M. and Blanquet, S. (1999) Crystal structure of *Escherichia coli* methionyl-tRNA synthetase highlights species-specific features. *J. Mol. Biol.* **294**: 1287-1297.

25. Takeuchi, N., Kawakami, M., Omori, A., Ueda, T., Spremulli, L.L. and Watanabe, K. (1998) Mammalian mitochondrial methionyl-tRNA transformylase from bovine liver: Purification, characterization and gene structure. *J. Biol. Chem.* **273**: 15085-15090.

26. Takeuchi, N., Vial, L., Panvert, M., Schmitt, E., Watanabe, K., Mechulam, Y. and Blanquet, S. (2001) Recognition of tRNAs by methionyl-tRNA transformylase from mammalian mitochondria. *J. Biol. Chem.* **276**: 20064-20068.

27. Schmitt, E., Blanquet, S. and Mechulam, Y. (1996) Structure of crystalline *Escherichia coli* methionyl-tRNA$_f^{Met}$ formyltransferase: comparison with glycinamide ribonucleotide formyltransferase. *EMBO J.* **15**: 4749-4758.

28. Lee, C., Seong, B. and RajBhandary, U. (1991) Structural and sequence elements important for recognition of *E. coli* formylmethionine tRNA by methionyl-tRNA transformylase are clustered in the acceptor stem. *J. Biol. Chem.* **266**: 18012-18017.

29. Andersen, G., Thirup, S., Spremulli, L.L. and Nyborg, J. (2000) High resolution crystal structure of bovine mitochondrial EF-Tu in complex with GDP. *J. Mol. Biol.* **297**: 421-436.

30. Nissen, P., Kjeldgaard, M., Thirup, S., Polekhina, G., Reshetnikova, L., Clark, B. and Nyborg, J. (1995) Crystal structure of the ternary complex of Phe-tRNA^{Phe}, EF-Tu and a GTP analog. *Science* **270**: 1464-1472.

31. Ramakrishnan,V. (2002) Ribosome structure and the mechanism of translation. *Cell* **108**: 557-572.

CHAPTER II

LACK OF SECONDARY STRUCTURE CHARACTERIZES THE 5′ ENDS OF

MAMMALIAN MITOCHONDRIAL mRNAs

INTRODUCTION

Mammalian mitochondria contain a double stranded genome of approximately 16 kilobase pairs (*1,2*). Encoded within the genome are 13 membrane proteins that function in the electron transfer chain or are components of the ATP synthase complex. The 13 mitochondrially encoded proteins are translated from 9 monocistronic and 2 dicistronic mRNAs. Both dicistronic mRNAs contain overlapping reading frames (*1,2*) (Fig. 2-1A). With the exception of the two internal start sites found in the dicistronic mRNAs, the remaining 11 start sites are located at or near the 5′ end of each mRNA *(3)*. These mRNAs therefore have no 5′ untranslated region and are leaderless. These leaderless mRNAs are translated by the specialized protein biosynthetic system found in mitochondria. The start codon at the 5′ end can be either AUG or AUA, both of which encode methionine in mammalian mitochondria. These codons direct the insertion of formylmethionine during initiation and methionine during chain elongation. In bovine mitochondria, AUG serves as the start codon for 10 genes while AUA is used for the remaining three genes.

An early and fundamental step in protein synthesis is recognition of the start codon in the mRNA by the ribosomal small subunit. This process is achieved by different, well established, mechanisms in prokaryotes and for nuclear encoded genes in eukaryotes. In prokaryotes, most mRNAs have an untranslated region upstream of the start codon that contains the Shine/Dalgarno (SD) sequence. This sequence base pairs with the anti-Shine/Dalgarno sequence in the 16S rRNA of the 30S subunit and positions the mRNA start codon at the P-site of the ribosome (*4,5*). In addition to the simple presence of the SD sequence, the physical accessibility of the SD sequence and its associated start codon is a

major determinant for translational initiation in prokaryotes (*6,7*). The underlying secondary structure of the mRNA can function to prevent initiation at incorrect methionine codons and to facilitate the recognition of the correct initiation codon (*6,7*). Translational initiation in eukaryotes functions by a different mechanism. Eukaryotic mRNAs contain a co‑transcriptionally added 7-methylguanosine triphosphate cap at their 5′ ends and are post-transcriptionally polyadenylated at their 3′ ends *(8)*. Eukaryotic initiation factors bind the 5′ cap and 3′ poly(A) tail and provide a platform for binding by the small 40S ribosomal subunit *(9)*. Once bound, the small subunit scans the mRNA in the 5′ to 3′ direction to locate the start codon.

In contrast to these well developed models, the mechanism by which the translational start codon is recognized in mammalian mitochondria is unknown. Mammalian mitochondrial mRNAs do not have a SD sequence upstream of the start codon nor does the small subunit (28S) ribosomal RNA (12S rRNA) contain an anti-SD sequence *(1)*. These mRNAs also lack a 5′ cap and thus resemble the rare leaderless mRNAs found in prokaryotes. Leaderless mRNAs in prokaryotes may actually be initiated on 70S ribosomes rather than on the 30S subunit (*10,11*).

The fact that mitochondrial mRNAs are leaderless raises the question of whether information exists at or near the 5′ ends of these RNAs that enables them to be efficiently recognized by the mitochondrial translational machinery. No *in vitro* translational system that might allow a direct test of this question has been established for mammalian mitochondria, nor have any additional protein factors that function in start site selection been identified. It is, therefore, possible that the structure of the mRNA alone guides the ribosome to the proper start codon. This guiding or recognition function could be achieved by a conserved structural

element detected by the ribosome. Alternatively, it could be based on the unique accessibility of the start codon at the 5′ end of the mRNA. To begin to address these models, we have analyzed the secondary structure at the 5′ ends of all 13 protein coding regions in the bovine mitochondrial transcriptome at single nucleotide resolution using RNA SHAPE chemistry. Secondary structure predictions based on thermodynamic free energy minimization calculations indicate that the 5′ ends of many mitochondrial mRNAs can, in principle, form short stable secondary structures. In contrast to predictions based on free energy parameters alone, when experimental SHAPE information is used to constrain secondary structure predictions, we find that the 5′ ends of bovine mitochondrial mRNAs show a strong propensity to be highly unstructured. Our analysis indicates that the start codon tends to lie in a single-stranded region or in a very weak duplex stem. These data support a model in which translational initiation in mitochondria is not guided by a conserved secondary structural element but, instead, suggest that the mitochondrial ribosome recognizes structurally accessible and single stranded start codons.

FIGURE 2-1. The mitochondrial genome and strategy for analyzing the 5′ ends of mitochondrial mRNAs. *(A)* The mammalian mitochondrial genome encodes 13 proteins, each of which are subunits of the oxidative phosphorylation machinery. Protein coding genes and the 2 overlapping dicistronic mRNAs are shown explicitly. The protein encoding genes are generally separated by one or more tRNA genes (white); noncoding rRNA genes are green. *(B)* Messenger RNA fragments used for SHAPE analysis. The 5′ and 3′ extensions facilitate structural analysis of the 5′ end of the mRNA sequence and provide an efficient reverse transcriptase primer binding site, respectively.

Fig. 2-1

A

B

12s
rRNA

Control
Region

Cytb

16s
rRNA

ND6

ND5

ND1

ND4L/4
overlap

ATP8/6
overlap

ND4

ND2

ND4L

COI

ND3

COIII

COII

ATP6

ATP8

primer
binding site

5' extension

5' ends of
mitochondrial mRNAs

3' extension

49
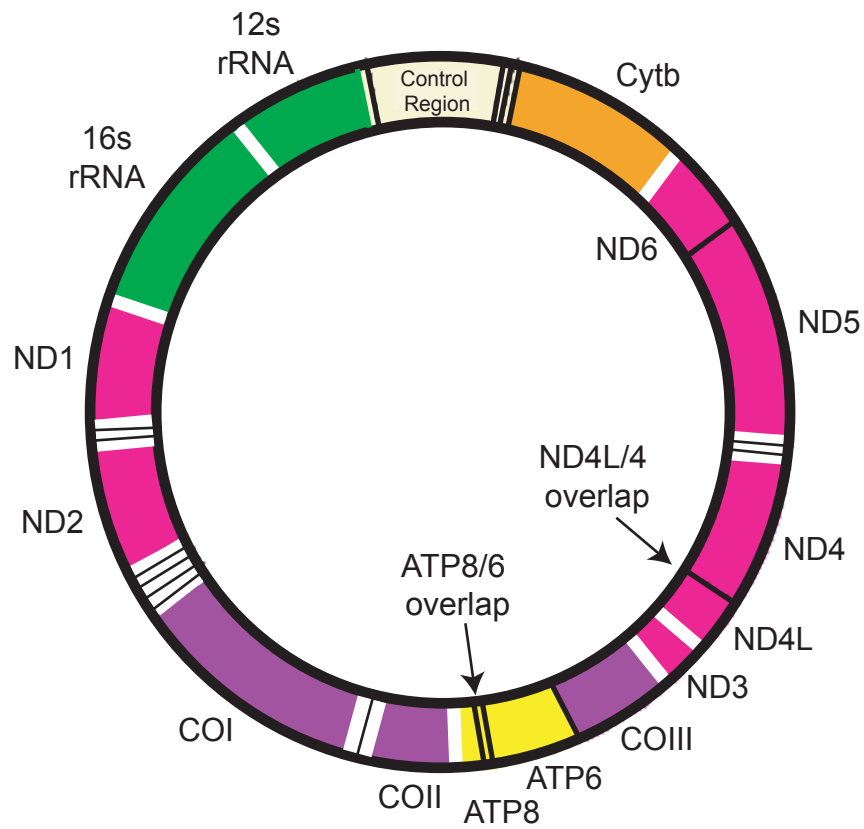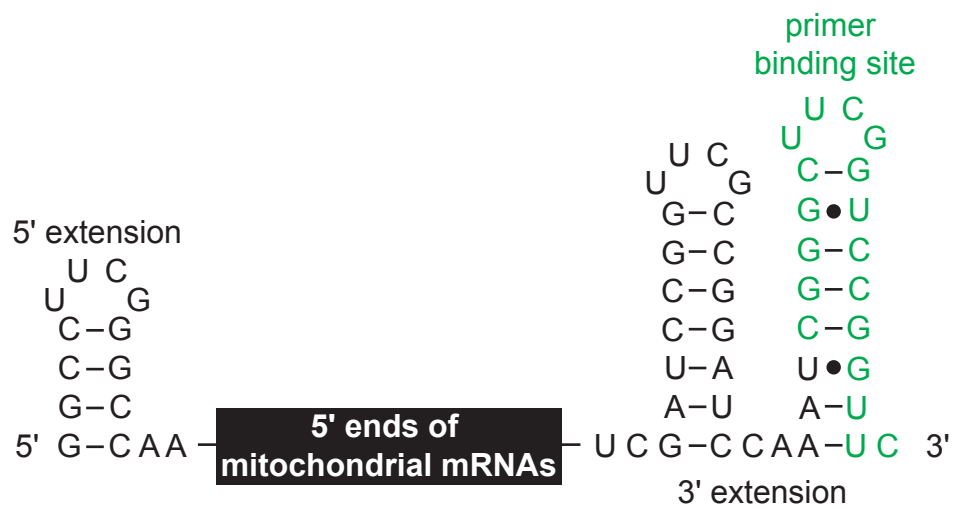
MATERIALS AND METHODS

Plasmids: The plasmids p11-1 and p11-5 *(12)*, containing the bovine mitochondrial genome, were kindly provided by Dr. Philip Laipis (University of Florida). The plasmid pTZ19R-CoII containing the bovine mitochondrial cytochrome oxidase subunit II gene was prepared as described *(13)*.

RNA synthesis: DNA transcription templates containing the 5′ portion of each mRNA, flanked on either side by a stably folding structural cassette *(14)* were prepared by PCR. Reactions (100 μL) contained 10 mM KCl, 10 mM $(NH_4)_2SO_4$, 20 mM Tris-HCl (pH 8.8), 2 mM $MgSO_4$, 0.1% Triton X-100, 250 μM each dNTP, 1 μM each forward and reverse primer, 15-30 ng linearized pTZ19R-CoII or 150-1,200 ng of linearized p11-1 or p11-5 plasmid DNA and 0.02 units/μL of Vent DNA polymerase (NEB) and were subjected to 33 cycles (denaturation at 95 ºC for 45 s; annealing 50-65 ºC for 30 s; elongation 72 ºC for 90 s). The specific primers (Table 2-1 and 2-2) and reaction conditions (Table 2-3) used to amplify each DNA are shown. The PCR product was recovered by ethanol precipitation and resuspended in 100 μL water. Transcription reactions (300 μL, 37 °C, 4-5 h) contained 40 mM Tris-HCl, pH 7.6, 20 mM $MgCl_2$, 2 mM spermidine, 10 mM dithiothreitol (DTT), 0.1 mg/mL bovine serum albumin, 0.2 U/μL SUPERase•In RNase inhibitor, 4 mM each NTP, 100 μL PCR-generated template, and a saturating amount of T7 RNA polymerase. The RNA product was precipitated with ethanol and resuspended in 100 μL water. The RNA was purified by denaturing (8%) polyacrylamide gel electrophoresis (29:1 acrylamide:bisacrylamide prepared with 7 M urea, 90 mM Tris-borate, 2 mM EDTA),

visualized by UV shadowing, excised from the gel, recovered by passive elution in water and ethanol precipitation, and resuspended in 100 µL water.

SHAPE Analysis: RNA (4 pmol) in 24 µL water was heated at 95 °C for 2 min and then cooled on ice for 2 min. The RNA was treated with 12 µL folding buffer (333 mM HEPES-KOH, pH 8, 20 mM MgCl$_2$, 333 mM NaCl) and incubated at 37 °C for 20 min. To 9 µL (1 pmol) of the folded RNA, 1 µL of 130 mM N-methylisatoic anhydride (NMIA, Molecular Probes) in anhydrous dimethyl sulfoxide (DMSO) or 1 µL of anhydrous DMSO alone (control) was added and allowed to react at 37 °C for 45 min *(15)*. The remaining 18 µL of folded RNA was divided into 2 aliquots (1 pmol RNA/tube) and stored on ice for sequencing.

Primer Extension: To the NMIA treated, DMSO control, or untreated RNA (1 pmol), 3 µL of a 0.3 µM 5′-[^{32}P] radiolabelled oligonucleotide (5′-^{32}P-GAACC GGACC GAAGC CCG or 5′-^{32}P-GCGTG TGGTC ATGAA AGTG, obtained from the Nucleic Acids Core Facility at UNC) was added and the samples were incubated at 65 °C for 5 min and then at 35 °C for 20 min for primer annealing. To each reaction, 6 µL of reverse transcription buffer (250 mM KCl, 167 mM Tris-HCl, pH 8.3, 17 mM DTT and 0.42 mM each dNTP) was added. For sequencing reactions using the untreated RNA, 2.5 µL of either 5 mM ddCTP or ddTTP were also added. After heating to 52 °C, 1 µL (200 Units) reverse transcriptase (Superscript III, InVitrogen) was added and the primer extension reaction was performed at 52 °C for 3 min. Reactions were quenched with 1 µL of 4 M NaOH and heated at 95 °C for 5 min. For gel analysis, 29 µL of a gel loading solution (40 mM Tris-borate, 5 mM EDTA, 276

mM unbuffered Tris-HCl, 0.01% (w/v) bromophenol blue and xylene cyanol and 73% (v/v) formamide) was added and the samples were heated at 95 °C for an additional 5 min *(15)*.

Analysis: cDNA products from the (+) and (-) NMIA and sequencing reactions were separated by denaturing gel electrophoresis (10% polyacrylamide). Gels (21 cm x 40 cm x 0.4 mm) were subjected to electrophoresis at 1400 V for 1.5 or 4 h. Bands were quantified by phosphorimaging (Molecular Dynamics). Band intensities in the (+) and (−) NMIA lanes were quantified using SAFA *(16)* and corrected for signal drop-off *(17)*. Normalized SHAPE reactivities were calculated by subtracting intensities from the (-) NMIA control from the (+) NMIA reaction and divided by the average reactivity of the 8% most reactive positions. These reactivity values were then used as quasi-energetic constraints to constrain a thermodynamic folding algorithm, as implemented in RNAstructure *(18)*; K.E. Deigan, T.W. Li, D.H. Mathews and K.M. Weeks, unpublished). Stabilities for individual helices, as reported in Figs. 2-2C through 2-14C, were calculated without adding SHAPE reactivities.

Table 2-1. PCR primers used to amplify mRNA gene regions of interest

mRNA	PCR Primers
COI	Forward 5' TAA TAC GAC TCA CTA TAG GCC TTC GGG CCA A ATG TTC ATT AAC CGC TGA C
	Reverse 5' GAA CCG GAC CGA AGC CCG ATT TGG ATC CGG CGA ACC GGA TCG AAA TAG TAG ATA AAG GGT ACC
COII fragment with 5' extension	Forward 5' TAA TAC GAC TCA CTA TAG GCC TTC GGG CCA AAT GGC ATA TCC CAT ACA AC
	Reverse 5' GAA CCG GAC CGA AGC CCG ATT TGG ATC CGG CGA ACC GGA TCG AGC GTG TGG TCA TGA AAG TG
COII full length with 5' extension	Forward 5' TAA TAC GAC TCA CTA TAG GCC TTC GGG CCA AAT GGC ATA TCC CAT ACA AC
	Reverse 5' TTA TAA TAT TGA CGC AGA TC
COIII with 5' extension	Forward 5' TAA TAC GAC TCA CTA TAG GCC TTC GGG CCA AAT GAC ACA CCA AAC TC
	Reverse 5' GAA CCG GAC CGA AGC CCG ATT TGG ATC CGG CGA ACC GGA TCG ACC TGT AAG AGG TCA AGG GC
COIII no 5' extension	Forward 5' TAA TAC GAC TCA CTA TAG ATG ACA CAC CAA ACT C
	Reverse 5' GAA CCG GAC CGA AGC CCG ATT TGG ATC CGG CGA ACC GGA TCG ACC TGT AAG AGG TCA AGG GC
Cyt B	Forward 5' TAA TAC GAC TCA CTA TAG GCC TTC GGG CCA AAT GAC TAA CAT TCG AAA GTC CC
	Reverse 5' GAA CCG GAC CGA AGC CCG ATT TGG ATC CGG CGA ACC GGA TCG AGG GGC TGG AAG GTC G
ATPase8	Forward 5' TAA TAC GAC TCA CTA TAG GCC TTC GGG CCA AAT GCC GCA ACT AGA CAC GTC
	Reverse 5' GAA CCG GAC CGA AGC CCG ATT TGG ATC CGG CGA ACC GGA TCG AGA TGA TAA AAA GGG TCA AG
ATPase6	Forward 5' TAA TAC GAC TCA CTA TAG GCC TTC GGG CCA ACC AGA ACT GAC ACC AAC
	Reverse 5' GAA CCG GAC CGA AGC CCG ATT TGG ATC CGG CGA ACC GGA TCG AGG GTT ACG AGA GGG AGA CC

Table 2-2. PCR primers used to amplify mRNA gene regions of interest

mRNA	PCR Primers
ND1	Forward 5' TAA TAC GAC TCA CTA TAG GCC TTC GGG CCA AAT GTT CAT AAT TAA CAT C
	Reverse 5' GAA CCG GAC CGA AGC CCG ATT TGG ATC CGG CGA ACC GGA TCG ACC ACT AAC GTA AGG AAT GC
ND2	Forward 5' TAA TAC GAC TCA CTA TAG GCC TTC GGG CCA A ATA AAC CCA ATT ATC TTT ATT ATT AT
	Reverse 5' GAA CCG GAC CGA AGC CCG ATT TGG ATC CGG CGA ACC GGA TCG ACA GTG AGA ACT GAT TAT GAC
ND3	Forward 5' TAA TAC GAC TCA CTA TAG GCC TTC GGG CCA AAT AAA TTT AAT ACT AGC CCT CC
	Reverse 5' GAA CCG GAC CGA AGC CCG ATT TGG ATC CGG CGA ACC GGA TCG AGG GGA AGT CAG AAT GCG ATG
ND4L	Forward 5' TAA TAC GAC TCA CTA TAG ATG TCT ATA GTA TAC ATA AAC
	Reverse 5' GAA CCG GAC CGA AGC CCG ATT TGG ATC CGG CGA ACC GGA TCG AGT AGT CCT ACA AGA G
ND4	Forward 5' TAA TAC GAC TCA CTA TAG GCC TTC GGG CCA ACA TAT GGT ACT GAT TAT GTA C
	Reverse 5' GAA CCG GAC CGA AGC CCG ATT TGG ATC CGG CGA ACC GGA TCG ACC AGG TTA GGG GTA TAA G
ND5	Forward 5' TAA TAC GAC TCA CTA TAG GCC TTC GGG CCA AAT AAA CAT ATT CTC CTC ACT C
	Reverse 5' GAA CCG GAC CGA AGC CCG ATT TGG ATC CGG CGA ACC GGA TCG AGC TTA TTA TTA TAA TGG G
ND6	Forward 5' TAA TAC GAC TCA CTA TAG GCC TTC GGG CCA AAT GAT ACT ATA CAT TGT ATT
	Reverse 5' GAA CCG GAC CGA AGC CCG ATT TGG ATC CGG CGA ACC GGA TCG ACG AAG AAA ACC CCA C

Table 2-3. PCR conditions used to amplify mRNA gene regions of interest

mRNA	plasmid	plasmid (ng)[1]		annealing temperature (°C)		
				5 cycles	28 cycles	33 cycles
COI	p11-1		300	45	65	
COII	pTZ19R	15	30	50	65	
full length COII with 5' extension	pTZ19R	15	23	50	65	
full length COII no 5' extension	pTZ19R	15	30			50
COIII	p11-5	600	1200	50	60	
Cyt B	p11-5		600	45	50	
ATPase8	p11-1	150	300	50	65	
ATPase6	p11-1	150	300	50	65	
ND1	p11-1		900			42
ND2	p11-1		900			42
ND3	p11-5	600	900			42
ND4L with 5' extension	p11-5	300	600	50	65	
ND4L no 5' extension	p11-5	300	600	50	65	
ND4	p11-1	150	300	50	65	
ND5	p11-5	300	600			42
ND6	p11-5	600	900			42

[1] For the amplification of some mRNA genes two separate concentrations of plasmid were used and the products were combined.

RESULTS

Strategy: To investigate the structure near the 5′ ends of mitochondrial mRNAs, RNA constructs containing approximately the first 70 nucleotides of each mRNA were prepared. The selected region of each mRNA was flanked on the 5′ end by an extension allowing structural analysis to include the entire 5′ end of the mRNA (Fig. 2-1B). On the 3′ end, the mRNA carried an extension that contained a strong primer binding site to ensure uniform reverse transcription *(19)*. The structure formed by the first ~70 nucleotides of each of the mRNAs was then analyzed using RNA SHAPE chemistry *(15)*.

In a SHAPE experiment, local nucleotide flexibility is detected as the preferential ability of the 2′-hydroxyl group of nucleotides at conformationally dynamic sites to react with an electrophile to form a 2′-O-adduct. The structure of each RNA was assessed by treating the RNA with N-methylisatoic anhydride (NMIA). Background was analyzed in a mock reaction omitting the reagent, performed in parallel. Sites of 2′-O-adduct formation were detected by primer extension. Two dideoxy sequencing reactions were performed in parallel to yield a sequencing ladder allowing identification of modified sites. The SHAPE extension reactions and sequencing ladders were resolved on a sequencing gel. The relative reactivities of each nucleotide were used as constraints in conjunction with structure prediction based on free energy minimization *(18)* to generate secondary structure models satisfying the imposed SHAPE constraints. We will focus on the analysis of three mitochondrial messages in detail (ND2, COIII and COII) and then briefly discuss the analysis and the experimentally supported structures for all 13 mRNAs (see Fig. 2-1A).

NADH Dehydrogenase Subunit 2 (ND2) mRNA: Of the 13 protein-coding sequences in the mitochondrial genome, seven open reading frames encode subunits of the NADH dehydrogenase complex (Complex I). Five of these are encoded as monocistronic mRNAs, while 2 are encoded in the form of the dicistronic ND4/4L transcript *(20)*.

In one representative example, we analyzed a 78 nucleotide fragment of the ND2 mRNA using RNA SHAPE chemistry (Fig. 2-2). The RNA was folded in the presence of Mg^{2+} and subsequently treated with NMIA to assess local RNA structure or subjected to a mock reaction omitting the reagent to assess background. There were no significant stops in the control experiment omitting NMIA. In contrast, the RNA was highly modified upon treatment with the reagent [compare (+) and (-) NMIA lanes, Fig. 2-2A]. Reactivities were normalized to a scale spanning 0 to ~1.2 in which the average intensity of highly reactive positions was defined as having a reactivity of 1.0 *(15)*. SHAPE reactivities can vary continuously from 0 to 1.2. To simplify visual analysis of this information, positions with high and medium reactivities will be colored red and yellow, respectively. Residues with little or no reactivity will be black.

Most nucleotides between positions 1 and 45 in the ND2 mRNA are highly susceptible to modification, indicating that a considerable portion of this RNA is flexible and consequently, has little or no secondary or tertiary structure. While most nucleotides in this RNA are highly modified, nucleotides 46-56, 61-65 and 67-72 are unreactive toward NMIA (Fig. 2-2B). We used the experimental SHAPE reactivities to predict a secondary structure for this RNA (Fig. 2-2C). The predicted structure contains a single hairpin with a C bulge. The calculated free energy of this stem-loop is -6.3 kcal/mol (Fig. 2-2C). The SHAPE reactivities exactly match the predicted structure because unmodified nucleotides lie in the

57

FIGURE 2-2. SHAPE analysis of the 5′ end of the ND2 mRNA. *(A)* Gel image showing the NMIA modification reaction (+), the no reagent control (-), and G and A dideoxy sequencing ladders. *(B)* Histogram of normalized SHAPE reactivities after correcting for drop off. The histogram bar colors correspond to SHAPE reactivities. Nucleotides are defined as having a high reactivity (red), moderate reactivity (yellow) or low reactivity (black). *(C)* Predicted secondary structure for the 5′ end of the ND2 mRNA as constrained by SHAPE reactivities. Nucleotide colors correspond to those in panel (B). The reactivities for nucleotides 68-73 were assigned by visual analysis of the gel. Although the first 10 nucleotides of this RNA have low (but still significant) reactivities, there are no obvious pairing partners for these positions in the RNA and flanking structure cassette. These nucleotides are thus predicted to be single stranded.

Fig. 2-2
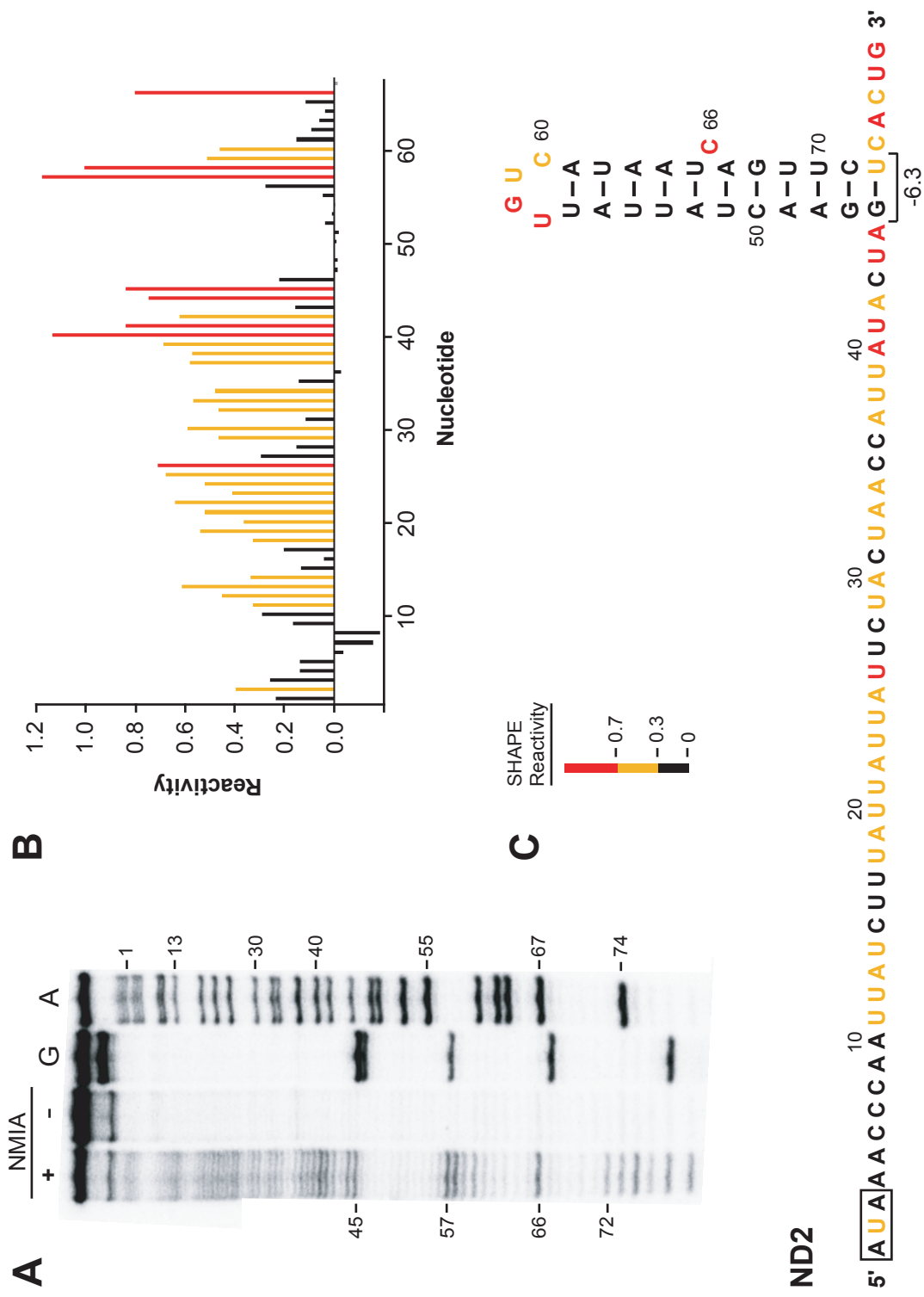
hairpin stem, while the single nucleotide bulge at position 66 is reactive. The remainder of this mRNA, including the AUA start codon, is predicted to be unstructured.

These data emphasize the high degree of structural detail that can be obtained in a SHAPE analysis. Even though mitochondrial mRNAs contain a low fraction of guanine residues, it is still possible for these RNAs to form stable secondary structures as evidenced by the stem-loop at positions 46-72 in the ND2 message. This well defined stable structure stands in strong contrast to the first 45 nucleotides in the ND2 message, which are highly flexible and do not form a stable secondary structure (Fig. 2-2C).

Cytochrome Oxidase Subunit II and III mRNA: Three subunits of cytochrome oxidase (Complex IV) in the oxidative phosphorylation pathway are encoded within the mitochondrial genome (COI, COII and COIII). The mRNA for the 30 kDa COIII subunit is 781 nucleotides in length and begins with an AUG start codon. We used SHAPE chemistry to analyze a 5′ fragment of the COIII RNA in the context of the 5′ and 3′ extensions of the structure cassette. To address the general possibility that the 5′ extension might affect the structure of the internal mRNA, we analyzed the same COIII RNA fragment lacking the 5′ extension. Comparison of the reactivity profiles revealed that the 5′ extension had no significant effect on nucleotide reactivity [see (+) NMIA lanes in the extension and no 5′ extension lanes, Fig. 2-3A]. Comparison of the integrated SHAPE intensities shows that the reactivities for the two RNAs are essentially identical (blue and green bars, Fig. 2-3B) In both cases, the 5′ end of the RNA is predicted to form the same structure (Fig. 2-3C). This structure contains a set of two stem-loops, with the potential to stack coaxially. However, these structures are just barely stable and have a net free energy of formation of -0.7 and -0.3

FIGURE 2-3. SHAPE analysis of the 5′ end of the COII mRNA. Panels A-C were generated as described for Fig. 2-2 with the following additions: *(A)* Gel image shows sites of 2′-O-adduct formation for the 82 nucleotide long COII fragment and for the full length mRNA. *(B)* Histograms for the COII fragment and full length mRNA reactivities are in blue and green respectively. *(C)* Secondary structure model for the COII mRNA fragment.

Fig 2-3
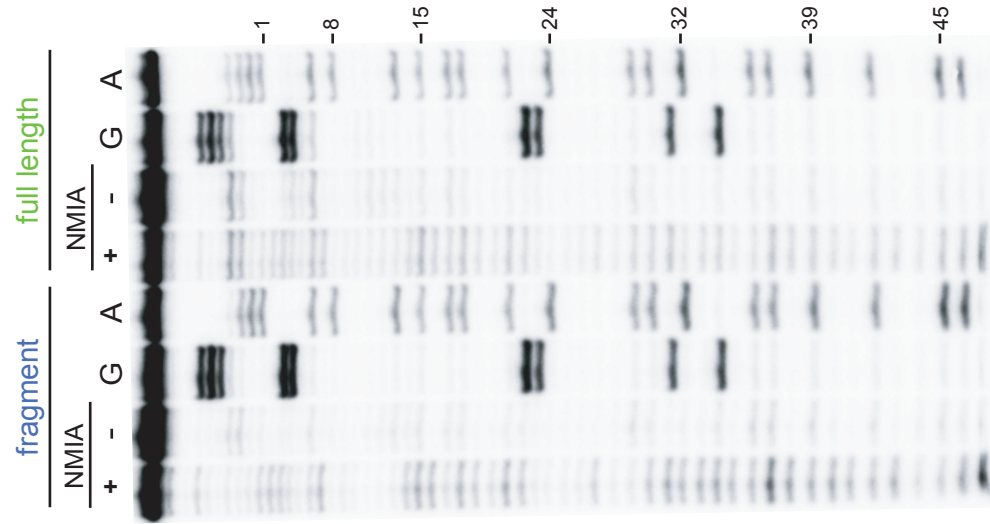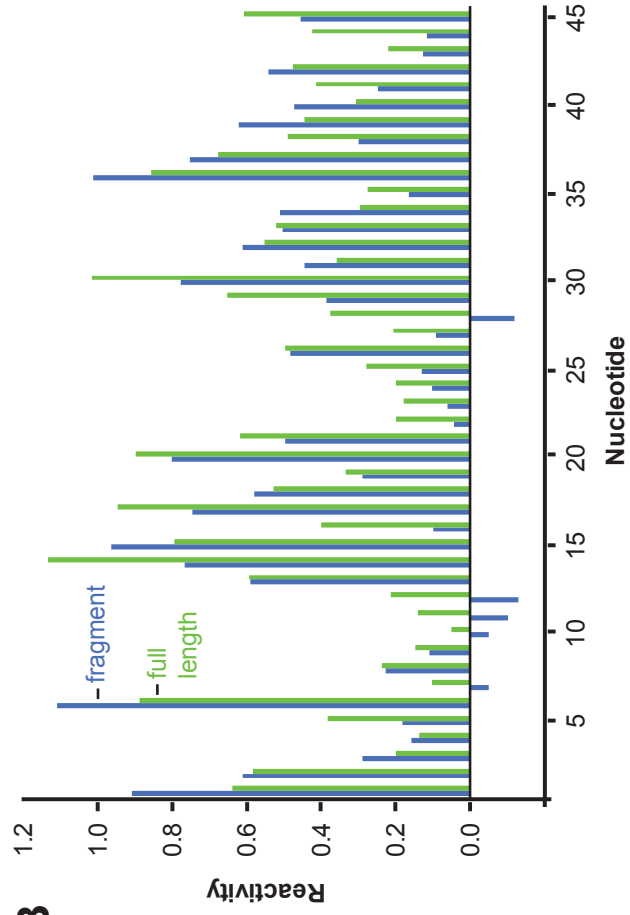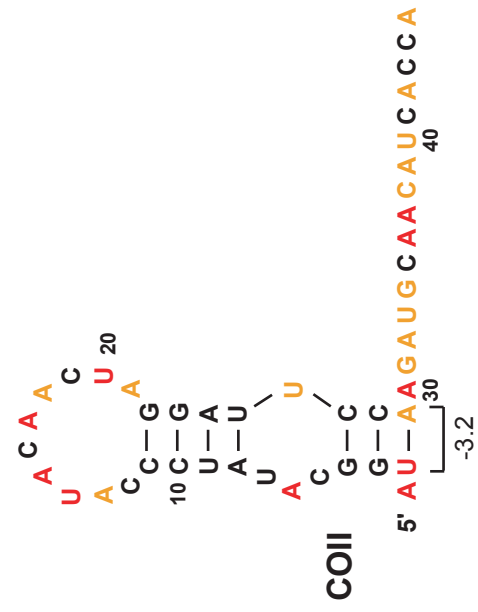
kcal/mol. It is likely that there are multiple weak structures in equilibrium. The AUG start codon at the 5′ end is predicted to be fully unpaired. These experiments emphasize that the structure cassette does not affect the folding of the internal mRNA sequence and that the 5′ end of the COIII mRNA lacks significant structure.

The mRNA for cytochrome oxidase subunit II (COII) is 684 nucleotides long and begins with an AUG start codon. For this RNA, we addressed the question of whether the structure of a 5′ fragment is a good model for the structure of the full mRNA. Hence, for this RNA, we analyzed both a 5′ fragment and an RNA spanning the full 684 nucleotides of the mRNA. This analysis allows us to assess whether long range pairings might be prevalent and affect the SHAPE profile at the 5′ ends of these RNAs. For both RNAs, SHAPE chemistry was performed under identical conditions and the sites of modification were analyzed using an internal DNA primer complementary to COII nucleotides 64-82 [compare 'fragment' and 'full length' lanes, Fig. 2-4A]. The two RNAs have very similar SHAPE reactivity patterns [compare blue and green bars in the histogram, Fig. 2-4B]. Both reactivity patterns also support essentially the same structure for the 5′ end of this RNA with one minor difference. The full length data supports a slightly less stable structure in which the U-A pair at the base of the stem (shown in Fig. 2-3C) does not form. The overall secondary structure features a single stem-loop, interrupted by an internal loop that partially incorporates the AUG start codon (Fig. 2-4C). Although the stem-loop structure spans 28 nucleotides, its overall stability is still low and has a total free energy of only -3.2 kcal/mol. This analysis supports the conclusion that the ~70 nucleotides at the 5′ end of the mRNA yields a SHAPE profile and overall structure that is representative of the full length mRNA.

FIGURE 2-4. SHAPE analysis of the 5′ end of the COIII mRNA. Panels A-C were generated as described for Fig. 2-2 with the following additions. *(A)* Gel image showing sites of 2′-O-adduct formation for the COIII mRNA fragment both with and without the 5′ extension from the structure cassette. G and A sequencing ladders correspond to the COIII RNA containing the 5′ extension. *(B)* Absolute SHAPE reactivities. Histograms for the COIII mRNA fragment without and with the 5′ extension are blue and green respectively. *(C)* Secondary structure model for the COIII mRNA fragment. Positions for which no data was obtained are gray. Identical structures are predicted for the RNAs without and with the 5′ extension.

Fig. 2-4
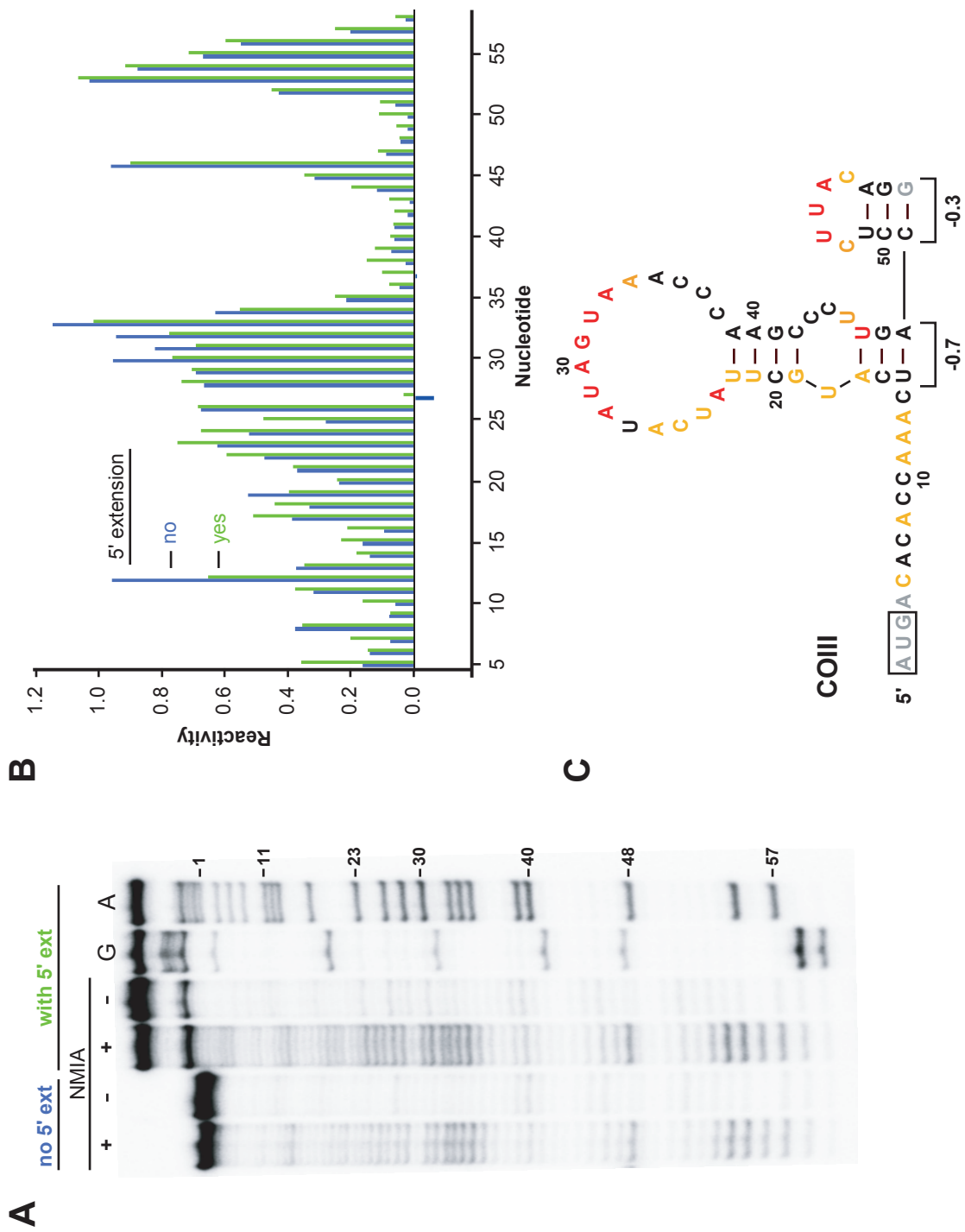
Other Monocistronic mRNAs: We analyzed 5′ RNA fragments for the other six

monocistronic mRNAs in mammalian mitochondria. These included the remaining subunit of

the cytochrome oxidase complex (COI, Fig. 2-5); the other four subunits of the NADH

dehydrogenase complex (Figs. 2-6 – 2-9); and of cytochrome b (Cytb), which is the only

subunit of complex III of the electron transfer chain encoded in the mitochondrial genome

(Fig. 2-10). Strikingly, SHAPE analysis reveals that all of these RNAs are largely

unstructured (note yellow and red nucleotides, Fig. 2-5 – 2-10). The most stable single

secondary structural element is found in the COI RNA and consists of a reasonably stable

stem-loop whose formation is 4.2 kcal/mol more stable than the corresponding single strand

(Fig. 2-5C). Note that this stable stem lies 39 nucleotides from the 5′ end of this RNA such

that the AUG start site is still in a conformationally flexible region (Fig. 2-5C). The 5′

regions of the remaining mRNAs are predicted to be essentially unstructured. For

completeness, the most stable secondary structure for each RNA is shown as panel C in

Figures 2-6 to 2-10 and none of these has a stability greater than 2.0 kcal/mol, a free energy

increment equivalent to a single A-U base pair *(21)*.

Dicistronic mRNAs: There are two dicistronic mRNAs in mammalian mitochondria.

One of these encodes the ND4L and ND4 proteins, both subunits of Complex I. This mRNA

initially codes for ND4L. The reading frames for the two proteins overlap such that the AUG

start codon of ND4 is 1 nucleotide upstream of the stop codon for ND4L (Fig. 2-12). The

second dicistronic mRNA encodes ATPase subunit 8 (ATP8) as the first cistron and ATPase

subunit 6 (ATP6) as the second cistron. Both of these subunits are components of

FIGURE 2-5. SHAPE analysis of the 5′ end of the COI mRNA. *(A)* Gel image showing the NMIA modification reaction (+), the no reagent control (-), and G and A dideoxy sequencing ladders. *(B)* Histogram of normalized SHAPE reactivities after correcting for drop off. The histogram bar colors correspond to SHAPE reactivities. Nucleotides are defined as having a high reactivity (red), moderate reactivity (yellow) or low reactivity (black). *(C)* Predicted secondary structure for the 5′ end of the COI mRNA as constrained by SHAPE reactivities with the start codon boxed. Nucleotide colors correspond to those in panel (B).

Fig. 2-5

68

FIGURE 2-6. SHAPE analysis of the 5′ end of the ND1 mRNA. *(A)* Gel image showing the NMIA modification reaction (+), the no reagent control (-), and G and A dideoxy sequencing ladders. *(B)* Histogram of normalized SHAPE reactivities after correcting for drop off. The histogram bar colors correspond to SHAPE reactivities. Nucleotides are defined as having a high reactivity (red), moderate reactivity (yellow) or low reactivity (black). *(C)* Predicted secondary structure for the 5′ end of the NDI mRNA as constrained by SHAPE reactivities with the start codon boxed. Nucleotide colors correspond to those in panel (B).

Fig. 2-6

70

FIGURE 2-7. SHAPE analysis of the 5′ end of the ND3 mRNA. *(A)* Gel image showing the NMIA modification reaction (+), the no reagent control (-), and G and A dideoxy sequencing ladders. *(B)* Histogram of normalized SHAPE reactivities after correcting for drop off. The histogram bar colors correspond to SHAPE reactivities. Nucleotides are defined as having a high reactivity (red), moderate reactivity (yellow) or low reactivity (black). *(C)* No secondary structure is predicted for the 5′ end of the ND3 mRNA when constrained by SHAPE reactivities. The start codon of the unstructured mRNA fragment is boxed. Nucleotide colors correspond to those in panel (B).

Fig. 2-7
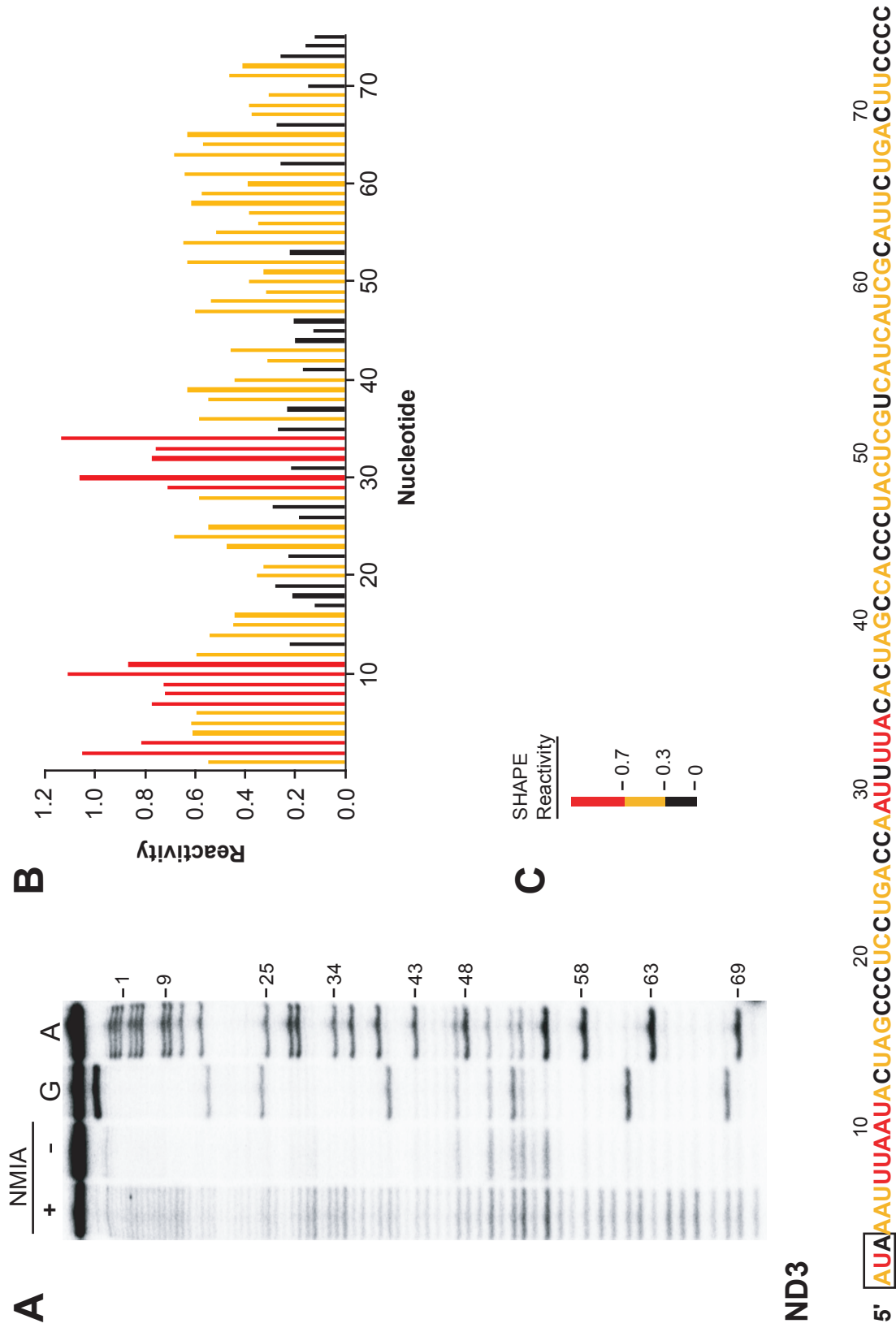
FIGURE 2-8. SHAPE analysis of the 5′ end of the ND5 mRNA. *(A)* Gel image showing the NMIA modification reaction (+), the no reagent control (-), and G and A dideoxy sequencing ladders. *(B)* Histogram of normalized SHAPE reactivities after correcting for drop off. The histogram bar colors correspond to SHAPE reactivities. Nucleotides are defined as having a high reactivity (red), moderate reactivity (yellow) or low reactivity (black). *(C)* Predicted secondary structure for the 5′ end of the ND5 mRNA as constrained by SHAPE reactivities with the start codon boxed. Nucleotide colors correspond to those in panel (B).
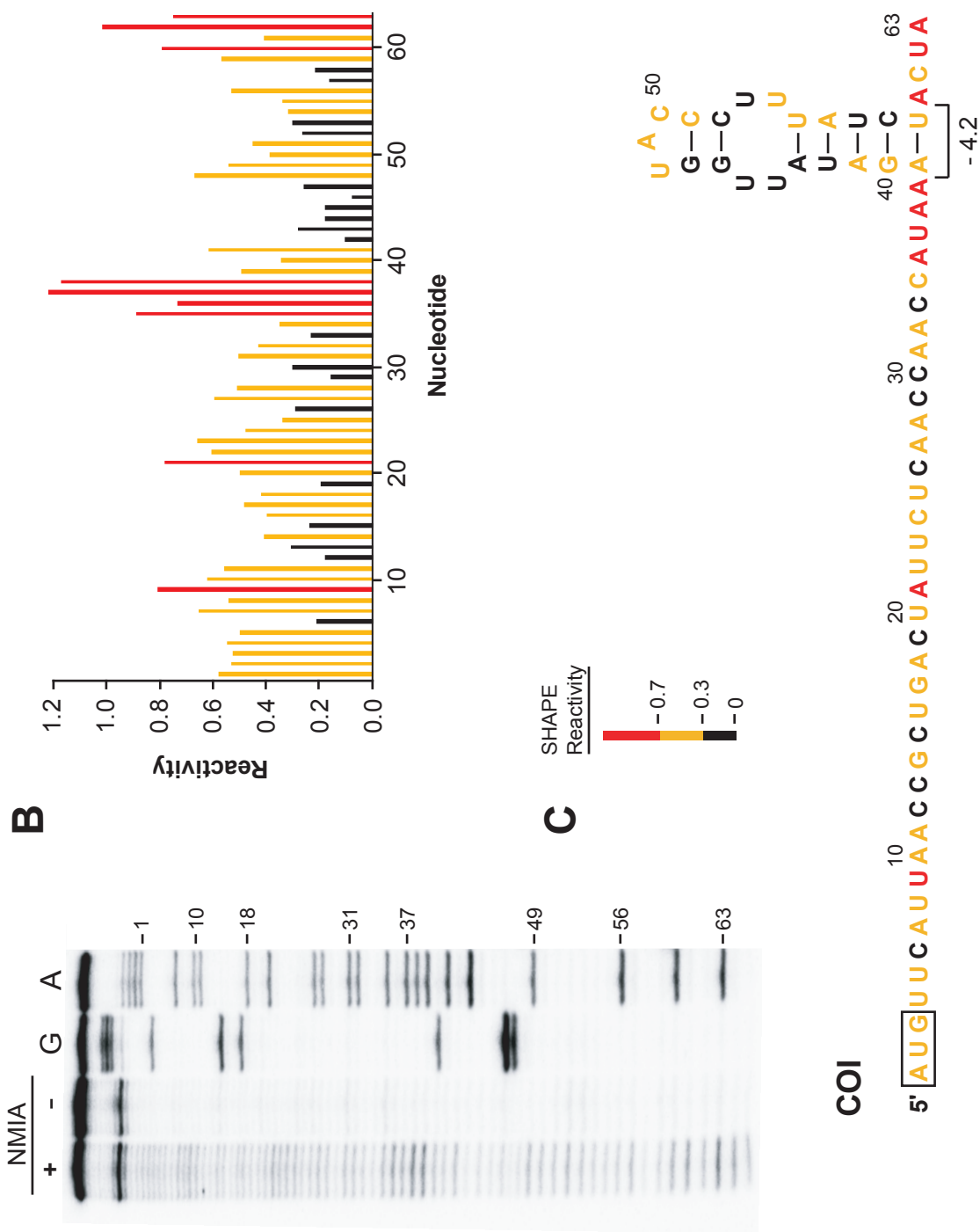
Fig. 2-8
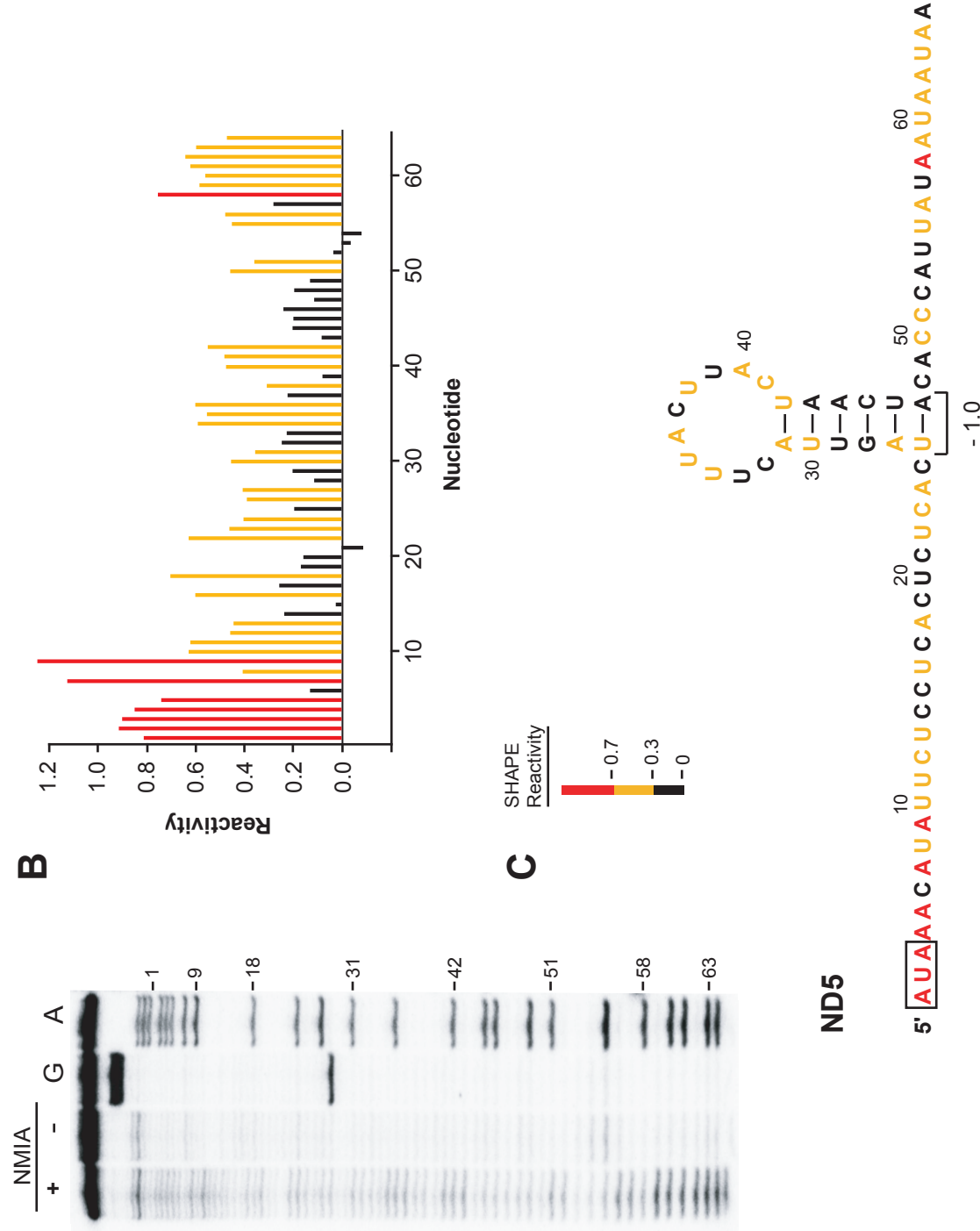
FIGURE 2-9. SHAPE analysis of the 5′ end of the ND6 mRNA. *(A)* Gel image showing the NMIA modification reaction (+), the no reagent control (-), and G and A dideoxy sequencing ladders. *(B)* Histogram of normalized SHAPE reactivities after correcting for drop off. The histogram bar colors correspond to SHAPE reactivities. Nucleotides are defined as having a high reactivity (red), moderate reactivity (yellow) or low reactivity (black). *(C)* Predicted secondary structure for the 5′ end of the ND6 mRNA as constrained by SHAPE reactivities with the start codon boxed. Nucleotide colors correspond to those in panel (B).
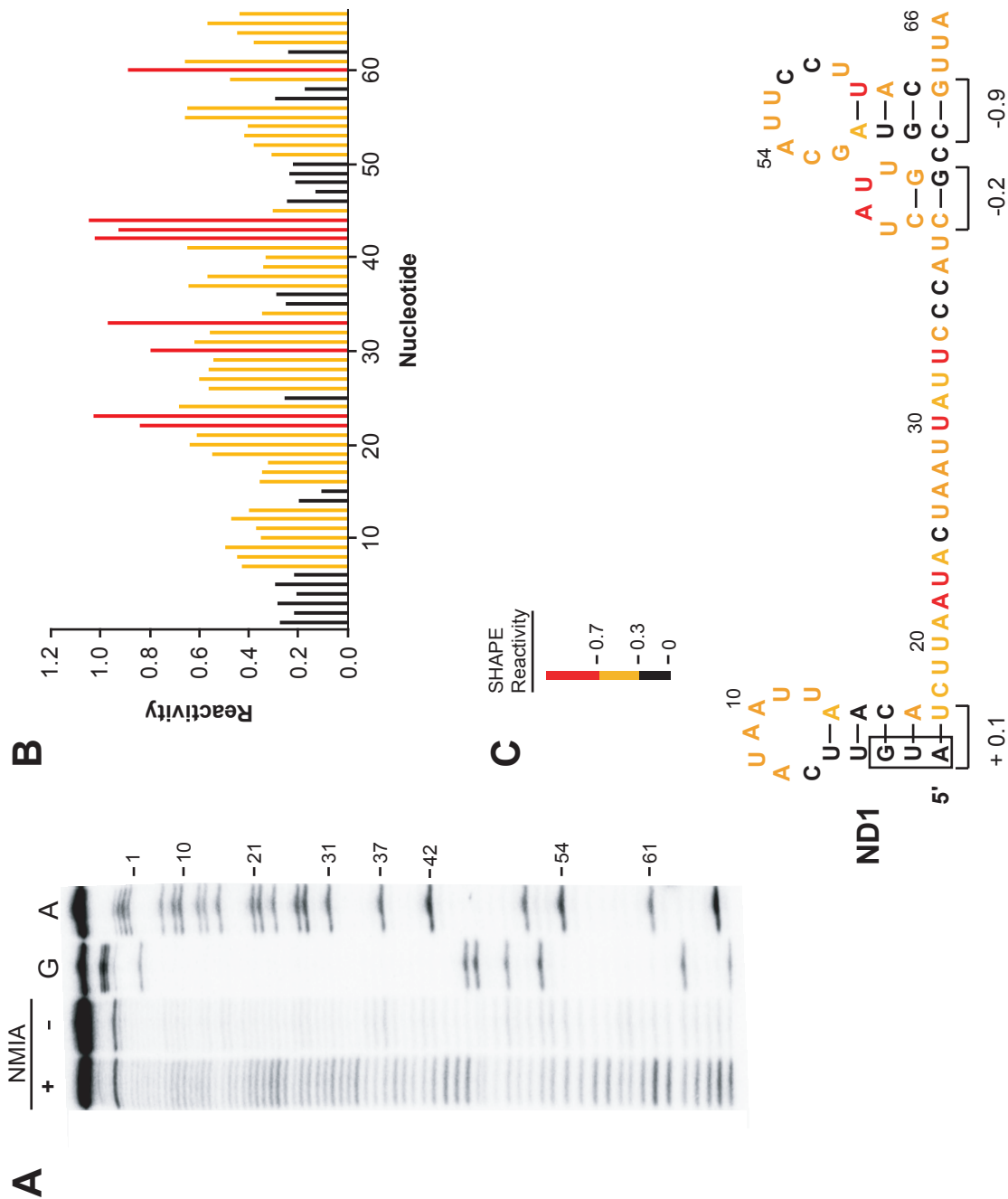
Fig. 2-9
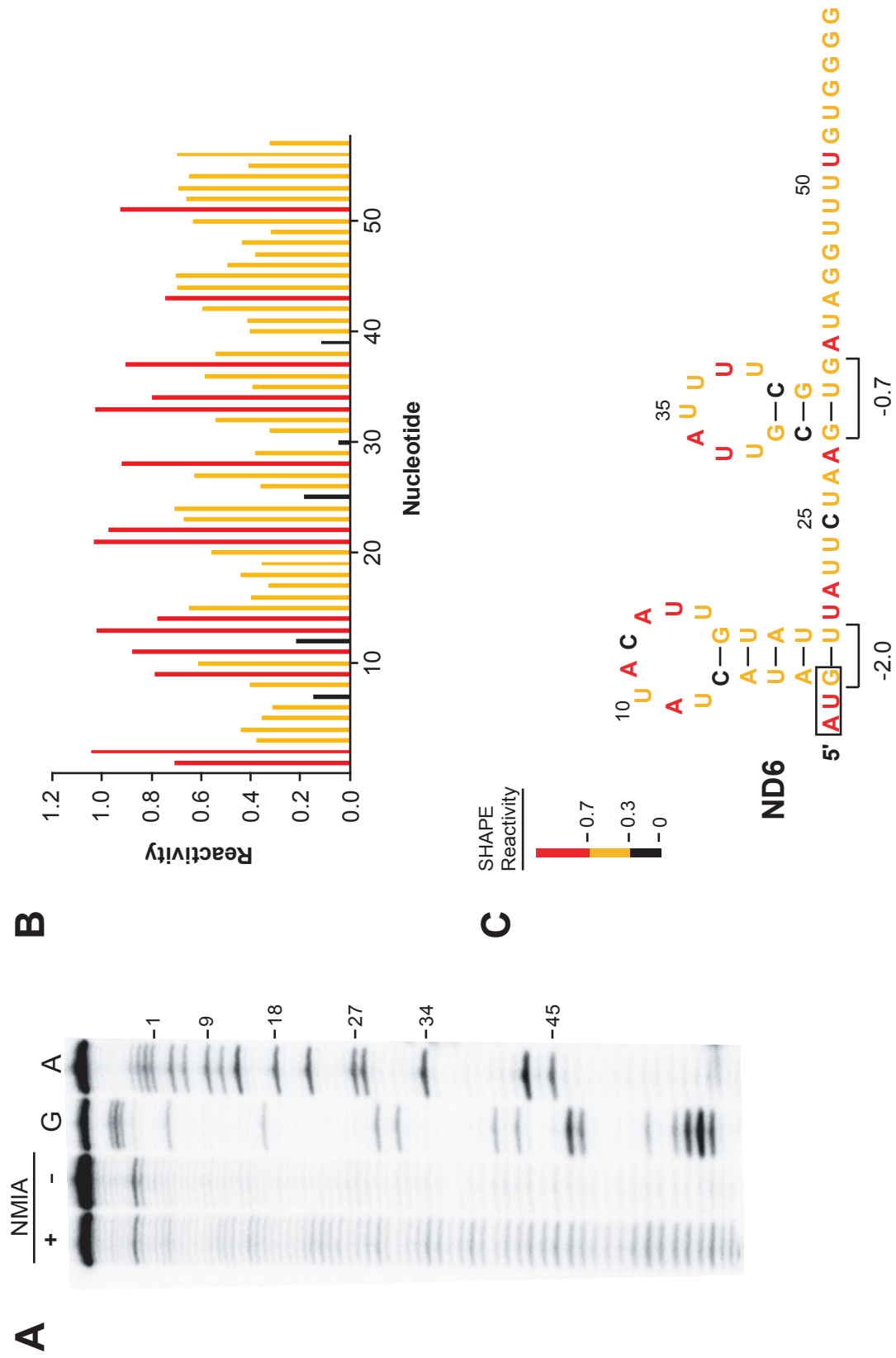
FIGURE 2-10. SHAPE analysis of the 5′ end of the CytB mRNA. *(A)* Gel image showing the NMIA modification reaction (+), the no reagent control (-), and G and A dideoxy sequencing ladders. *(B)* Histogram of normalized SHAPE reactivities after correcting for drop off. The histogram bar colors correspond to SHAPE reactivities. Nucleotides are defined as having a high reactivity (red), moderate reactivity (yellow) or low reactivity (black). *(C)* Predicted secondary structure for the 5′ end of the CytB mRNA as constrained by SHAPE reactivities with the start codon boxed. Nucleotide colors correspond to those in panel (B).

Fig. 2-10
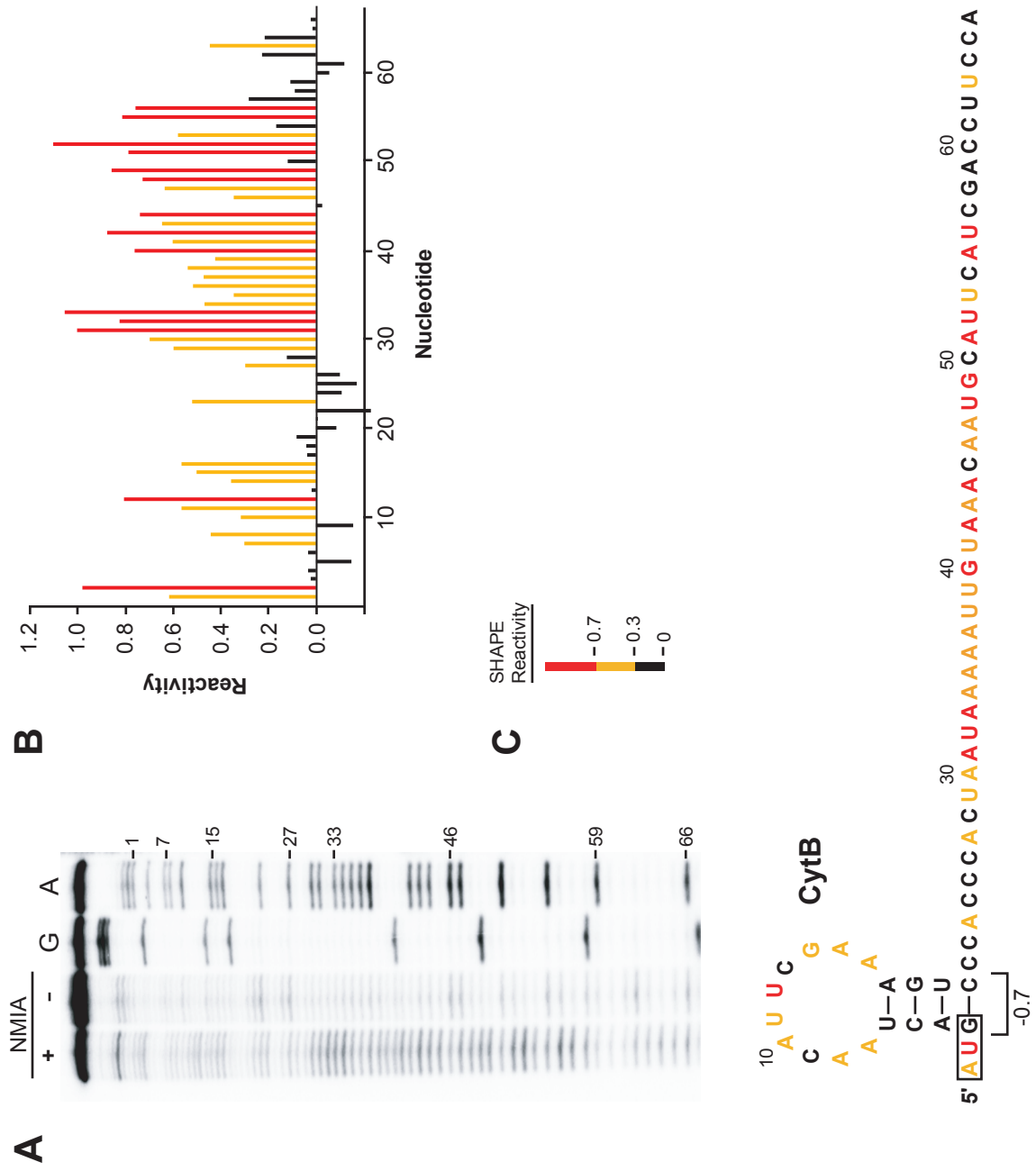
mitochondrial Complex V (the ATP synthase). The reading frames for these proteins overlap by 40 nucleotides (Fig. 2-14).

The 5′ end fragments of both dicistronic mRNAs (corresponding to synthesis of ND4L and ATP8) were analyzed by SHAPE. Both RNAs have the ability to form single stem-loop structures (Figs. 6A and C); however, neither is more stable than a single G-C base pair (stabilities are -0.1 and -2.7 kcal/mol, respectively). The start codon for both ND4L and ATP8 lie in very weakly or unstructured regions that would be readily accessible to the ribosome. Thus, the 5′ ends of the two dicistronic messages conform to the pattern identified for the monocistronic messages (Fig. 2-2C to 2-10C) and have no stable secondary structural elements near the 5′ start codons.

We next analyzed fragments containing the overlapping coding regions for the ND4L/ND4 and ATP8/ATP6 messages, which spanned 88 and 92 nucleotides, respectively (Fig. 2-12 and 2-14). The start codon of ND4 and the stop codon of ND4L both lie in highly unstructured regions and both are predicted to be single-stranded. Moreover, these codons lie in a large unstructured domain. We speculate that the initiation of translation at the ND4 start site occurs by slippage of the ribosome or small subunit from the ND4L stop codon back to the ND4 start codon. However, if *de novo* initiation occurs, then the lack of structure may be important for facilitating the process.

At the ATP8/ATP6 junction, there is also essentially no significant structure (Fig. 2-14). Both the start codon of ATP6 and the stop codon of ATP8 lie in unstructured, and likely highly accessible, regions. There are 40 nucleotides between the beginning of the start codon of ATP8 and the end of the stop codon of ATP8. Initiation of translation of the ATP6 message may require an independent initiation event, rather than ribosome slippage. An

independent initiation event is likely to be strongly facilitated by the absence of structure in the region. One interesting observation in this case is the absence of AUG or AUA triplets in or around the overlapping reading frames, possibly facilitating correct translational initiation at the ATP6 start site. Interestingly, initiation of these internal messages occurs at the first codon located upstream of the stop codon for the initial message in RNA regions devoid of measurable secondary structure (Figs. 6B & D).

FIGURE 2-11. SHAPE analysis of the 5′ translational start site for the ND4L dicistronic mRNA. *(A)* Gel image showing the NMIA modification reaction (+), the no reagent control (-), and G and A dideoxy sequencing ladders. *(B)* Histogram of normalized SHAPE reactivities after correcting for drop off. The histogram bar colors correspond to SHAPE reactivities. Nucleotides are defined as having a high reactivity (red), moderate reactivity (yellow) or low reactivity (black). *(C)* Predicted secondary structure for the 5′ end of the ND4L mRNA as constrained by SHAPE reactivities with the start codon boxed. Nucleotide colors correspond to those in panel (B).

Fig. 2-11
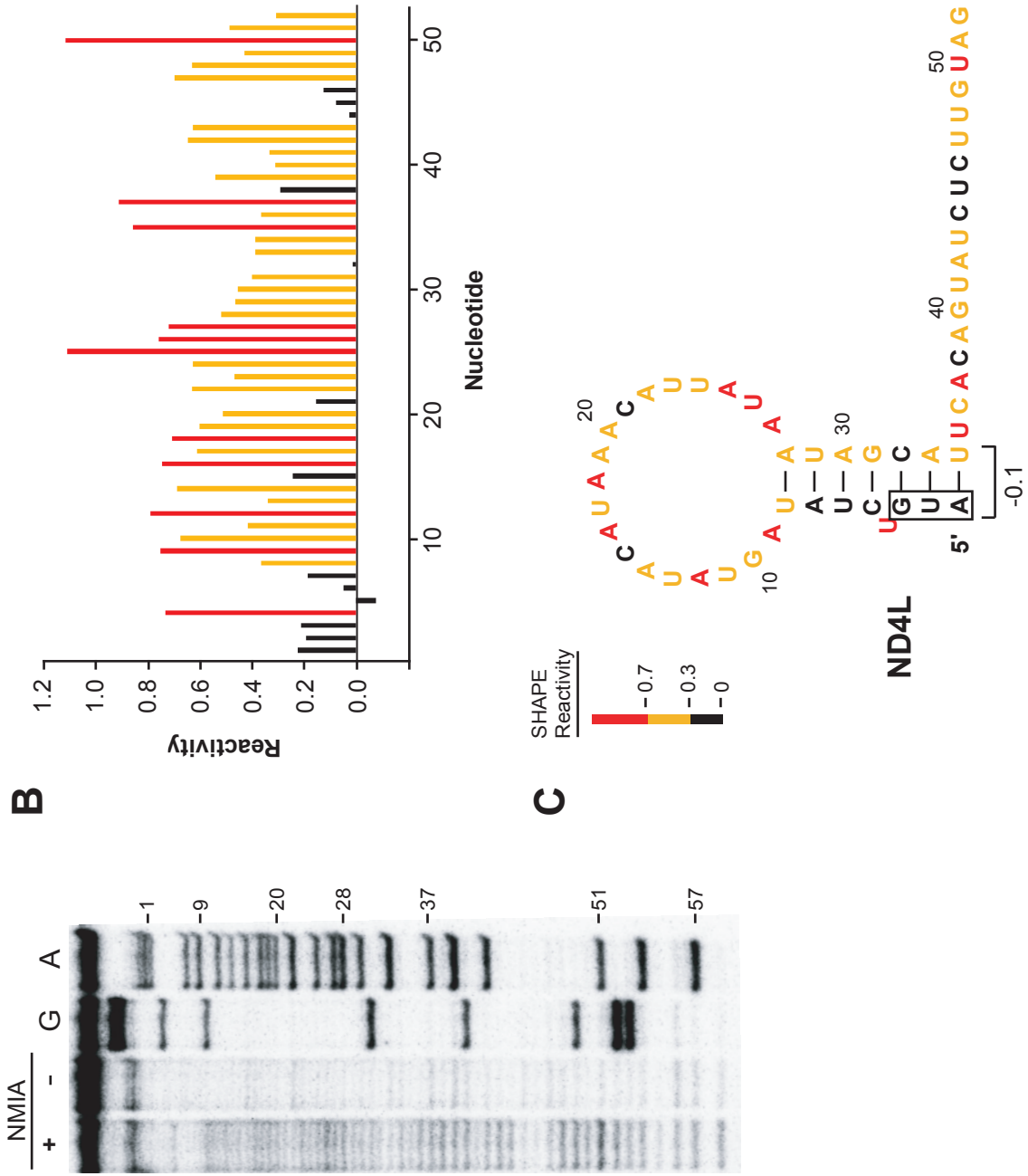
FIGURE 2-12. SHAPE analysis at the junction between coding regions for the dicistronic ND4 mRNA. *(A)* Gel image showing the NMIA modification reaction (+), the no reagent control (-), and G and A dideoxy sequencing ladders. *(B)* Histogram of normalized SHAPE reactivities after correcting for drop off. The histogram bar colors correspond to SHAPE reactivities. Nucleotides are defined as having a high reactivity (red), moderate reactivity (yellow) or low reactivity (black). *(C)* Predicted secondary structure for the coding region junction of the dicistronic ND4 mRNA as constrained by SHAPE reactivities. The start codon for ND4 is boxed and the stop codon for the ND4L coding region is underlined. Nucleotide colors correspond to those in panel (B).

Fig. 2-12

84
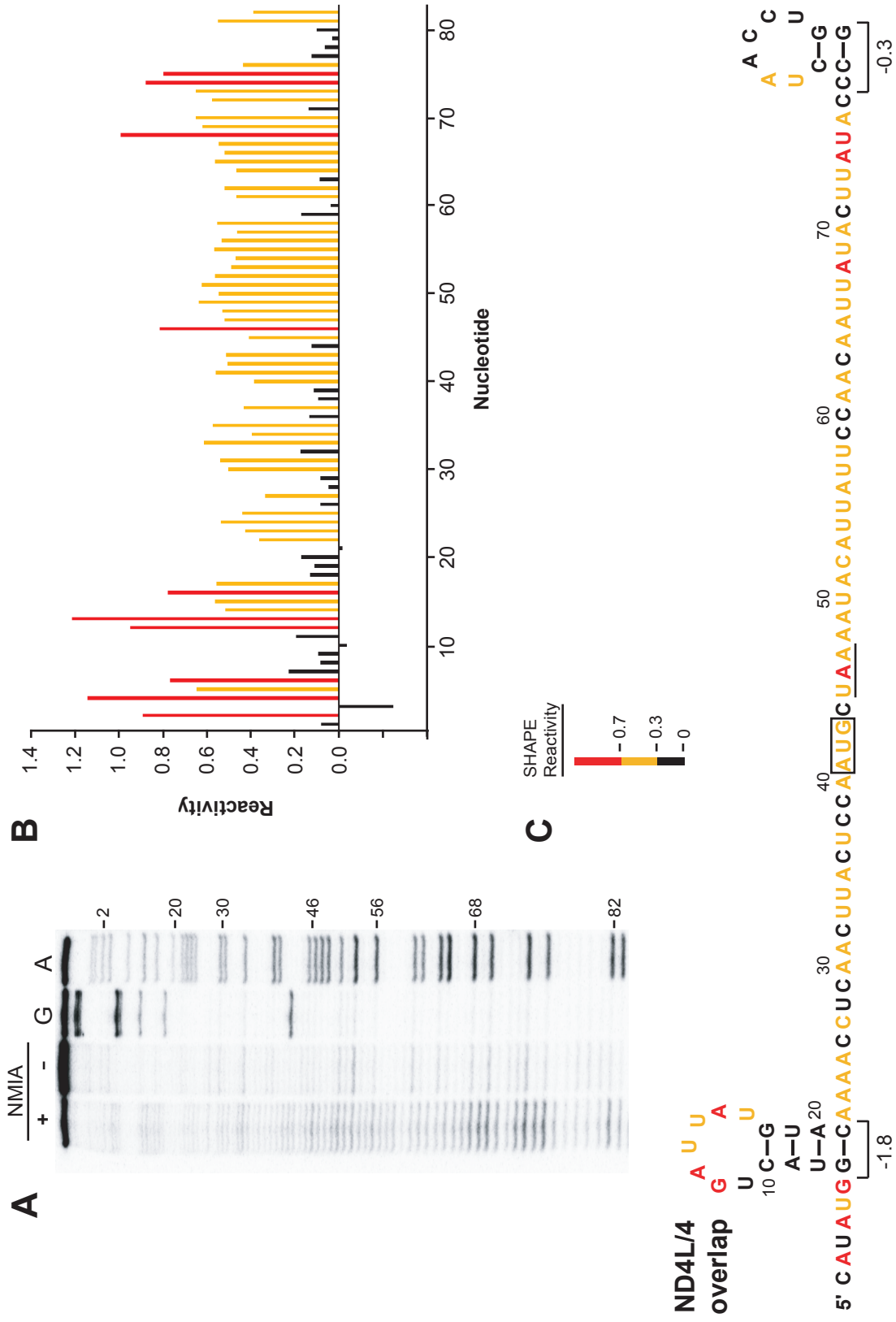
FIGURE 2-13. SHAPE analysis of the 5′ translational start site for the ATP8 dicistronic mRNA. *(A)* Gel image showing the NMIA modification reaction (+), the no reagent control (-), and G and A dideoxy sequencing ladders. *(B)* Histogram of normalized SHAPE reactivities after correcting for drop off. The histogram bar colors correspond to SHAPE reactivities. Nucleotides are defined as having a high reactivity (red), moderate reactivity (yellow) or low reactivity (black). *(C)* Predicted secondary structure for the 5′ end of the ATP8 mRNA as constrained by SHAPE reactivities with the start codon boxed. Nucleotide colors correspond to those in panel (B).

Fig. 2-13

A

B

C

SHAPE Reactivity

ATP8

86
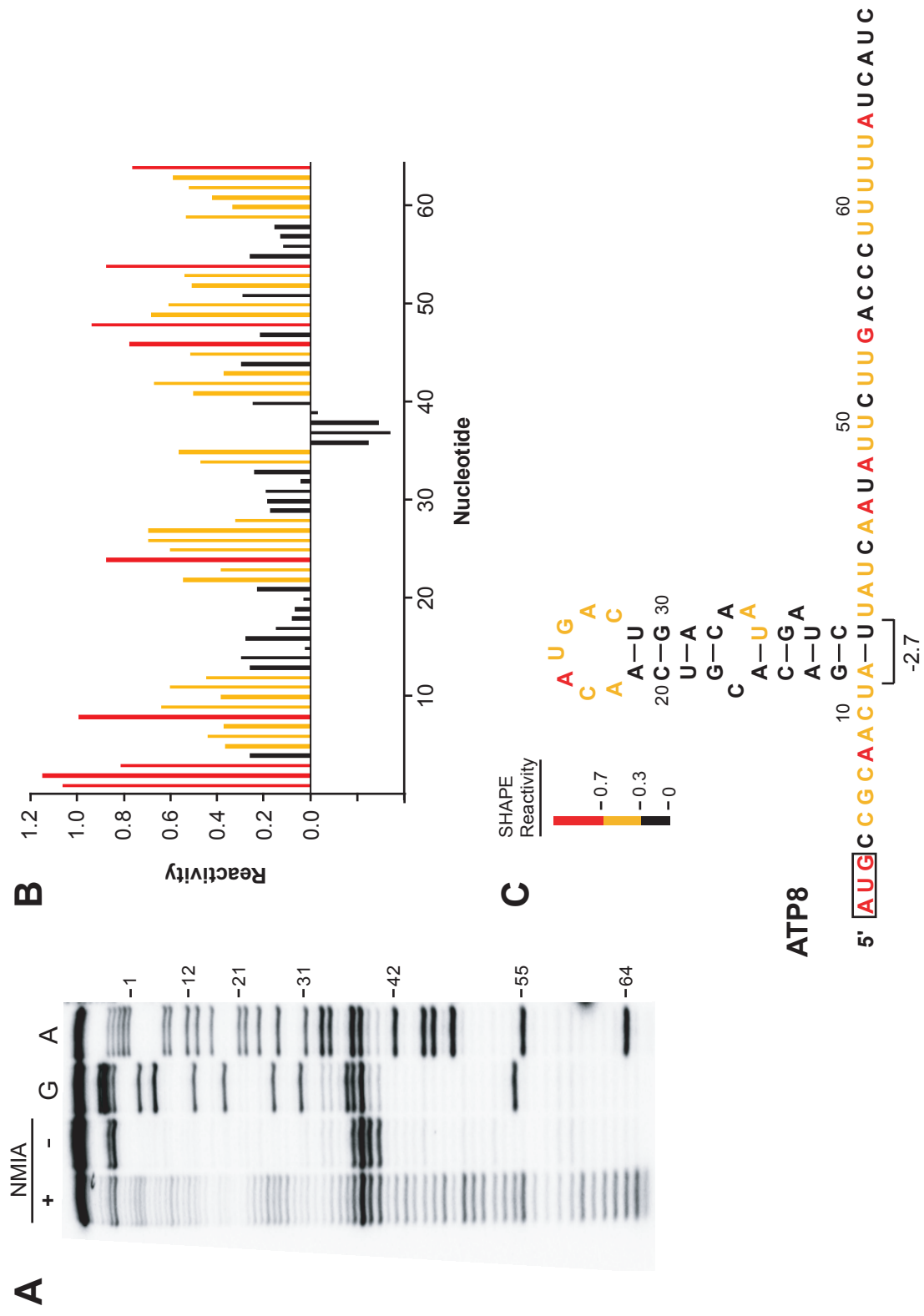
FIGURE 2-14. SHAPE analysis at the junction between coding regions for the dicistronic ATP6 mRNA. *(A)* Gel image showing the NMIA modification reaction (+), the no reagent control (-), and G and A dideoxy sequencing ladders. *(B)* Histogram of normalized SHAPE reactivities after correcting for drop off. The histogram bar colors correspond to SHAPE reactivities. Nucleotides are defined as having a high reactivity (red), moderate reactivity (yellow) or low reactivity (black). *(C)* Predicted secondary structure for the coding region junction of the dicistronic ATP6 mRNA as constrained by SHAPE reactivities. The start codon for ATP6 is boxed and the stop codon for the ATP8 coding region is underlined. Nucleotide colors correspond to those in panel (B).

Fig. 2-14

A

B

C

ATP8/6 overlap
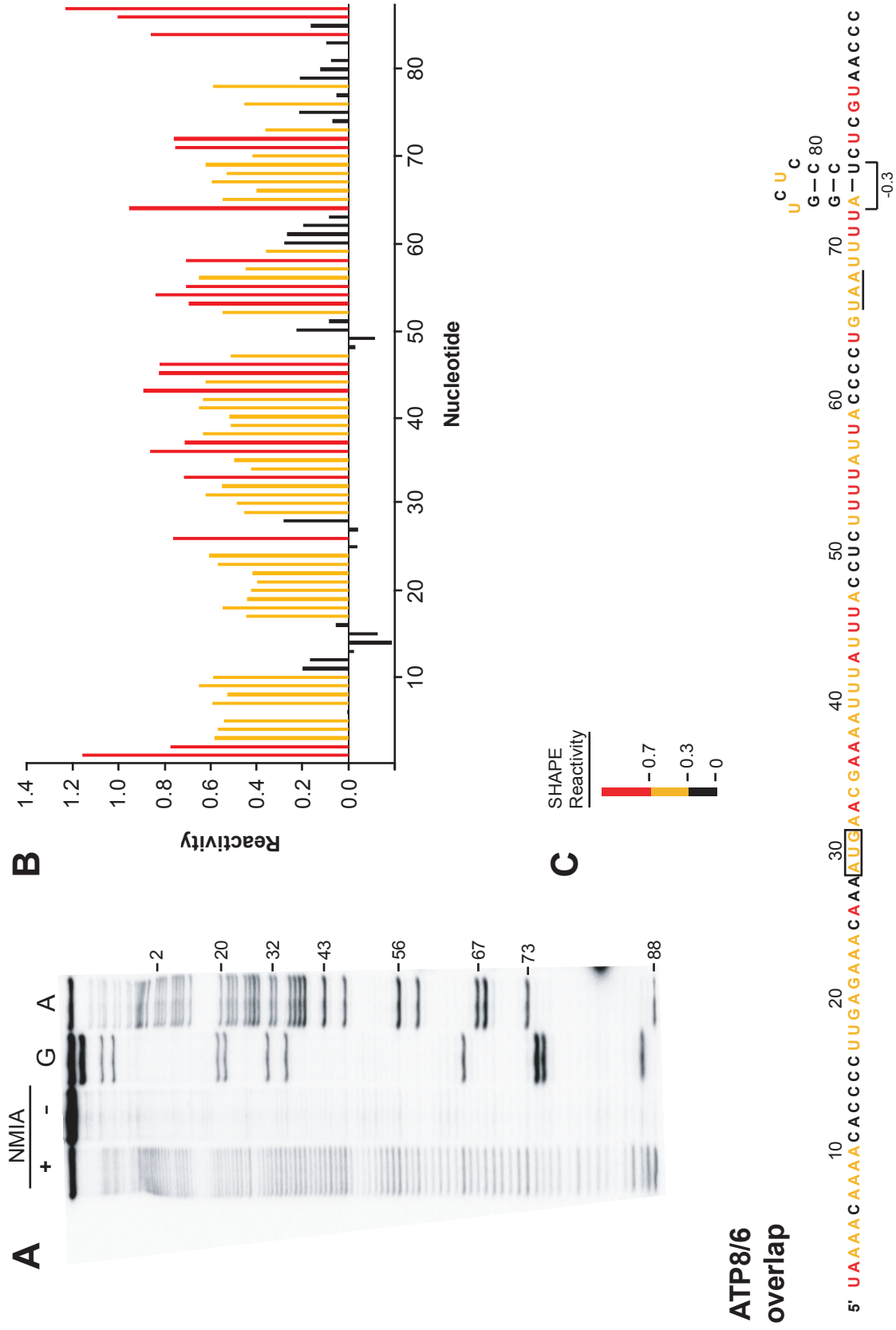
DISCUSSION

mRNA Structure in a Small Transcriptome

We have analyzed the 5′ ends of all translated RNAs in a single, small transcriptome. This analysis reveals that all 11 mRNAs in bovine mitochondria are highly unstructured. Specifically, as judged by SHAPE-constrained secondary structure prediction, there are no structures with a net stability greater than -3 kcal/mol in the first 35 nucleotides of any of these RNAs and, for most mRNAs, no structure forms that has a calculated stability of even -1.0 kcal/mol (Figs. 2-2C to 2-11C, 2-13C).

Mitochondrial genomes tend to be A/U rich and one explanation for the low extent of secondary structure might simply reflect the lower stability of A-U base pairs as compared with G-C base pairs. However, we find that some mRNA sequences do form stable secondary structures near their 5′ ends: the ND2 and COI messages contain stem-loops with calculated stabilities of -6.3 and -4.2 kcal/mol, respectively (Figs. 2-2C and 2-5C). These structures lie 45 and 39 nucleotides from the 5′ ends of their respective mRNAs. Furthermore, the structured mitochondrial tRNAs and rRNAs are also A/U rich indicating that the high A/U content by itself does not preclude the formation of significant structure. Thus, these data suggest mitochondrial mRNAs have the potential to form stable local structures but that such structures do not form near the 5′ ends of these mRNAs.

Requirement for Experimental Information in Inferring Mitochondrial mRNA Structure

We also assessed the extent to which the SHAPE reactivity information modulates the predicted secondary structure models for the mitochondrial mRNA leader sequences. In the

absence of experimental structural information, the most stable structure for an RNA can be estimated using thermodynamic parameters based on a dinucleotide sequence model, supplemented by other information for loops and multi-helix junctions (22-24). We calculated secondary structures for the 5′ ends of all 11 bovine mitochondrial mRNAs using a well-established thermodynamic model *(18)*. In general, the 5′ ends of these leaderless mRNAs are predicted to contain significant structure with free energies ranging from -2.0 to -7.1 kcal/mol (Fig. 2-15).

Comparison of the thermodynamic-only versus SHAPE-constrained predictions reveals that the differences fall into 3 classes. For three RNAs (ND2, ND5 and COI) the predicted models are identical. For the COIII RNA, there are minor differences between the structural models. In the third class, encompassing seven of the 11 leader sequences, there are large differences between the thermodynamic-only and SHAPE-constrained structures (compare structures in Fig. 2-15 with those in other figures). The differences between structures show a clear pattern. Structures predicted based on thermodynamic parameters alone contain many more base paired regions than do the SHAPE-constrained models. In general, the 'extra' helical regions tend to involve nucleotides that have high experimental SHAPE reactivities and, thus, are not consistent with direct experimental tests of these structures (see Fig. 2-15). These data are consistent with the general observation that thermodynamic models alone tend to over-predict secondary structures for RNAs of known structure *(24)*. Importantly, the clear demonstration that the 5′ leaders of bovine mitochondrial mRNAs are characterized by a lack of stable secondary structure was dependent on having single nucleotide resolution SHAPE information. We hypothesize that

the conserved lack of structure at the 5′ ends of mitochondrial mRNAs plays a functional role in mitochondrial translational initiation.

Structural Requirements for Translation Initiation in Mammalian Mitochondria

Overall, the mechanism of translational initiation for the leaderless mitochondrial mRNAs remains poorly understood. This mechanism is likely to be distinct from initiation of leaderless mRNAs in prokaryotes. In prokaryotes, initiation of leaderless mRNAs is thought to occur on preformed 70S ribosomes rather than on the small subunit, as is the predominant mechanism in the cytoplasm of both prokaryotes and eukaryotes (*5,9,11*). In the model for leaderless prokaryotic translational initiation, IF2 promotes binding of fMet-tRNA to the intact 70S ribosome instead of to the small 30S ribosomal subunit *(11)*. In contrast, the presence of an IF3 homolog in mitochondria (IF3$_{mt}$) argues that initiation on mitochondrial mRNAs occurs on 28S subunits. IF3 functions to dissociate intact ribosomes into their constituent subunits, in both the prokaryotic and mitochondrial systems. In prokaryotes, IF3 antagonizes initiation of leaderless mRNAs, which require intact 70S ribosomes *(11)*. Whereas, IF3$_{mt}$ stimulates initiation complex formation in the presence of mitochondrial 55S ribosomes *(25)*. This stimulation is consistent with the ability of IF3$_{mt}$ to dissociate 55S ribosomes and, thereby, to increase the concentration of initiation-active 28S subunits *(25)*.

The small ribosomal subunit must then select the correct AUG or AUA start codon. The unifying characteristic among the mitochondrial mRNAs is that the start codon generally lies at the 5′ end of the message. SHAPE analysis indicates that all start codons in mammalian mitochondrial mRNAs lie in mRNA regions with little or no local structure. It is likely that this structural accessibility is important for providing a suitable platform for the

initiating ribosome, as has been suggested for the leaderless mRNAs found in the prokaryotic system *(26)*.

One of the most distinctive differences between mitochondrial and bacterial ribosomes is the presence of a triangular gate-like structure at the mRNA entrance site on the small subunit of the mitochondrial ribosome *(27)*. The mRNA gate is formed almost completely by proteins that are specific to the mammalian mitochondrial ribosome. Thus, in the small 11 mRNA transcriptome of bovine mitochondria, both the mRNA start codon and also the mRNA entry site appear to have developed distinctive adaptations. The distinctive mitochondrial mRNA entry gate *(27)* may function to allow passage of only unstructured mRNA 5′ sequences into the small subunit for subsequent recognition of the start codon and translational initiation.

REFERENCES

1. Anderson, S., de Brujin, M., Coulson, A., Eperon, I., Sanger, F., and Young, I. (1982) Complete sequence of bovine mitochondrial DNA: Conserved features of the mammalian mitochondrial genome. *J. Mol. Biol.* **156:** 683-717.

2. Anderson, S., Bankier, A.T., Barrell, B.G., de Bruijn, M.H.L., Coulson, A.R., Drouin, J., Eperon, I.C., Nierlich, D.P., Roe, B.A., Sanger, F., Schreier, P.H., Smith, A.J.H., Staden, R., and Young, I.G. (1981) Sequence and organization of the human mitochondrial genome. *Nature* **290:** 457-465.

3. Montoya, J., Ojala, D., and Attardi, G. (1981) Distinctive features of the 5′-terminal sequences of the human mitochondrial mRNAs. *Nature* **290:** 465-470.

4. Shine, J. and Dalgarno, L. (1974) The 3′-terminal sequence of *Escherichia coli* 16S ribosomal RNA: complementarity to nonsense triplets and ribosome binding sites. *Proc. Natl. Acad. Sci.* **71:** 1342-1346.

5. Gualerzi, C.O., Brandi, L., Caserta, E., Teana, A., Spurio, R., Tomsic, J., and Pon, C.L. (2000) Translation initiation in bacteria. In the ribosome: Sructure, function, antibiotics, and cellular interactions, R.A. Garrett, S.R. Douthwaite, A. Liljas, A.T. Matheson, P.B. Moore, and H.F. Noller, eds. (Washington D.C.: ASM Press), pp. 477-494.

6. Boni, I.V. (2006) Diverse molecular mechanisms for translation initiation in prokaryotes. *Mol. Biol. (Mosk)* **40:** 658-668.

7. Nakamoto, T. (2006) A unified view of the initiation of protein synthesis. *Biochem. Biophys. Res. Commun.* **341:** 675-678.

8. Sachs, A., Sarnow, P., and Hentze, M.W. (1997) Starting at the beginning, middle, and end: Translation initiation in eukaryotes. *Cell* **89:** 831-838.

9. Kapp, L.D. and Lorsch, J.R. (2004) The molecular mechanics of eukaryotic translation. *Ann. Rev. Biochem.* **73:** 657-704.

10. Moll, I., Hirokawa, G., Kiel, M.C., Kaji, A., and Blasi, U. (2004) Translation initiation with 70S ribosomes: an alternative pathway for leaderless mRNAs. *Nucleic Acids Res.* **32:** 3354-3363.

11. Udagawa, T., Shimizu, Y., and Ueda, T. (2004) Evidence for the translation initiation of leaderless mRNAs by the intact 70 S ribosome without its dissociation into subunits in eubacteria. *J. Biol. Chem.* **279:** 8539-8546.

12. Hauswirth, W.W. and Laipis, P.J. (1982) Mitochondrial DNA polymorphism in a maternal lineage of holstein cows. *Proc. Natl. Acad. Sci USA.* **79:** 4686-4690.

13. Liao, H.-X. and Spremulli, L.L. (1989) Interaction of bovine mitochondrial ribosomes with messenger RNA. *J. Biol. Chem.* **264:** 7518-7522.

14. Merino, E.J., Wilkinson, K.A., Coughlan, J.L., and Weeks, K.M. (2005) RNA structure analysis at single nucleotide resolution by selective 2′-hydroxyl acylation and primer extension (SHAPE). *J. Am. Chem. Soc.* **127:** 4223-4231.

15. Wilkinson, K.A., Merino, E.J., and Weeks, K.M. (2006) Selective 2′-hydroxyl acylation analyzed by primer extension (SHAPE): quantitative RNA structure analysis at single nucleotide resolution. *Nat. Protocols* **1:** 1610-1616.

16. Das, R., Laederach, A., Pearlman, S.M., Herschlag, D., and Altman, R.B. (2005) SAFA: Semi-automated footprinting analysis software for high-throughput quantification of nucleic acid footprinting experiments. *RNA* **11:** 344-354.

17. Badorrek, C.S. and Weeks, K.M. (2006) Architecture of a gamma retroviral genomic RNA dimer. *Biochem.* **45:** 12664-12672.

18. Mathews, D.H., Disney, M.D., Childs, J.L., Schroeder, S.J., Zuker, M., and Turner, D.H. (2004) Incorporating chemical modification constraints into a dynamic programming algorithm for prediction of RNA secondary structure. *Proc. Natl. Acad. Sci. USA* **101:** 7287-7292.

19. Wilkinson, K.A., Merino, E.J., and Weeks, K.M. (2005) RNA SHAPE chemistry reveals non-hierarchical interactions dominate equilibrium structural transitions in tRNA[Asp] transcripts. *J. Am. Chem. Soc.* **127:** 4659-4667.

20. Taanman, J.-W. (1999) The mitochondrial genome: structure, transcription, translation and replication. *Biochim. Biophys. Acta* **1410:** 103-123.

21. Mathews, D.H., Sabina, J., Zuker, M., and Turner, D.H. (1999) Expanded sequence dependence of thermodynamic parameters improves prediction of RNA secondary structure. *J. Mol. Biol.* **288:** 911-940.

22. Zuker, M. (2003) Mfold web server for nucleic acid folding and hybridization prediction. *Nucleic Acids Res.* **31:** 3406-3415.

23. Eddy, S.R. (2004) How do RNA folding algorithms work? *Nat. Biotechnol.* **22:** 1457-1458.

24. Mathews, D.H. and Turner, D.H. (2006) Prediction of RNA secondary structure by free energy minimization. *Curr. Opin. Struct. Biol.* **16:** 270-278.

25. Koc, E.C. and Spremulli, L.L. (2002) Identification of mammalian mitochondrial translational initiation factor 3 and examination of its role in initiation complex formation with natural mRNAs. *J. Biol. Chem.* **277:** 35541-35549.

26. Moll, I., Grill, S., Gualerzi, C.O., and Blasi, U. (2002) Leaderless mRNAs in bacteria: surprises in ribosomal recruitment and translational control. *Mol. Microbiol.* **43:** 239-246.

27. Sharma, M.R., Koc, E.C., Datta, P.P., Booth, T.M., Spremulli, L.L., and Agrawal, R.K. (2003) Structure of the mammalian mitochondrial ribosome reveals an expanded functional role for its component proteins. *Cell* **115:** 97-108.

CHAPTER III

A SINGLE POINT MUTATION IN HUMAN MITOCHONDRIAL tRNA^{Met} CAUSES DISEASE BY DISRUPTING Mg^{2+} BINDING LEADING TO tRNA MISFOLDING

INTRODUCTION

Human mitochondria are subcellular organelles that produce more than 90% of the energy required by the cell. The mitochondrial genome encodes 13 proteins necessary for energy production, two rRNAs and all of the 22 tRNAs that are necessary for the synthesis of these proteins *(1,2)*. Mammalian mitochondrial tRNAs have a number of unusual features that distinguish them from canonical tRNAs. In many cases, they lack a number of the conserved or semi-conserved nucleotides that play important roles in creating the L-shaped tertiary structure of prokaryotic and eukaryotic cytoplasmic tRNAs *(3)*. There is little detailed structural information on these tRNAs. No data is currently available that examines the structure of mammalian mitochondrial tRNAs with single nucleotide resolution. However, chemical and enzymatic probing has lead to the idea that these tRNAs have retained the basic cloverleaf structure of canonical tRNAs but that they lack a number of conserved tertiary interactions leading to a weaker tertiary structure *(4-8)*. In particular, a number of the long-range interactions between the D-and T-arms of the tRNAs appear to be missing.

All 22 tRNAs that function in mammalian mitochondria are encoded in the mitochondrial DNA. Considerable interest in mitochondrial tRNAs centers on the occurrence of diseases arising from mutations in their genes that lead to a number of maternally inherited genetic disorders *(9-12)*. The diseases associated with mitochondrial tRNA mutations may arise from failure in the processing of the tRNA *(13)*, from reduced stability of the tRNA *(14,15)*, from a reduction in aminoacylation *(12,16,17)*, from a reduced ability of the mutated

aminoacyl-tRNA to interact with mitochondrial elongation factor Tu (EF-Tu$_{mt}$) *(16)* and from the failure of the tRNA to be correctly modified leading to translational defects *(18)*.

Normally, protein biosynthetic systems have two tRNA^{Met} species. One is used solely for initiation while the other functions in polypeptide chain elongation. Animal mitochondria are quite unusual in that they contain a single gene for tRNA^{Met}, which functions in both polypeptide chain initiation and chain elongation. As a result of this dual role, mitochondrial Met-tRNA^{Met} must be recognized by the mitochondrial Met-tRNA transformylase (MTF$_{mt}$) and be brought as fMet-tRNA^{Met} to the ribosome for translational initiation. In addition Met-tRNA^{Met} must interact with elongation factor EF-Tu$_{mt}$ and bind to the A-site of the ribosome during translational elongation. Thus, this tRNA^{Met} is of central importance in mitochondrial translation.

Human tRNA^{Met} has a number of interesting features (Fig. 3-1A). The D-loop is somewhat small and lacks the classical GG sequence found in most tRNAs. It has no dihydrouridine modification. The D-loop lacks the G at 19 that facilitates interactions with the T-loop through the tertiary interaction G19 with C56. The first position of the anticodon contains the unusual modified base 5-formylcytidine. This modification may play a role in the unusual codon recognition requirements of this tRNA which must recognize both AUG and AUA codons. The minor loop is short lacking the usual G47 and the T-stem has two adjacent pyrimidine:pyrimidine pairs (U-U and U-Ψ). Further, the T-loop contains only 6 nucleotides instead of the normal 7. These unusual structural features suggest that human mitochondrial tRNA^{Met} may have an intrinsically weak tertiary structure.

Three interesting point mutations (T4409C, A4435G and G4450A) occur in the gene for human tRNA^{Met} (hmtRNA^{Met}). The T4409C mutation (Fig. 3-1A) results in a U8 to C

change at the corner of the acceptor stem and D-stem of hmtRNA^{Met}. This mutation leads to

mitochondrial myopathy resulting in dystrophic muscles and exercise intolerance *(19)*. The

A4435G mutation leads to the change of A37 to G37 in the anticodon loop of the tRNA *(20)*.

This mutation acts as a modulator of Leber's hereditary optic neuropathy increasing the

severity of this condition when it arises due to other mutations in the mitochondrial DNA.

The G4450A mutation leads to loss of the final base pair in the T-stem (Fig. 3-1A). This

mutation presents as splenic lymphoma, is largely confined to lymphocyte cells, and results

in severely abnormal mitochondria leading to serious defects in energy production *(21)*. A

systematic examination of the structural and biochemical consequences of these mutations is

lacking. Here we examine the structure of human mitochondrial tRNA^{Met} and probe the

effects of the U8C mutation on the structure and function of this tRNA.

FIGURE 3-1: The sequence of the normal and U8C hmtRNA^{Met} and the effect of the

mutation on the aminoacylation of the tRNA. *(A)* Primary sequence of hmtRNA^{Met} indicating

the position of the U8C mutation. The Sprinzl numbering system is used throughout *(40)*. *(B)*

Aminoacylation of the normal (circles) and U8C transcripts (squares) of hmtRNA^{Met} by

hmMetRS. *(C)* Aminoacylation of the normal (circles) and U8C transcripts (squares) of

hmtRNA^{Met} by *E. coli* MetRS.

Fig. 3-1

A

3'
A
C
C
A
5' A — U
G — C
U — A 70
A — U
A ● G
G — C
G — [U]
C

acceptor stem

T-arm

A U
C A 55
C C U U
60
C U U C C G [G] U
● ● ● |
G Ψ U G G
U 48
A 46
A A
G53A

U8C

D-arm
A U C G A
| | | |
A A G C U
A A
17 A
U A 21

Ψ — A A
Ψ — A
C — G
G — C
G — C
G — C
30 G — C 40
G — C
C — C
C A
5fC
A37G
[A]
U

anticodon stem and loop

B hmMetRS

hmtRNA^Met

U8C mutant

[³⁵S]-Met-tRNA^Met (pmol)

Time (min)

C E. coli MetRS

hmtRNA^Met

U8C mutant

[³⁵S]-Met-tRNA^Met (pmol)

Time (min)

101

MATERIALS AND METHODS

RNA synthesis: Human mitochondrial tRNA^{Met} transcripts for aminoacylation experiments were prepared by *in vitro* transcription (22), purified by denaturing (10%) polyacrylamide gel electrophoresis (29:1 acrylamide:bisacrylamide prepared with 7M urea, 90 mM Tris-borate, 2 mM EDTA), visualized by UV shadowing, excised from the gel and recovered by passive elution in water followed by ethanol precipitation. HmtRNA^{Met} transcripts for selective 2′-hydroxyl acylation and primer extension (SHAPE) experiments were prepared in the context of the structure cassette as described *(23)*. D- and T-half molecules were chemically synthesized (Dharmacon), purified and analyzed as previously described *(24)*.

Purification of E. coli MetRS: A saturated overnight culture of JM109 cells carrying the pQE60-*E. coli* MetRS plasmid construct (kindly provided by Uttam RajBhandary, MIT) was grown at 37 °C in 2xYT media (20 mL) supplemented with 50 µg/mL Ampicillin and used to inoculate 2 L of 2xYT media (50 µg/mL ampicillin). The cells were grown at 37 °C for 4 hours (A_{600}= 0.6), induced with 50 µM isopropyl-β-D-thiogalactopyranoside (IPTG) and then grown at 37 °C for 4 h post-induction. The cells were harvested by centrifugation at 4000 rpm for 30 min. The cell pellet was resuspended in 500 mL of 10 mM Tris-HCl (pH 7.6) and then re-collected by low speed centrifugation. The cell pellet was fast frozen and stored at -80 °C until used for purification of MetRS as described below.

The cell pellet (7 g) was resuspended in 100 mL of lysis buffer (50 mM Tris-HCl pH 7.6, 50 mM KCl, 10 mM MgCl$_2$, 200 µM phenylmethylsulphonyl fluoride (PMSF), 0.1%

Triton X-100 and 7 mM β-mercaptoethanol (βME)) and sonicated on ice for 7 min with 10 s

bursts followed by a 50 s cooling periods. The cell lysate was separated by centrifugation at

15k rpm for 30 min at 4 °C. *E. coli* MetRS was purified from the supernatant using 400 µL of

a 50% Ni-NTA slurry in wash buffer (100 mM Tris-HCl, pH 7.6, 1 M KCl, 10 mM $MgCl_2$,

10 mM imidazole, 200 µM PMSF and 7 mM βME). The resin was washed with 200 mL of

wash buffer. The protein was eluted with 4 mL of elution buffer (100 mM Tris-HCl, pH 7.6,

50 mM KCl, 10 mM $MgCl_2$, 150 mM imidazole, 200 µM PMSF and 7 mM βME). The

protein sample was dialyzed against 2 volumes of 500 mL of dialysis buffer (50 mM Tris-

HCl pH, 7.6, 50 mM KCl, 2.5 mM $MgCl_2$, 0.1 mM EDTA, 10% glycerol and 7 mM βME)

for 1 h.

Purification of bovine MTF$_{mt}$: A saturated culture of *E. coli* BL21 cells carrying the

pET15-bovine MTF$_{mt}$ plasmid construct (kindly provided by Nono Takeuchi, Univ. of

Tokyo) was grown at 37 °C in LB media (20 mL, with 50 µg/mL ampicillin) and used to

inoculate 2 L of LB media (50 µg/mL ampicillin). The cells were grown at 37 °C until an

A_{600} of 0.6 was reached, induced with 140 µM IPTG and then grown at 18 °C overnight (~16

h). The cells were harvested by low speed centrifugation. The cell pellet was washed with

500 mL of 50 mM Tris-HCl, pH 7.6 and then re-collected by low speed centrifugation. The

cell pellet was fast frozen and stored at -80 °C until used for purification of MTF$_{mt}$ as

described below.

The cell pellet (9 g) was resuspended in 100 mL of MTF lysis buffer (50 mM Tris-

HCl, pH 7.6, 40 mM KCl, 7 mM $MgCl_2$, 10% glycerol, 100 µM PMSF, 0.1% Triton X-100

and 7 mM βME) and sonicated on ice for 7 min with 10 s bursts followed by a 50 s cooling

periods. The cell lysate was separated by centrifugation at 15k rpm for 30 min at 4 °C. MTF_{mt} was purified from the supernatant using 600 µL of a 50% Ni-NTA slurry in MTF wash buffer (50 mM Tris-HCl, pH 7.6, 1 M KCl, 7 mM $MgCl_2$, 10 mM imidazole, 10% glycerol and 7 mM βME). The resin was washed with 100 mL of MTF wash buffer. The protein was eluted with 6 mL of MTF elution buffer (50 mM Tris-HCl, pH 7.6, 40 mM KCl, 7 mM $MgCl_2$, 150 mM imidazole, 10% glycerol and 7 mM βME). The protein sample was dialyzed against 2 volumes of 500 mL of MTF dialysis buffer (20 mM Tris-HCl, pH 7.6, 100 mM KCl, 10% glycerol and 3 mM βME) for 1 h.

Aminoacylation of human mitochondrial tRNA^{Met}: The aminoacylation reactions for both the wild-type and U8C mutant tRNA^{Met} transcripts were performed essentially as described *(22)*. Reaction mixtures (100 µL) containing 50 mM Tris-HCl, pH 7.6, 2.5 mM $MgCl_2$, 2.5 mM ATP, 200 nM spermine, 200 µg/mL BSA, 0.2 U/µL SUPERase•In RNase Inhibitor, 40 µM [^{35}S] methionine (4000 cpm/pmol), 50 nM human mitochondrial MetRS (hmMetRS, prepared as described *(22)*) or 8 nM *E. coli* MetRS and 1 µM U8 or U8C hmtRNA^{Met} were used.

SHAPE analysis of wild-type and U8C mutated hmtRNA^{Met} transcripts: Wild-type or U8C mutated tRNA (14 pmol, 0.33 µM) in 42 µL of nuclease free water (Ambion) was incubated at 50 °C for 2 min and then cooled on ice for 2 min. The RNA was divided into two aliquots of 12 µL (4 pmol) and 24 µL (8 pmol). The 4 pmol of RNA was treated with 6 µL of no Mg^{2+} folding buffer (333 mM Hepes-KOH, pH 8, 333 mM NaCl) and the 8 pmol of RNA was treated with 12 µL of with Mg^{2+} folding buffer (333 mM Hepes-KOH, pH 8, 20

mM MgCl$_2$, 333 mM NaCl) and incubated at 37 °C for 20 min. To 1 µL of 100 mM 1-methyl-7-nitro-isotoic anhydride (1M7) in anhydrous DMSO or 1 µL of anhydrous DMSO (control), 9 µL (2 pmol) of folded RNA was added and allowed to react at 37 °C for 70 s (5 half lives). The remaining 18 µL of folded RNA was divided into 2 aliquots of 9 µL (2 pmol) each and stored at 37 °C for sequencing. To the RNA treated with the no Mg^{2+} folding buffer 1 µL of 64 mM MgCl$_2$ was added. To the 1M7 treated, DMSO treated or untreated RNA (2 pmol), 3 µL of a 0.3 µM 5′-[^{32}P] radiolabelled oligonucleotide (5′-^{32}P-GAACCGGACCGAAGCCCG, obtained from the Nucleic Acids Core Facility at UNC) was added and the samples were incubated at 65 °C for 5 min and then at 35 °C for 20 min for primer annealing. To each reaction, 6 µL of reverse transcription buffer (250 mM KCl, 167 mM Tris-HCl, pH 8.3, 17 mM DTT and 0.42 mM each dNTP) was added. To the untreated RNA 1 µL of 5 mM ddCTP or ddTTP (Amersham) was added. After heating to 52 °C, 1 µL (200 Units) reverse transcriptase (Superscript III, InVitrogen) was added and the primer extension reaction was performed at 52 °C for 5 min. Reactions were quenched with 1 µL of 4 M NaOH and heated at 95 °C for 5 min. For gel analysis, 29 µL of a gel loading solution (138 mM unbuffered Tris HCl, 73% (v/v) formamide, 2 mM Tris-borate, 86 mM EDTA pH 8, with xylene cyanol and bromophenol blue) was added and the samples were heated at 95 °C for an additional 5 min. The cDNA products from the (+) and (-) 1M7 and sequencing reactions were separated by denaturing gel electrophoresis (10% polyacrylamide). Gels (21 cm x 40 cm x 0.4 mm) were electrophoresed at 1400 V for ~2.5 h. Gels were visualized by phosphorimaging (Molecular Dynamics). The (+) and (-) 1M7 band intensities were quantified using SAFA *(25)* and corrected for signal drop-off *(26)*. SHAPE reactivities were normalized by subtracting intensities from the (-) 1M7 control from the (+) 1M7 reaction and

divided by the average reactivity of the most reactive 7%. The reactivity of each nucleotide was assigned a value between 0 and 1. Nucleotides fall into 1 of 4 categories; unreactive (0-0.055), low reactivity (0.055-0.11), moderately reactive (0.11-0.22) or highly reactive (0.22-1).

Structural Studies of hmtRNA[Met] half molecules: Reconstitution of hmtRNA[Met] from U8 and U8C D-half molecules with T-half molecules required Mg^{2+} and was assessed by gel mobility shift assays using native, 15% polyacrylamide gel electrophoresis in Tris-borate buffer (89 mM Tris base, 89 mM boric acid, pH 8.3) with and without 3 mM Mg^{2+} at 4 °C *(24)*. The concentration of the D-half molecule was held constant at 31.2 μM while the concentration of the T-half molecule was varied from 4.2 to 112 μM.

UV monitored thermodynamic experiments: The half-molecule RNA samples were dissolved in the above Tris-borate buffer used for the PAGE experiments to obtain a concentration of 1.2 μM. $MgCl_2$ was added to a concentration of 3 mM. UV-monitored, thermal denaturations and re-naturations were replicated 10 times and monitored by measuring UV absorbance (260 nm) using a Cary 3 spectrophotometer as published *(27,28)*. The data points were averaged over 20 s and recorded with a temperature change of 1 °C per min from 4 to 90 °C. The least inconsistent of the ten melting transitions (either a denaturation or renaturation) was discarded from each set and the resulting data averaged on a point-by-point basis. The data was analysed as described by Serra and Turner *(29)* and the thermodynamic parameters were determined using Meltwin *(30)*.

106

For UV melts, the normal U8 tRNA and the U8C hmtRNA^{Met} was dialyzed against water using 10 kDa cutoff dialysis cups (Stratagene). The U8 and U8C hmtRNA^{Met} transcripts were diluted to 0.5 μM in a buffer containing 10 mM NaCl and 10 mM HEPES-KOH, pH 8.0. The thermal denaturation of the tRNAs was monitored by UV absorbance at 260 nm using a Cary 3 spectrophotometer. Data points were recorded once per min from 4-95 °C with a temperature change of 1 °C per min. Following thermal renaturation, 6 mM Mg^{2+} was added to the U8 and U8C transcripts and the UV-monitored thermal denaturation experiments were repeated.

RESULTS

Aminoacylation of the normal and U8C mutated tRNA^{Met}: Previous studies *(22)* have shown that the transcript of mitochondrial tRNA^{Met} has aminoacylation properties similar to those observed with the native tRNA. The U8C mutation leads to a myopathy presumably arising from a reduction in translational activity in mitochondria. To determine the biochemical consequence of the U8C mutation, the ability of the U8 and U8C hmtRNA^{Met} transcripts to be aminoacylated by the human mitochondrial methionyl-tRNA synthetase (hmMetRS) was tested. Aminoacylation is an early step required for the tRNA to be used in either the elongation or initiation phase of protein synthesis, and is, thus, of central importance for protein synthesis in mitochondria. The normal U8 transcript aminoacylates as expected *(22)*; however the U8C mutation causes a drastic reduction in the rate of aminoacylation of the tRNA (Fig. 3-1B).

Interestingly, though U8C hmtRNA^{Met} is anemically aminoacylated by hmMetRS, it is not aminoacylated at all by *E. coli* MetRS (Fig. 3-1C). The hmMetRS is believed to be both structurally and functionally homologous to its prokaryotic counterpart *(22)*. However, this work demonstrates that the hmMetRS is less discriminatory than *E. coli* MetRS for the structure of the tRNA. Since a major determinant in the recognition of tRNA^{Met} by the MetRS is thought to lie in the anticodon sequence which is unchanged *(31)*, this observation then leads to the question of why the mutated tRNA is less active in aminoacylation.

Chemical probing of the structure of the normal U8 tRNA^{Met} in the presence and absence of Mg²⁺: The structures of the hmtRNA^{Met} transcript containing the normal U8 and

the transcript containing the disease causing U8C mutation were probed using SHAPE chemistry *(23,32)*. SHAPE chemistry relies on the differential reactivity of the 2′ OH of nucleotides in different conformational states within the RNA (single stranded versus base paired) to the small molecule 1-methyl-7-nitroisatoic anhydride (1M7) *(23,32)*. Residues in flexible regions of the RNA are preferentially modified by this reagent. The tRNA was reverse transcribed using a radio-labeled primer and sites of modification were identified based on their ability to obstruct reverse transcription. The cDNA products were analyzed on a denaturing polyacrylamide gel. When residues in unstructured or flexible regions of the tRNA are modified, the reverse transcriptase stops, leading to a labeled band observed on the gel one residue shorter than the position of the modification. Comparison of the position of these bands to a sequencing ladder allows the identification of residues susceptible to modification *(33)*. The reactivity of each nucleotide toward 1M7 is quantified and the relative reactivity of each nucleotide is assigned a value between 0 and 1. The higher the value, the more propensity the nucleotide has to be unstructured. This information allows us to evaluate the legitimacy of the modeled tRNA structure *(34)*.

SHAPE chemistry was performed on the normal U8 hmtRNA^{Met} transcript in the presence of Mg^{2+} (Fig. 3-2A). A number of distinct structural features can be observed (Fig. 3-2B). No modification is observed for residues predicted to form the acceptor stem and the D-stem indicating that they are largely paired as expected. A single residue in the D-loop is highly reactive suggesting that most of the residues in this region of the tRNA are involved in tertiary interactions that reduce their reactivity. The anticodon stem is clearly protected, but, as expected, residues in the anticodon loop are available for modification. The variable loop again shows limited modification indicating tertiary interactions. These interactions are

FIGURE 3-2: Structural consequence of the U8C mutation in hmtRNA^{Met} and the effect of

Mg^{2+}. *(A)* Gel image showing the reactivity to 1M7 of the U8 hmtRNA^{Met} transcript.

Reactions were performed in the presence (lane 3) and absence (lane 1) of Mg^{2+} and control

reactions were performed lacking 1M7. Dideoxy NTP sequencing reactions were also

performed and those gel bands are 1 nucleotide longer than the corresponding bands in the

reaction lanes. The reactivities of the various tRNA loops are highlighted. A line on the gel

indicates the acceptor stem. Bands above the 5′ end of the acceptor stem correspond to the

structure cassette. *(B)* The structure of the hmtRNA^{Met} transcript indicating structural regions

of interest. The U8 which is changed in the U8C tRNA is red. *(C)* Gel image showing the

1M7 reactivity of the U8C hmtRNA^{Met} in the presence (lane 3) and absence (lane 1) of Mg^{2+}.

The gel is annotated as in A. *(D)* The structure formed by the U8C hmtRNA^{Met} transcript in

the presence of Mg^{2+} with the mutated nucleotide, C8, shown in red.

Fig. 3-2

A — wild-type

Lane	1	2	3	4	5	6
1M7	+	−	+	−	G	U
Mg²⁺	−	−	+	+	+	+

5' end acceptor stem

D loop

Anticodon loop

Variable loop

T loop

3' end acceptor stem

ACCA end

B

3'
ACCA end

D-loop

T-loop

acceptor stem

variable loop

anticodon loop

C — U8C mutant

Lane	1	2	3	4	5	6
1M7	+	−	+	−	G	U
Mg²⁺	−	−	+	+	+	+

5' end acceptor stem

D loop

Anticodon loop

Variable loop

T loop

3' end acceptor stem

ACCA end

D

3'

anticodon loop

111

FIGURE 3-3: Tertiary interactions in the hmtRNA^{Met} and the effect of mutating U8 to C on these interactions. *(A)* Histogram showing the reactivity of nucleotides in the U8 hmtRNA^{Met} transcript. Nucleotides with high, medium, low and no reactivity are shown in red, orange, green and black respectively. Structural regions in the tRNA are shown above the histogram. *(B)* The L-shaped structure of hmtRNA^{Met}. Possible tertiary interactions occurring in the tRNA are shown and are based on conserved interactions in canonical tRNAs. The nucleotides are colored based on reactivity as in A. *(C)* The histogram showing the reactivity of nucleotides in the U8C hmtRNA^{Met}. The histogram is labeled and colored as in A. *(D)* A possible unfolded structure of the mutated U8C hmtRNA^{Met} is shown with the nucleotides colored based on the nucleotide reactivity shown in the histogram in C. The Sprinzyl numbering system is used.

Fig. 3-3
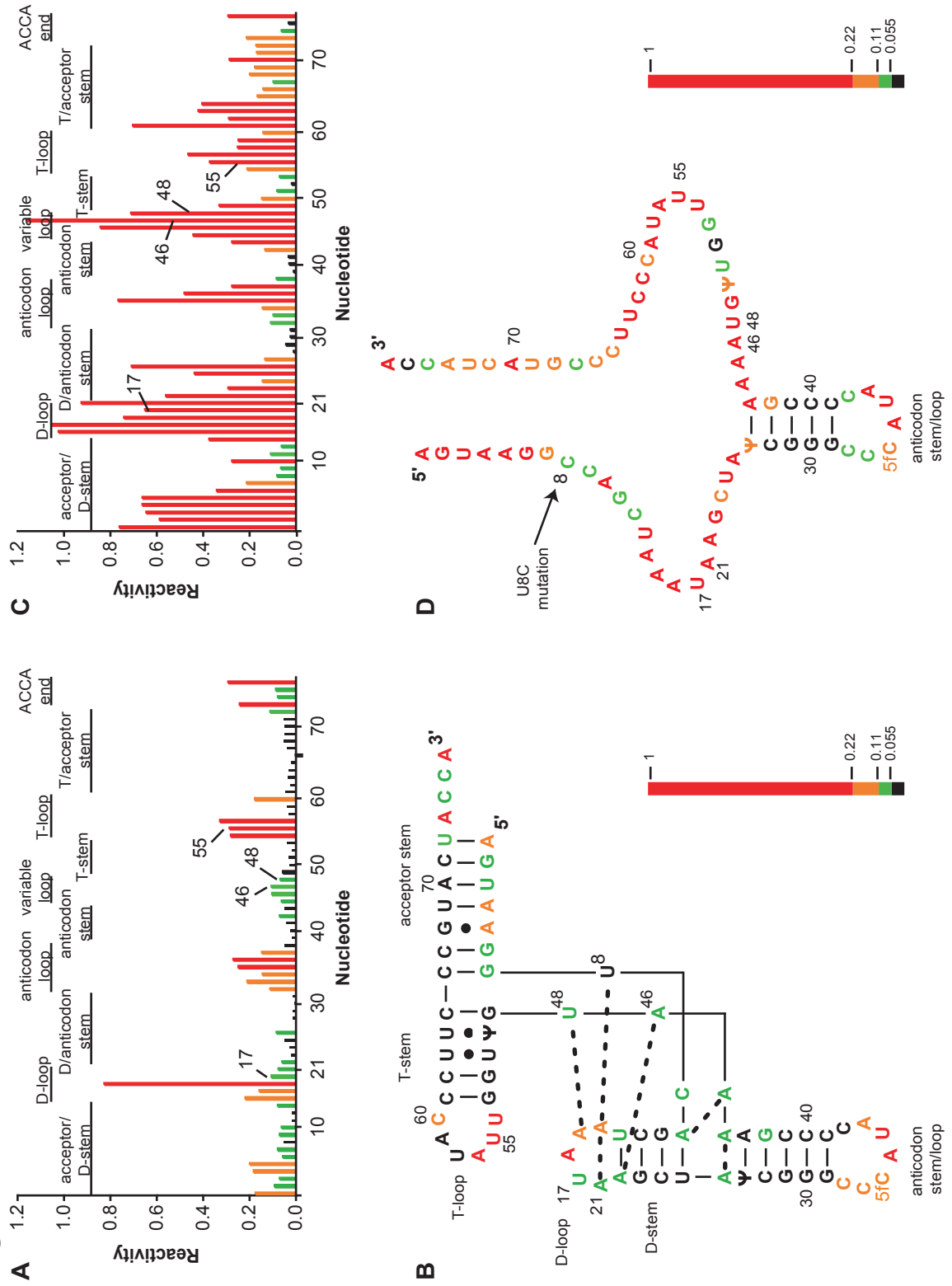
expected to take place primarily with residues in the D-loop as would be expected from tertiary contacts observed in canonical tRNAs. The T-stem apparently forms despite the presence of the U-U pairs. However, in contrast to other tRNAs *(35)*, residues in the T-loop are quite reactive indicating that they are accessible in the tertiary structure of this tRNA.

A more thorough analysis of the SHAPE data through quantitation of the individual nucleotide reactivities provides additional insight into the 3-dimensional structure formed by the unusual hmtRNA^{Met}. The SHAPE reactivity pattern is suggestive of a fully folded L-shaped tRNA and is similar to the reaction pattern observed with other tRNAs *(35)* (Fig. 3-3A). Superimposition of the nucleotide reactivities on the L-shaped tRNA structure *(34)* (Fig. 3-3B) provides additional information about possible tertiary interactions within the tRNA. For clarity, we have colored nucleotides according to their level of reactivity. As expected, the most reactive portion of the tRNA is the anticodon loop. The reactivity data support a structure in which many of the conserved canonical tertiary interactions are preserved. For example, nucleotides U8, A14, and A21 which in canonical tRNAs, form a triple base pair are all modestly reactive or non-reactive in hmtRNA^{Met}. Other possible preserved tertiary interactions are shown in Fig. 3-3B and include the expected interaction between nucleotides in the D-loop and the variable loop such as between A15 and U48.

Despite the likely presence of many conserved tertiary interactions in hmtRNA^{Met}, other interactions are probably not occurring due to the shortened sequence of this tRNA. For example, interactions between the D- and T-loops may be different than in canonical tRNAs since the D-loop is short and lacks the common GG sequence while the T-loop is only 6-nucleotides instead of the universal 7-nucleotides found in classical tRNAs. Also, A58 in the T-loop is not reactive while its expected partner U54 shows significant reactivity, suggesting

that this expected canonical tertiary interaction may not occur. This may be indicative of significant differences in the tertiary interactions occurring in the T-loop of this tRNA when compared to a canonical tRNA.

The reactivity of 1M7 is not Mg^{2+}-sensitive, hence, SHAPE chemistry was used to examine the influence of Mg^{2+} on the structure formed by the hmtRNA^{Met}. As indicated in Fig. 3-2A (compare lanes 1 and 3) the structure of this tRNA is sensitive to the presence of Mg^{2+} as would be expected for stabilization of the negatively charged backbone. In the absence of Mg^{2+}, the tRNA structure is opened and highly reactive with 1M7 indicating that both secondary and tertiary interactions have been lost (Fig. 3-2A lane 1).

Chemical probing of the structure of the U8C mutated tRNA in the presence and absence of Mg^{2+}: The structure of the U8C mutated hmtRNA was probed in the presence of Mg^{2+} (Fig. 3-2C, lane 3). The single nucleotide mutation (U8C) at the corner of the acceptor stem and D-stem of the hmtRNA^{Met} results in a drastic loss of structure that is seen even in the presence of Mg^{2+} (Fig. 3-2C, lane 3). An increase in reactivity is seen in the region of the D-loop, the variable loop, acceptor stem and T-stem. For example, all of the residues in the D-loop and most of the residues in the variable loop are now reactive. Further, the residues in the acceptor stem, which are base paired in the wild-type tRNA, are now reactive. Only the G•C pairs of the anticodon stem appear to be forming stably in the mutated tRNA (Fig. 3-2D). These changes indicate that the tertiary structure and a large portion of the secondary structure have been lost due to the mutation.

As expected, this tRNA, like the wild-type hmtRNA has essentially no structure in the absence of Mg^{2+} (Fig. 3-2C lane 1). Even the anticodon stem has now melted. Clearly,

the mutated tRNA has lost most of its Mg^{2+} sensitivity so that even the presence of Mg^{2+} is not sufficient to correctly fold the tRNA. It is likely that the loss in structure observed upon mutation of U8C results from a loss of stabilizing tertiary interactions that are present in the wild-type tRNA and that are dependent on the presence of Mg^{2+}.

Analysis of the U8C mutated tRNA clearly shows a global increase in reactivity (Fig. 3-3C and D). This increase is seen in all of the stems accept the anticodon stem suggesting a loss of these secondary structural elements. Both the D- and T-loops also significantly increase in reactivity, suggesting a loss in stabilizing tertiary interactions. The variable loop, which makes extensive tertiary interactions in the U8 hmtRNA^{Met}, becomes highly reactive in the U8C tRNA. While the mutated U8C residue itself shows only a slight increase in reactivity, its tertiary interaction partners, A14 and A21, become highly reactive suggesting that they are unable to form the necessary stabilizing tertiary interactions in this region of the tRNA. When these reactivities are superimposed on the L-shaped hmtRNA^{Met} structure it is clear that changing the single U8 nucleotide to a C results in loss of both secondary and tertiary interactions resulting in a tRNA that is largely unstructured (Fig. 3-3D).
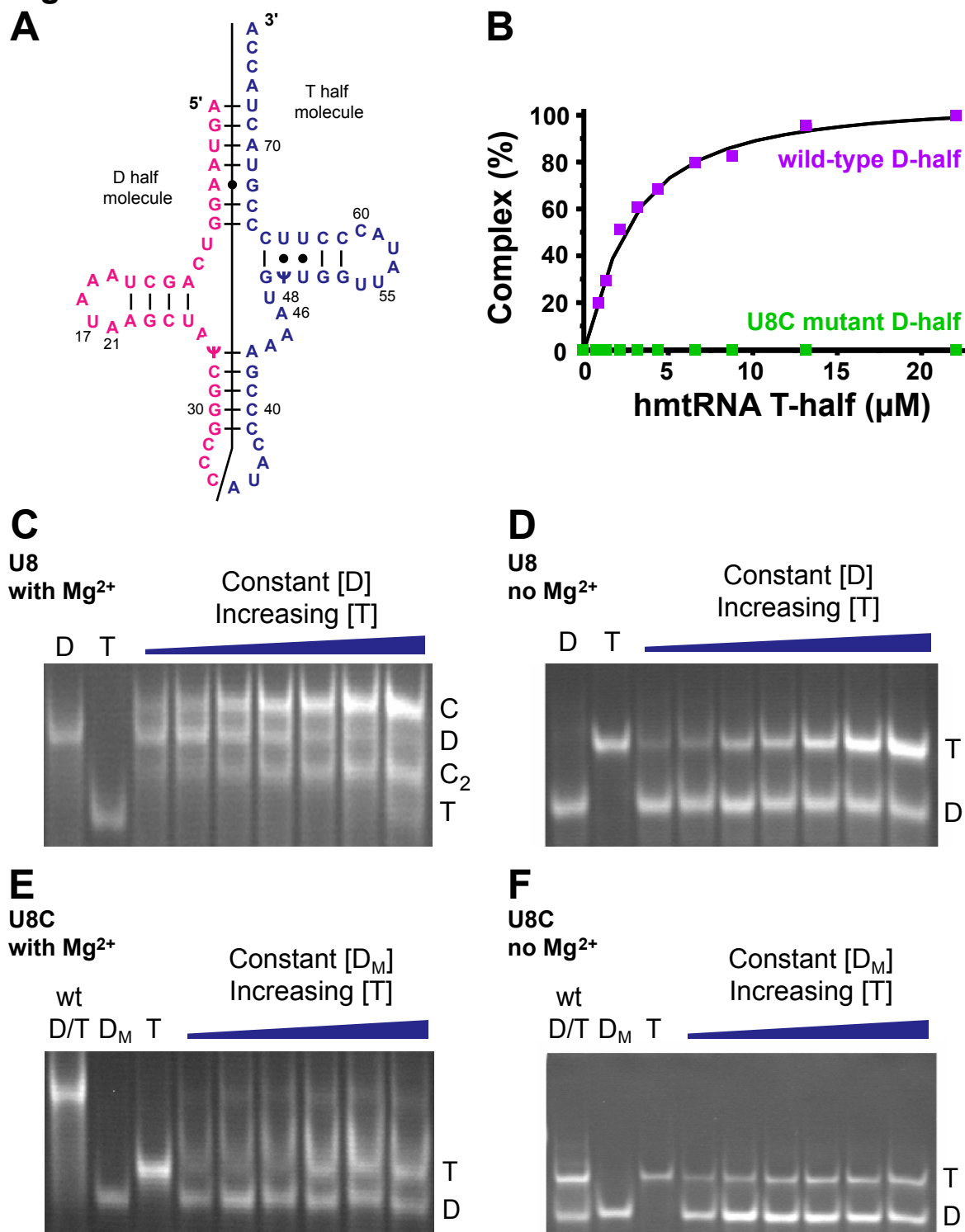
Association of T-half molecules with U8 and U8C D-half molecules: The secondary structure probing was performed on an *in vitro* transcript of the tRNA, which replaces two pseudouridines (Ψ_{27} and Ψ_{50}) with uridines and a single 5-formylcytosine (C34) with cytosine *(36)*. To further probe the effect of the U8C mutation on the structure of the tRNA, D- and T-domain tRNA half molecules were prepared containing the two pseudouridines and either U8 or U8C in the D-half molecule (Fig. 3-4A). Previously, we demonstrated that incubation of the wild type D- and T-half molecules of bovine mtRNA^{Met} in the presence of Mg^{2+} resulted

in reconstitution of the mtRNA^{Met} *(24)*. The reconstituted tRNA could be observed as a slow moving band under native conditions in polyacrylamide gel electrophoresis (PAGE). The effect of the U8C mutation on the reconstitution of the human mtRNA^{Met} was assessed using PAGE migration in the presence and absence of Mg^{2+}. The thermal stabilities of the U8 and U8C D-half molecules and the wild type T-half molecule were also determined in the presence and absence of Mg^{2+}.

In PAGE, when the slower migrating mtRNA^{Met} D-half molecule containing the normal U8 is titrated with the faster migrating T-half molecule at 3 mM Mg^{2+}, a gel shift is observed which corresponds to the formation of a complex between the two half molecules (Fig. 3-4C) *(24)*. In fact, two new bands attributed to the reconstituted tRNA appear to increase with increasing amounts of the T-half molecule. This increase is accompanied by the expected decrease in the D-half molecule (Fig. 3-4C). The two gel bands attributed to the reconstituted mtRNA^{Met} contained both half molecules, as determined by denaturing PAGE (data not shown). The slower moving mtRNA^{Met} approximated 70% of the reconstituted tRNA and migrated in a fashion similar to that of *E. coli* cytoplasmic tRNA (Fig. 3-4C), and to the migration found for the complex of bovine mtRNA^{Met} half molecules *(24)*. The faster moving band representing some 30% of the reconstituted human mtRNA^{Met} migrated faster than the D-half and slower than the T-half. It is believed to be folded into a second, but non-native, conformation. In the absence of Mg^{2+} the migration of the D-half molecule is more rapid than in the presence of Mg^{2+} suggesting a Mg^{2+}-dependent conformational change in the half molecule. In the absence of Mg^{2+}, the two half molecules could not form a complex (Fig. 3-4C and D).

FIGURE 3-4: Effect of Mg^{2+} and the U8C mutation on complex formation between the tRNA D-half and T-half molecules. *(A)* The D-half molecule (A_1- C_{32}, pink) and the T-half molecule (A_{33}-A_{76}, blue) were chemically synthesized to include Ψ_{27} and Ψ_{50}. *(B)* Summary of the efficiency of complex formation between the normal (purple) and mutated (green) D-half and T-half molecules in the presence of Mg^{2+}. *(C)* Titration of the U8 D-half molecule (D) with increasing concentrations of the T-half molecule (T) at 3 mM Mg^{2+} showing the formation of two complexes (C_1 and C_2). *(D)* Titration of the U8 D-half molecule with increasing concentrations of the T-half molecule in the absence of Mg^{2+} showing that no complex is formed. *(E)* Titration of the U8C D-half molecule with increasing concentrations of the T-half molecule at 3 mM Mg^{2+} showing that little complex is formed. *(F)* Titration of the U8C D-half molecule with increasing concentration of the T-half molecule in the absence of Mg^{2+} showing that no complex is formed. The first lane labeled wt D/T is a positive control showing the formation of the complex between the wild-type D-half molecule (37.6 μM) and the wild-type T-half molecule (37.1 μM). The lane labeled D_m indicates the migration of the mutated D-half molecule alone, while the T lane indicates the migration of the wild-type T-half molecule. Done in collaboration with C. Jones, W. Graham and P. Agris (NCSU).

Fig. 3-4

A

B

C

U8
with Mg²⁺

Constant [D]
Increasing [T]

D

U8
no Mg²⁺

Constant [D]
Increasing [T]

E

U8C
with Mg²⁺

Constant [D_M]
Increasing [T]

F

U8C
no Mg²⁺

Constant [D_M]
Increasing [T]

The mutated U8C D-half and wild-type T-half molecules are incapable of forming a complex either in the presence or absence of Mg^{2+} (Fig. 3-4E, F and B). The migration of the mutant U8C D-half molecule is much faster than the wild-type D-half in the presence of Mg^{2+}, suggesting a conformational difference in the half molecule resulting from the U8C change. In addition, the rapid migration of the U8C D-half molecule was not affected by Mg^{2+}. These results suggest that the U8C D-half molecule has lost the ability to bind one or more structurally important Mg^{2+} ions.

Native gel electrophoresis was also carried out on the hmtRNA^{Met} transcripts in the presence and absence of Mg^{2+} (data not shown). There was a noticeable shift to a slower migration of the U8C transcript in the presence of Mg^{2+} compared to the wild-type. In the absence of Mg^{2+} only a slight difference in migration was observed. This data again indicates that the U8C and wild-type transcripts respond differently to Mg^{2+}.

Thermal denaturation of the mutated tRNA: The addition of counterions, particularly Mg^{2+}, to RNA stabilizes its structure. Apparently, the U8C D-half molecule has lost the ability to bind one or more critical Mg^{2+}. We are able to observe this difference between the U8 and U8C D-half molecule by UV-monitored denaturation and renaturation. In the absence of Mg^{2+}, the U8 D-half molecule began to denature at low temperatures, but did exhibit a major transition (Fig. 3-5A). However, in the presence of Mg^{2+}, the RNA melted earlier and with a lower hyperchromicity. This response to Mg^{2+} is similar to that of the bovine mtRNA^{Met} D-half molecule *(24)*.

In contrast, the thermal denaturation of the human mtRNA^{Met} U8C D-half molecule lacked a major thermal transition, and was little effected by the presence of Mg^{2+} (Fig. 3-5B). This observation again argues that the mutation has led to the loss of a Mg^{2+} binding site.

The wild type T-half molecule exhibited a major thermal transition that was stabilized by the presence of Mg^{2+} (Fig. 3-5C). This is surprising considering that the T-stem contains two adjacent U-U mismatches (Fig. 3-1A). However, tandem U-U mismatches form one of the most stable internal loops in RNA and, despite the stem distortion that results, their presence actually stabilizes duplex RNA *(37,38)*.

Thermal denaturation of the intact U8 hmtRNA^{Met} transcript similarly demonstrates the importance of Mg^{2+} for correctly folding of hmtRNA^{Met}. In the absence of Mg^{2+} the U8 tRNA began melting at low temperatures, but demonstrated a major transition at around 30 °C (Fig. 3-6A, blue). In the presence of Mg^{2+} the U8 tRNA was stably folded until about 50°C were a major transition occurred (Fig. 3-6A, pink). The shift in melting temperature in the presence of Mg^{2+} demonstrates the increased structure resulting from the presence of Mg^{2+}. Conversely, melting the U8C hmtRNA^{Met} transcript did not show a strong dependence on Mg^{2+}. In both the presence and absence of Mg^{2+} the U8C transcript failed to show a major thermal transition, although significant hyperchromicity was observed (Fig. 3-6B). Clearly the U8C tRNA does not show the same structural response to Mg^{2+} as the U8 tRNA.

FIGURE 3-5: Effect of Mg^{2+} on the thermal stabilities of the hmtRNA^{Met} wild type and mutant D-half molecules and the wild type T-half molecule. The wild type *(A)* and mutant *(B)* D-half molecules and the wild type T-half molecule *(C)* were subjected repeatedly to thermal denaturation and renaturation monitored at 260 nm. The average of nine melt profiles conducted on different days are plotted for each RNA in the absence (blue) and presence (pink) of 3 mM Mg^{2+}. Done in collaboration with C. Jones, W. Graham and P. Agris (NCSU).
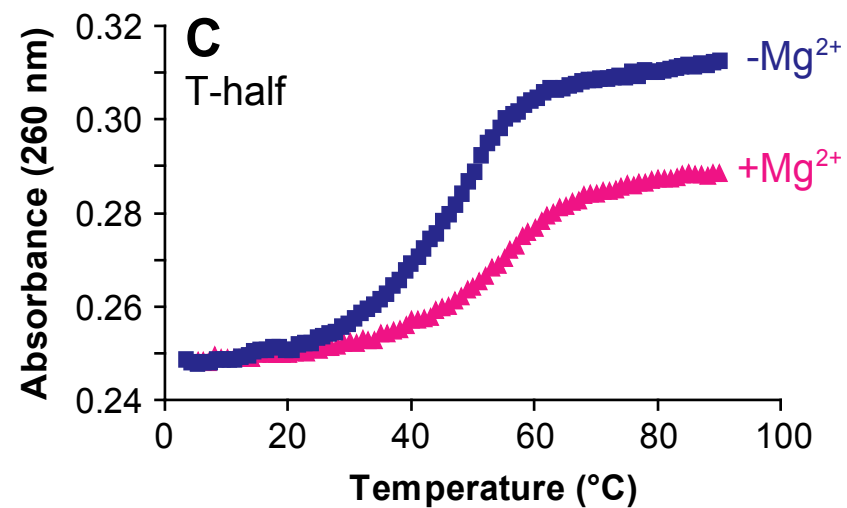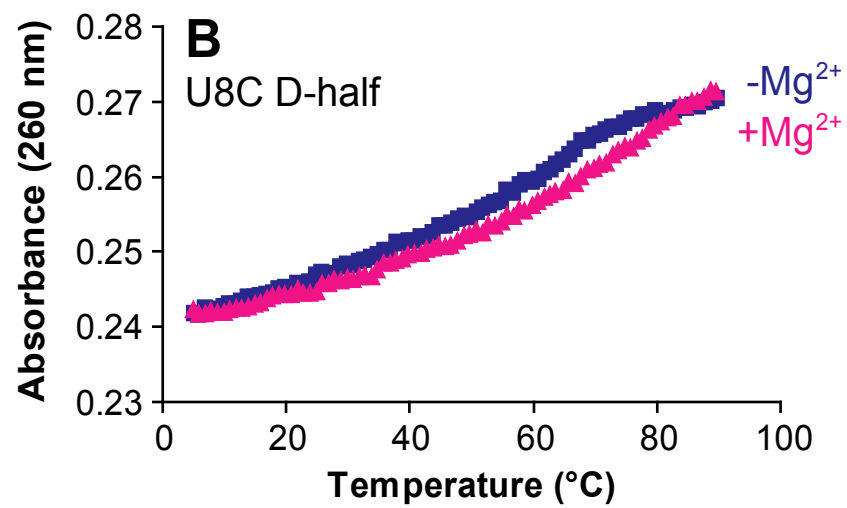
Fig. 3-5

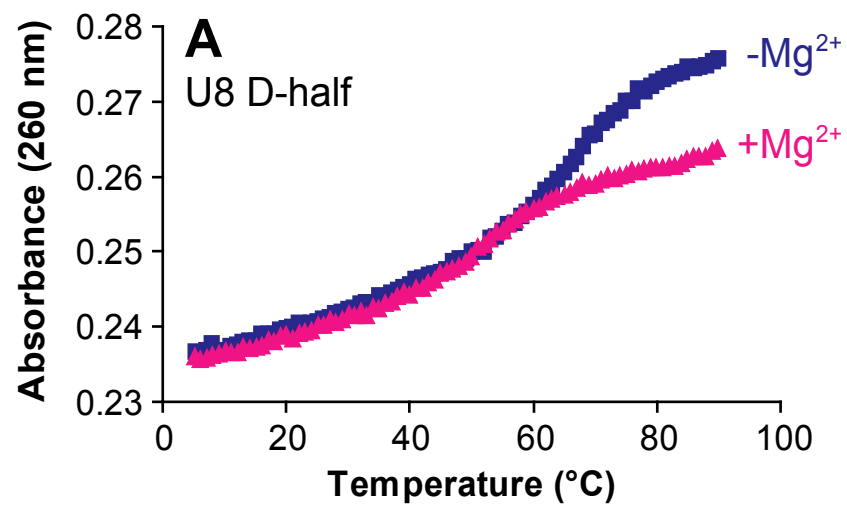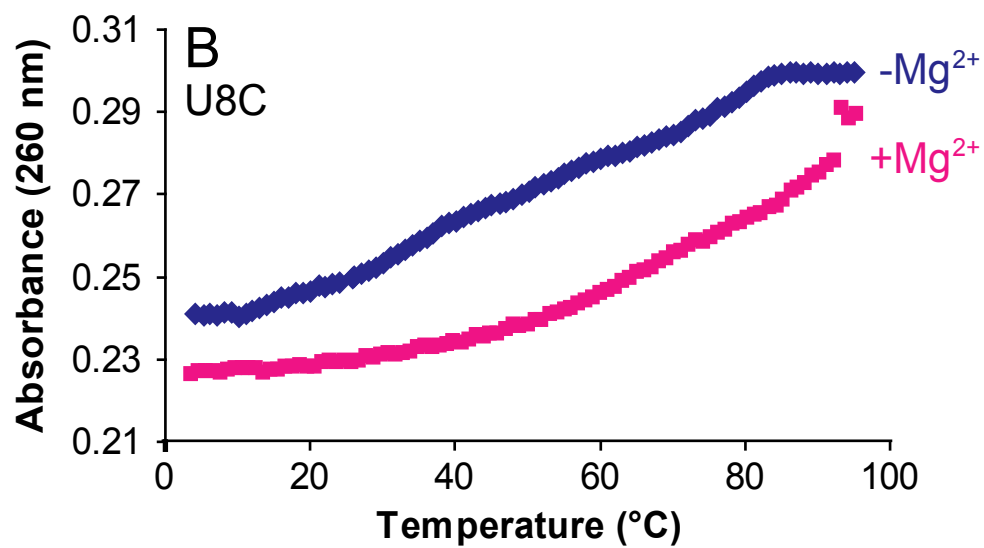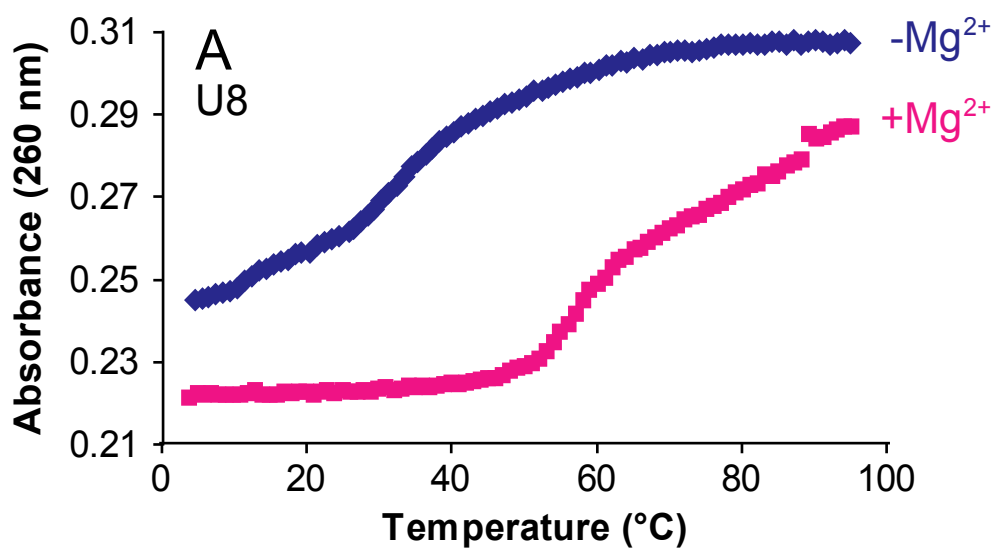**FIGURE 3-6:** Thermal denaturation of the U8 and U8C transcripts in the presence and absence of Mg^{2+}. *(A)* The thermal denaturation of the U8 transcript was monitored at 260 nm in the absence (blue) and presence (pink) of 6 mM Mg^{2+}. *(B)* The U8C transcript in the absence (blue) and presence (pink) of 6 mM Mg^{2+} was subjected to thermal denaturation monitored at 260 nm.

Fig. 3-6

125

DISCUSSION

The data presented here represent the first analysis of the structure of a human mitochondrial tRNA at single nucleotide resolution. Our data indicate that, despite an overall weaker structure, hmtRNA^{Met} displays an overall secondary and tertiary structure that is compatible with the L-shaped structure of canonical tRNAs. The drastic effect of the U8C mutation on the ability of this tRNA to fold even in the presence of Mg^{2+} suggests that the nucleotide at position 8 is critical for the structure of this tRNA and for the ability of the tRNA to take advantage of the stabilization from a site-specifically bound Mg^{2+}.
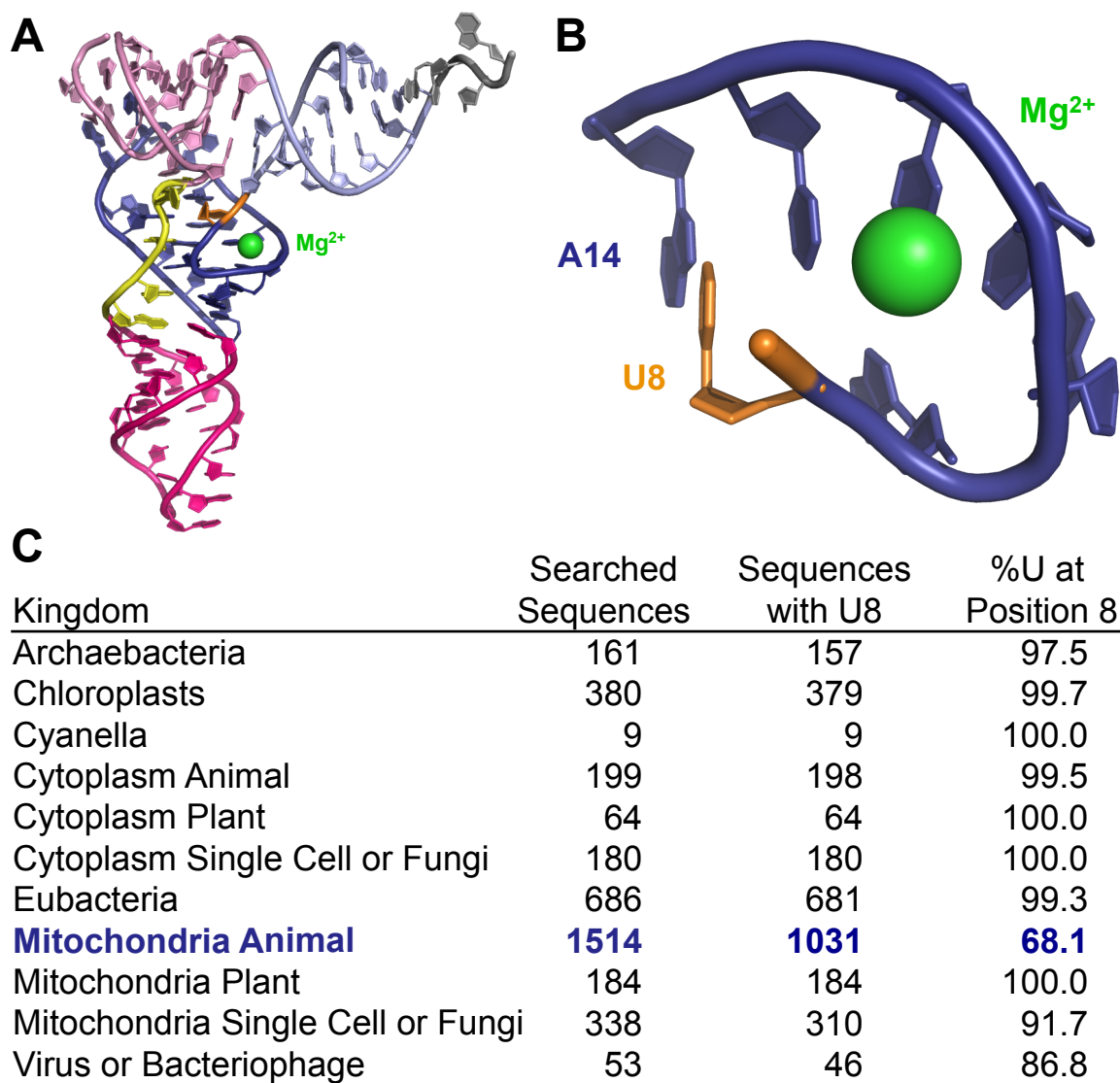
The crystal structure of yeast tRNA^{Phe} clearly shows that Mg^{2+} binds tightly and site specifically to binding pockets formed by tertiary interactions in the tRNA *(39)*. It is believed that formation of these binding pockets precedes Mg^{2+} binding, and that the subsequent binding of Mg^{2+} then stabilizes the 3-dimensional architecture of the tRNA (39). A single tightly coordinated Mg^{2+} is bound at the elbow of tRNA^{Phe}. The binding site for this ion is formed by nucleotides in the D-arm and at the corner of the D-stem and acceptor stem (Fig. 3-7A). The phosphate of U8 contacts this Mg^{2+} through a bridging water molecule. U8 is also involved in a triple non-Watson-Crick pairing interaction with nucleotides A14 and A21 forming the binding pocket (Fig. 3-7B). Our work suggests that mutation of this single nucleotide to cytosine (U8C) in hmtRNA^{Met} prevents formation of this Mg^{2+} binding pocket, resulting in a tRNA that fails to fold in the presence of Mg^{2+}. The loss of the structure of the tRNA could occur because of a disruption in the base pairing between nucleotides U8 and either A14 or A21, that in turn would destabilize the sharp turn and the Mg^{2+} binding pocket. Alternatively, loss of structure could result from an inability to properly coordinate the Mg^{2+}

126

ion via a water molecule in the pocket. Without the stabilizing effect of Mg^{2+} bound at this site, a drastic loss of structure results leading to a tRNA that is not readily aminoacylated.

Interestingly, in canonical tRNAs U8 is highly conserved and is considered a universal nucleotide (Fig. 3-7C) underlying the critical role of this nucleotide in forming the site-specific Mg^{2+} binding pocket that leads to a correctly folded, functional L-shaped tRNA. Of the 22 tRNAs present in human mitochondria, 16 of them have a U at position 8 and 14 of them have the U8--A14--A21 combination seen in hmtRNA^{Met}. It is of interest to note that the most common mutation in human mitochondrial tRNAs (the A3243G mutation in the tRNA^{Leu} gene associated with MELAS) is the mutation of A14 to G. The extremely deleterious effect of this mutation is also likely to arise from an inability to form the tertiary interaction involving the U8--A14--A21 triple base triple.

FIGURE 3-7: The location of the Mg^{2+} binding pocket in yeast $tRNA^{Phe}$ involving the highly conserved U8. *(A)* Tertiary structure of yeast $tRNA^{Phe}$ showing the Mg^{2+} (green) bound near U8. The tRNA is colored by secondary structure domain. The acceptor arm is light pink, the T-arm is light blue, the D-arm is sky blue, the anticodon arm is pink, the variable loop is yellow, the corner of the D-stem and acceptor stem is orange, the ACCA end is grey, and the Mg^{2+} is green. *(B)* Close-up view of the Mg^{2+} binding pocket colored as in A. *(C)* Table showing conservation of U8 among various organisms and organelles. The conservation of U8 in mammalian mitochondrial is shown in pink.

Fig. 3-7

	Searched Sequences	Sequences with U8	%U at Position 8
Kingdom			
Archaebacteria	161	157	97.5
Chloroplasts	380	379	99.7
Cyanella	9	9	100.0
Cytoplasm Animal	199	198	99.5
Cytoplasm Plant	64	64	100.0
Cytoplasm Single Cell or Fungi	180	180	100.0
Eubacteria	686	681	99.3
Mitochondria Animal	**1514**	**1031**	**68.1**
Mitochondria Plant	184	184	100.0
Mitochondria Single Cell or Fungi	338	310	91.7
Virus or Bacteriophage	53	46	86.8

REFERENCES

1. Attardi, G. (1985) Animal mitochondrial DNA: An extreme example of genetic economy. *Int. Rev. Cytology* **93:** 93-145.

2. Anderson, S., de Brujin, M., Coulson, A., Eperon, I., Sanger, F., and Young, I. (1982) Complete sequence of bovine mitochondrial DNA: Conserved features of the mammalian mitochondrial genome. *J. Mol. Biol.* **156:** 683-717.

3. Dirheimer, G., Keith, G., Dumas, P. and Westhof, E. (1995) Primary, secondary and tertiary structures of tRNAs. U. RajBhandary and D. Soll, eds. *tRNA: Structure, biosynthesis and function*. (Washington, D.C.: ASM Press), pp. 93-126.

4. Watanabe, Y.-I., Kawai, G., Yokogawa, T., Hayashi, N., Kumazawa, Y., Ueda, T., Nishikawa, K., Hirao, I., Miura, K. I. and Watanabe, K. (1994) Higher-order structure of bovine mitochondrial tRNA(SerUGA): chemical modification and computer modeling. *Nucleic Acids Res.* **22:** 347-353.

5. Yokogawa, T., Watanabe, Y.-I., Kumazawa, Y., Ueda, T., Hirao, I., Miura, K.-I. and Watanabe, K. (1991) A novel cloverleaf structure found in mammalian mitochondrial tRNA(Ser)(UCN). *Nucleic Acids Res.* **19:** 6101-6105.

6. Wakita, K., Watanabe, W., Yokogawa, T., Kumazawa, Y., Nakamura, S., Ueda, T., Watanabe, K. and Nishikawa, K. (1994) Higher-order structure of bovine mitochondrial tRNA[Phe] lacking the 'conserved' GG and TYCG sequences as inferred by enzymatic and chemical probing. *Nucleic Acids Res.* **22:** 347-353.

7. Helm, M., Giege, R. and Florentz, C. (1999) A Watson-Crick base pair disrupting methyl group (m^1A) is sufficient for cloverleaf folding of human mitochondrial RNA[Lys]. *Biochem.* **38:** 13338-13346.

8. Helm, M., Brule, H., Friede, D., Giege, R., Putz, D. and Florentz, C. (2000) Search for characteristic structural features of mammalian mitochondrial tRNAs. *RNA* **6:** 1356-1379.

9. Wittenhagen, L. M. and Kelley, S. O. (2003) Impact of disease-related mitochondrial mutations on tRNA structure and function. *Trends Biochem. Sci.* **28:** 605-611.

10. King, M., Koga, Y., Davidson, M. and Schon, E. (1992) Defects in mitochondrial protein synthesis and respiratory chain activity segregate with tRNA(Leu(UUR)) mutation associated with mitochondrial myopathy, encephalopathy, lactic acidosis, and strokelike episodes. *Mol. Cell. Biol.* **12:** 480-490.

11. Sternberg, D., Chatzoglou, E., Laforet, P., Fayet, G., Jardel, C., Blondy, P., Fardeau, M., Amselem, S., Eymard, B. and Lombes, A. (2001) Mitochondrial DNA transfer RNA gene sequence variations in patients with mitochondrial disorders. *Brain* **124:** 984-994.

12. Enriquez, J., Chomyn, A. and Attardi, G. (1995) MtDNA mutation in MERRF syndrome causes defective aminoacylation of tRNA[Lys] and premature translation termination. *Nat. Genet.* **10:** 47-55.

13. Levinger, L., Jacobs, O. and James, M. (2001) In vitro 3'-end endonucleolytic processing defect in a human mitochondrial tRNA(Ser(UCN)) precursor with the U7445C substitution, which causes non-syndromic deafness. *Nucleic Acids Res.* **29:** 4334-4340.

14. Hao, H. and Moraes, C. T. (1997) A disease-associated G5703A Mutation in human mitochondrial DNA causes a conformational change and a marked decrease in steady-state levels of mitochondrial tRNA[Asn]. *Mol. Cell. Biol.* **17:** 6831-6837.

15. Kelley, S. O., Steinberg, S. V. and Schimmel, P. (2000) Functional defects of pathogenic human mitochondrial tRNAs related to structural fragility. *Nat. Struct. Biol.* **7:** 862-865.

16. Ling, J., Roy, H., Qin, D., Rubio, M. A., Alfonzo, J. D., Fredrick, K. and Ibba, M. (2007) Pathogenic mechanism of a human mitochondrial tRNA[Phe] mutation associated with myoclonic epilepsy with ragged red fibers syndrome. *Proc. Nat. Acad. Sci. U.S.A.* **104:** 15299-15304.

17. Cenatiempo, Y., Deville, F., Dondon, J., Grunberg-Manago, M., Sacerdot, C., Hershey, J. W., Hansen, H. F., Petersen, H. U., Clark, B. F., Kjeldgaard, M. *et al.* (1987) The protein synthesis initiation factor 2 G-domain. Study of a functionally active C-terminal 65-kilodalton fragment of IF2 from Escherichia coli. *Biochem.* **26:** 5070-5076.

18. Kirino, Y., Yasukawa, T., Ohta, S., Akira, S., Ishihara, K., Watanabe, K. and Suzuki, T. (2004) Codon-specific translational defect caused by taurine-modification deficiency of mutant tRNA in MELAS, a human mitochondrial disease. *Proc. Nat. Acad. Sci. U.S.A.* **101:** 15070-15075.

19. Vissing, J., Salamon, M. B., Arlien-Soborg, P., Norby, S., Manta, P., DiMauro, S. and Schmalbruch, H. (1998) A new mitochondrial tRNA(Met) gene mutation in a patient with dystrophic muscle and exercise intolerance. *Neurology* **50:** 1875-1878.

20. Qu, J., Li, R., Zhou, X., Tong, Y., Lu, F., Qian, Y., Hu, Y., Mo, J. Q., West, C. E. and Guan, M. X. (2006) The novel A4435G mutation in the mitochondrial tRNA[Met] may modulate the phenotypic expression of the LHON-Associated ND4 G11778A mutation. *Invest. Ophth. Vis. Sci*, **47:** 475-483.

21. Lombes, A., Bories, D., Girodon, E., Franchon, P., Ngo, M., Breton-Gorious, J., Tulliez, M. and Goossens, M. (1998) The first pathogenic mitochondrial methionine tRNA point mutation is discovered in splenic lymphoma. *Hum. Mutat.* Supplement 1, S175-S183.

22. Spencer, A. C., Heck, A. H., Takeuchi, N., Watanabe, K. and Spremulli, L. L. (2004) Characterization of the human mitochondrial methionyl-tRNA synthetase. *Biochem.* **43:** 9743-9754.

23. Wilkinson, K. A., Merino, E. J. and Weeks, K. M. (2006) Selective 2′-hydroxyl acylation analyzed by primer extension (SHAPE): quantitative RNA structure analysis at single nucleotide resolution. *Nat. Protocols* **1:** 1610-1616.

24. Jones, C., Spencer, A. C., Hsu, J., Spremulli, L. L., Martinis, S. A., DeRider, M. and Agris, P. F. (2006) A counterintuitive Mg^{2+}-dependent and modification-assisted functional folding of mitochondrial tRNAs. *J.Mol. Biol.* **362:** 771-786.

25. Das, R., Laederach, A., Pearlman, S. M., Herschlag, D. and Altman, R. B. (2005) SAFA: semi-automated footprinting analysis software for high-throughput quantification of nucleic acid footprinting experiments. *RNA* **11:** 344-354.

26. Badorrek, C. S. and Weeks, K. M. (2006) Architecture of a gamma retroviral genomic RNA dimer. *Biochem.* **45:** 12664-12672.

27. Ashraf, S. S., Guenther, R. H., Ansari, G., Malkiewicz, A., Sochacka, E. and Agris, P. F. (2000) Role of modified nucleosides of yeast tRNA[Phe] in ribosomal binding. *Cell Biochem. Biophys.* **33:** 241-252.

28. Yarian, C. S., Basti, M. M., Cain, R. J., Ansari, G., Guenther, R. H., Sochacka, E., Czerwinska, G., Malkiewicz, A. and Agris, P. F. (1999) Structural and functional roles of the N1- and N3-protons of psi at tRNA's position 39. *Nucleic Acids Res.* **27:** 3543-3549.

29. Serra, M. J. and Turner, D. H. (1995) Predicting thermodynamic properties of RNA. *Methods Enzymol.* **259:** 242-261.

30. McDowell, J. A. and Turner, D. H. (1996) Investigation of the structural basis for thermodynamic stabilities of tandem GU mismatches: solution structure of (rGAGGUCUC)2 by two-dimensional NMR and simulated annealing. *Biochem.* **35:** 14077-14089.

31. Schulman, L. H. and Pelka, H. (1988) Anticodon switching changes the identity of methionine and valine transfer RNAs. *Science* **242:** 765-768.

32. Mortimer, S. A. and Weeks, K. M. (2007) A fast-acting reagent for accurate analysis of RNA secondary and tertiary structure by SHAPE chemistry. *J. Am. Chem. Soc.* **129:** 4144-4145.

33. Wilkinson, K. A., Merino, E. J. and Weeks, K. M. (2005) RNA SHAPE chemistry reveals non-hierarchical interactions dominate equilibrium structural transitions in tRNA[Asp] transcripts. *J. Am. Chem. Soc.* **127:** 4659-4667.

34. Florentz, C., Sohm, B., Tryoen-Toth, P., Putz, J. and Sissler, M. (2003) Human mitochondrial tRNAs in health and disease. *Cell. Mol. Life Sci.* **60:** 1356-1375.

35. Merino, E. J., Wilkinson, K. A., Coughlan, J. L. and Weeks, K. M. (2005) RNA structure analysis at single nucleotide resolution by selective 2'-hydroxyl acylation and primer extension (SHAPE). *J. Am. Chem. Soc.* **127:** 4223-4231.

36. Moriya, J., Yokagawa, T., Wakita, K., Ueda, T., Nishikawa, K., Crain, P., Hashizume, T., Pomerantz, S. C., McCloskey, J. A., Kawai, G. *et al.* (1994) A novel modified nucleoside found at the first position of the anticodon of methionine tRNA from bovine liver mitochondria. *Biochem.* **33:** 2234-2239.

37. SantaLucia, J., Kierzek, R. and Turner, D. H. (1991) Stabilities of consecutive AC, CC, GG, UC, and UU mismatches in RNA internal loops: Evidence for stable hydrogen-bonded UU and CC+ pairs. *Biochem.* **30:** 8242-8251.

38. Baeyens, K. J., De Bondt, H. L. and Holbrook, S. R. (1995) Structure of an RNA double helix including uracil-uracil base pairs in an internal loop. *Nat. Struct. Biol.* **2:** 56-62.

39. Jovine, L., Djordjevic, S. and Rhodes, D. (2000) The crystal structure of yeast phenylalanine tRNA at 2.0 Å resolution: cleavage by Mg^{2+} in 15-year old crystals. *J. Mol. Biol.* **301:** 401-414.

40. Sprinzl, M., Horn, C., Brown, M., Ioudovitch, A. and Steinberg, S. (1998) Compilation of tRNA sequences and sequences of tRNA genes. *Nucleic Acids Res*. **26**: 148-153.